PBPK models for CYP3A4 and P-gp DDI prediction: a modeling network of rifampicin, itraconazole, clarithromycin, midazolam, alfentanil and digoxin

Supplementary document

Nina Hanke [1], Sebastian Frechen [2], Daniel Moj [1], Hannah Britz [1], Thomas Eissing [2], Thomas Wendl [2] and Thorsten Lehr [1]

[1] Clinical Pharmacy, Saarland University, Saarbrücken, Germany

[2] Clinical Pharmacometrics, Bayer AG, Leverkusen, Germany

Corresponding Author: Thorsten Lehr, Clinical Pharmacy, Saarland University, Campus C2 2, 66123 Saarbrücken. Fax: +49 681 302 70258; Phone: +49 681 302 70255; E-mail: thorsten.lehr@mx.uni-saarland.de

Table of contents

1 Mathematical implementation of drug-drug interactions

1.1 DDI modeling: Induction

Induction of enzymes and transporters was implemented by substitution of the protein synthesis rate R_{syn} in the enzyme turnover equation by the apparent protein synthesis rate in the presence of an inducer $R_{syn,app}$:

$$d[E]/dt = R_{syn,app} - k_{deg} * [E] \quad (1)$$

$$R_{syn,app} = R_{syn} * (1 + (E_{max} * [I]) / (EC_{50} + [I])) \quad (2)$$

with d[E]/dt = enzyme or transporter turnover, $R_{syn,app}$ = rate of enzyme or transporter synthesis in the presence of an inducer, k_{deg} = degradation rate constant, [E] = enzyme or transporter concentration, R_{syn} = rate of enzyme or transporter synthesis in the absence of inducer, E_{max} = maximal induction effect in vivo, [I] = free inducer concentration, EC_{50} = concentration for half-maximal induction in vivo.

This increased R_{syn} value results in increased protein synthesis, increased metabolism or transport and, in our case of CYP3A4 or P-gp induction, decreased plasma concentrations of the victim drug. Implementation into the model is accomplished by addition of an induction process targeting an enzyme or transporter and information of this process with values for E_{max} and EC_{50}. In PK-Sim, induction and inhibition processes take effect in all organs and tissues that express the affected enzymes or transporters.

1.2 DDI modeling: Competitive inhibition

Competitive inhibition was implemented by substitution of the Michaelis-Menten constant K_M in the Michaelis-Menten reaction velocity equation by the apparent Michaelis-Menten constant in the presence of an inhibitor $K_{M,app}$:

$$v = (v_{max} * [S]) / (K_{M,app} + [S]) = (k_{cat} * [E] * [S]) / (K_{M,app} + [S]) \quad (3)$$

$$K_{M,app} = K_M * (1 + [I] / K_i) \quad (4)$$

with v = reaction velocity, v_{max} = maximum reaction velocity, [S] = free substrate concentration, $K_{M,app}$ = Michaelis-Menten constant in the presence of inhibitor, k_{cat} = catalytic rate constant, [E] = enzyme or transporter concentration, K_M = Michaelis-Menten constant in the absence of inhibitor, [I] = free inhibitor concentration, K_i = dissociation constant of the inhibitor-enzyme complex. As [E] is not influenced by pure competitive inhibition, here d[E]/dt = 0. During simultaneous simulation of induction or mechanism-based inactivation processes (see below), the change in [E] is dynamically calculated in PK-Sim.

This increased K_M value results in reduced reaction velocity, reduced metabolism or transport and, in the case of CYP3A4 or P-gp inhibition, increased plasma concentrations of the victim drug. Implementation into the model is accomplished by addition of a competitive inhibition process targeting an enzyme or transporter and information of this process with a value for K_i.

1.3 DDI modeling: Mechanism-based inactivation

Mechanism-based inactivation is an irreversible type of inhibition and was implemented by substitution of the protein degradation rate constant k_{deg} in the enzyme turnover equation by the apparent protein degradation rate constant in the presence of a mechanism-based inactivator $k_{deg,app}$:

$$d[E]/dt = R_{syn} – k_{deg,app} * [E] \quad (5)$$

$$k_{deg,app} = k_{deg} + (k_{inact} * [I]) / (K_I + [I]) \quad (6)$$

with $k_{deg,app}$ = enzyme or transporter degradation rate constant in the presence of mechanism-based inactivator, k_{deg} = enzyme or transporter degradation rate constant in the absence of mechanism-based inactivator, k_{inact} = maximum inactivation rate constant, [I] = free mechanism-based inactivator concentration, K_I = concentration for half-maximal inactivation. As mechanism-based inactivators are also competitive inhibitors, K_M in the Michaelis-Menten reaction velocity equation is to be substituted by $K_{M,app}$ as in equation (3).

This increased k_{deg} value results in increased protein degradation, reduced metabolism or transport and, in the case of CYP3A4 or P-gp inhibition, increased plasma concentrations of the victim drug. Return to baseline activity requires clearance of the mechanism-based inactivator and de novo synthesis of the inactivated protein. Implementation into the model is accomplished by addition of a mechanism-based inactivation process targeting an enzyme or transporter and information of this process with values for k_{inact} and K_I.

2 Model development and evaluation

2.1 Model establishment – general

The PBPK models of **rifampicin**, **itraconazole**, **clarithromycin**, **midazolam**, **alfentanil** and **digoxin** were developed with clinical data of healthy subjects covering the broadest dosing range possible for intravenous as well as oral administration of all drugs. Plasma concentrations following multiple-dose application, fractions excreted to urine or bile and other clinical measurements were included for model development whenever available.

The following sections on the six different models will all contain (a) a study table, listing details on the studies used as training and test data, (b) a parameter table listing the drug-dependent parameters of the final models, (c) a model performance figure showing predicted compared to observed plasma concentration-time profiles of all available studies in semilogarithmic plots, (d) a model performance figure showing the same predicted compared to observed plasma concentration-time profiles of all available studies in linear plots and (e) sensitivity analysis results. Furthermore, predicted and observed AUC and C_{max} values for all studies are given in the study tables (a), together with the calculated GMFEs as a measure of the descriptive and predictive performance of the established models.

System-dependent parameters, such as reference concentrations (concentration in the tissue with the highest expression) and tissue expression profiles of metabolizing enzymes, transporters and binding partners, are listed in Table S7. To enable enterohepatic cycling, the fraction of bile continuously entering the duodenum was set to 1 in all individuals and populations.

2.2 Rifampicin model establishment

Rifampicin is an antibiotic used for the treatment of mycobacterium infections, including tuberculosis and leprosy. For the investigation of DDIs, rifampicin is an established potent inducer of multiple drug metabolizing enzymes (CYP3A4, CYP2B6, CYP2C8, CYP2C9, CYP2C19) and transporters (P-gp, MRP2, MRP3, MRP4, OATP1A2). In addition to its inducing capabilities, rifampicin also competitively inhibits enzymes and transporters like CYP3A4, P-gp, OATP1B1 and OATP1B3 [1]. This study focuses on the CYP3A4 and P-gp effects of rifampicin. While induction by rifampicin involves gene expression and therefore takes several days to fully develop, competitive inhibition has an instantaneous effect and is strongest at the time of highest exposure to the inhibitor. As a consequence, the effects of rifampicin caused via competitive inhibition are most prominent 1 - 2 h after its oral administration and of relatively short duration. These complex and opposing actions of rifampicin demand careful consideration of the timing of interacting drugs during clinical studies and modeling.

The rifampicin model was established using 16 clinical studies, covering a dosing range from 300 to 600 mg (Table S1a). Integrating and testing processes that were described as vital to the pharmacokinetics of rifampicin resulted in a final model that applies transport by

OATP1B1, metabolism by arylacetamide deacetylase (AADAC), transport by P-gp and glomerular filtration. Furthermore, auto-induction of OATP1B1, AADAC and P-gp expression has been incorporated (Table S1b). Studies that measured pharmacokinetic profiles of rifampicin at different days of a 600 mg po QD regimen indicate that the clearance of rifampicin increases over time because of auto-induction of elimination processes. Therefore, we implemented induction of OATP1B1, AADAC and P-gp expression into the rifampicin model. While the induction of P-gp expression by rifampicin has been quantified in the duodenum of humans, induction of OATP1B1 has only been shown in vitro and although the enzyme catalyzing the main metabolic pathway of rifampicin has been identified as AADAC in 2011 [2], it is not yet known if the expression of AADAC is induced by rifampicin. Induction of P-gp was modeled using the same EC_{50} = 0.34 µmol/L as reported for the induction of CYP3A4 [3]. This assumption was made based on the knowledge that the co-induction of CYP3A4 and P-gp by rifampicin is mediated via binding of rifampicin to the same nuclear receptor (pregnane X receptor (PXR)) [4]. For E_{max} = 2.5 we used a value measured in human duodenal biopsies after treatment of healthy volunteers with rifampicin (600 mg po QD, 9 days) [5]. Induction of OATP1B1 was modeled using EC_{50} = 0.34 µmol/L and a fitted E_{max} = 0.38, based on in vitro reports showing induction of OATP1B1 by rifampicin in human hepatocytes [6,7]. Induction of AADAC was modeled using EC_{50} = 0.34 µmol/L and a fitted E_{max} = 0.99. The hypothesis of AADAC induction by rifampicin was based on the fact, that (1) rifampicin induces its own metabolism and (2) B-esterases are inducible by rifampicin via PXR [8,9].

The good descriptive and predictive performance is demonstrated in semilogarithmic (Figure S1c) as well as linear plots (Figure S1d) of population predicted compared to observed plasma concentration-time profiles of all clinical studies. In addition, predicted and observed AUC and C_{max} values of rifampicin with calculated GMFEs are presented in Table S1a.

Sensitivity analysis of a simulation of 600 mg rifampicin po QD with a threshold of 0.5 reveals that the rifampicin model is sensitive to the values of lipophilicity (optimized), OATP1B1 catalytic rate constant (optimized), AADAC catalytic rate constant (optimized), blood/plasma ratio (calculated) and fraction unbound (literature value) (Figure S1e).

Table S1a. Clinical studies used for rifampicin model establishment

Dose [mg]	Route	n	Males [%]	Age [years]	Weight [kg]	Data set	Pred AUC	Obs AUC	Pred/Obs AUC	Pred C_{max}	Obs C_{max}	Pred/Obs C_{max}	Reference
Rifampicin							[h*µg/mL]	[h*µg/mL]		[µg/mL]	[µg/mL]		
300	iv (0.5 h)	12	100	-	-	i	35.1	21.6	1.63	14.1	9.0	1.57	Sanofi 2013 [10]
300	iv (3 h)	2	-	-	-	i	29.7 [a]	17.6 [a]	1.69	6.2	4.1	1.50	Nitti 1977 [11]
450	iv (3 h)	3	-	-	-	i	47.7 [a]	50.5 [a]	0.94	10.0	12.4	0.81	Nitti 1977 [11]
600	iv (0.5 h)	12	100	-	-	i	82.4	58.7	1.40	30.4	17.5	1.74	Sanofi 2013 [10]
600	iv (3 h)	6	-	-	-	i	67.6 [a]	64.1 [a]	1.05	14.2	13.5	1.05	Nitti 1977 [11]
600, QD	iv (3 h)	5	100	58-68	46-65	i	-	-	-	-	-	-	Acocella 1977 [12]
300	po (cap)	12	50	39.0 (20-53)	63.4 (48-88)	i	24.0 [b]	26.1 [b]	0.92	5.0	6.6	0.75	Chouchane 1995 [13]
450	po (tab)	8	62.5	44.0	77.0	i	47.9	37.7	1.27	8.4	(6.3)	1.33	Blume 1989 [14]
450	po (-)	5	0	-	-	i	-	-	-	8.4	13.4	0.62	Acocella 1972 [15]
450, QD	po (-)	5	0	-	-	i	-	-	-	7.7	8.9	0.87	Acocella 1972 [15]
600	po (cap)	6	100	-	-	e	-	-	-	-	-	-	Acocella 1972 [16]
600	po (tab)	12	50	42.8 (26-57)	71.6 (55-89)	e	71.8	52.8	1.36	12.1	9.5	1.27	Blume 1989 [14]
600	po (cap)	38	100	29.2 (20-45)	71.2 (61-88)	i	74.4	59.9	1.24	12.1	10.8	1.12	FDA 1997 [17]
600	po (cap)	24 °	100	27.5 (19-45)	76.9 (60-101)	i	74.4	79.8	0.93	12.1	13.6	0.89	Peloquin 1997 [18]
600, QD, 4thd	po (-)	12	100	-	-	i	56.3	60.8	0.93	11.4	(12.5)	0.92	Baneyx 2014 [3]
600, QD, 7thd	po (-)	12	100	-	-	i	52.7	47.3	1.11	11.2	11.0	1.01	Baneyx 2014 [3]
							GMFE (range)		**1.24 (1.05-1.69)**			**1.28 (1.01-1.74)**	
							Pred/Obs within 2-fold		**12/12**			**14/14**	

° rifampicin + isoniazid + pyrazinamide, [a]: AUC_{0-12}, [b]: AUC_{0-10}, AUC values are 0-∞ if not specified differently, cap: capsule, d: day, e: test dataset, i: training dataset, iv: intravenously, po: orally, QD: once daily, tab: tablet, -: not given

Table S1b. Drug-dependent parameters of the final rifampicin PBPK model

Parameter	Unit	Rifampicin model	Rifampicin literature	Description
Rifampicin				
MW	g/mol	822.94		Molecular weight
pKa		1.7 (acid), 7.9 (base)	[19]	Acid dissociation constant
Solubility (pH)	mg/L	2800 (7.5)	1100 (6.5), 1400 (6.8), 2540 (6.8), 2800 (7.5), 3350 (7.4) [3,20–22]	Solubility
logP		2.50	1.30, 2.70 [3,23]	Lipophilicity
fu	%	17.0	11.0, 16.0, 17.0, 17.5 [3,22,24,25]	Fraction unbound
B/P ratio		0.89 calculated	0.9° [26]	Blood/plasma ratio
OATP1B1 K_M	µmol/L	1.5	[27]	Michaelis-Menten constant
OATP1B1 k_{cat}	1/min	7.80	n.a.	OATP1B1 catalytic rate constant
AADAC K_M	µmol/L	195.1	[2]	Michaelis-Menten constant
AADAC k_{cat}	1/min	9.87	n.a.	AADAC catalytic rate constant
P-gp K_M	µmol/L	55.0	[28]	Michaelis-Menten constant
P-gp k_{cat}	1/min	0.61	n.a.	P-gp catalytic rate constant
GFR fraction		1		Fraction of filtered drug reaching the urine
Induction EC_{50}	µmol/L	0.34	[24,25]	Conc. for half-maximal induction
E_{max} OATP1B1		0.38	n.a.	Maximum in vivo induction effect
E_{max} AADAC		0.99	n.a.	Maximum in vivo induction effect
E_{max} P-gp		2.5	[5]	Maximum in vivo induction effect
E_{max} CYP3A4		9.0	[24]	Maximum in vivo induction effect
Inhibition K_i P-gp	µmol/L	169.0	[29]	Conc. for half-maximal inhibition
Inhibition K_i CYP3A4	µmol/L	18.5	[30]	Conc. for half-maximal inhibition
Formulation		solution		Formulation used in predictions
Cell permeabilities		calculated	PK-Sim [31]	Permeation across cell membranes
Partition coefficients		calculated	R + R [32,33]	Organ-plasma partition coefficients
Specific intest. perm.	dm/min	1.24E-06	n.a.	Normalized to surface area
Specific organ perm.	dm/min	2.93E-06	calculated	Normalized to surface area

°: Blood/serum concentration ratio, AADAC: arylacetamide deacetylase, conc.: concentration, CYP3A4: cytochrome P450 3A4, GFR: glomerular filtration rate, intest.: intestinal, n.a.: not available, OATP1B1: organic anion transporting polypeptide 1B1, perm.: permeability, P-gp: P-glycoprotein, PK-Sim: PK-Sim Standard calculation method, R + R: Rodgers and Rowland calculation method

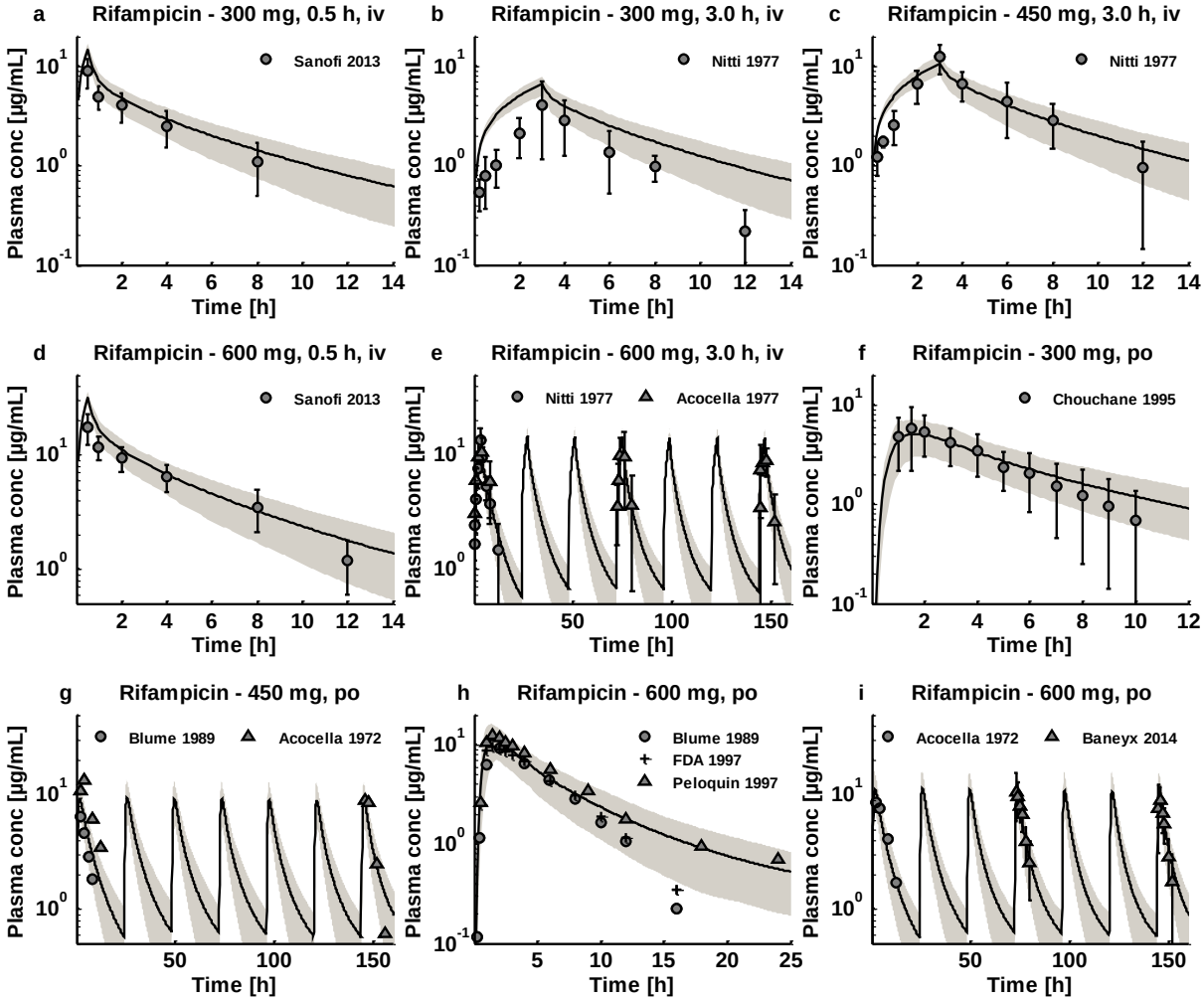

Figure S1c. Rifampicin (iv, po) semilog. Population predictions of rifampicin plasma concentration-time profiles, compared to observed data. Observed data are shown as dots, triangles or crosses ± SD. Population simulation arithmetic means are shown as lines; the shaded areas illustrate the 68% population prediction intervals. Details on dosing regimens, study populations, predicted and observed PK parameters are summarized in Table S1a.

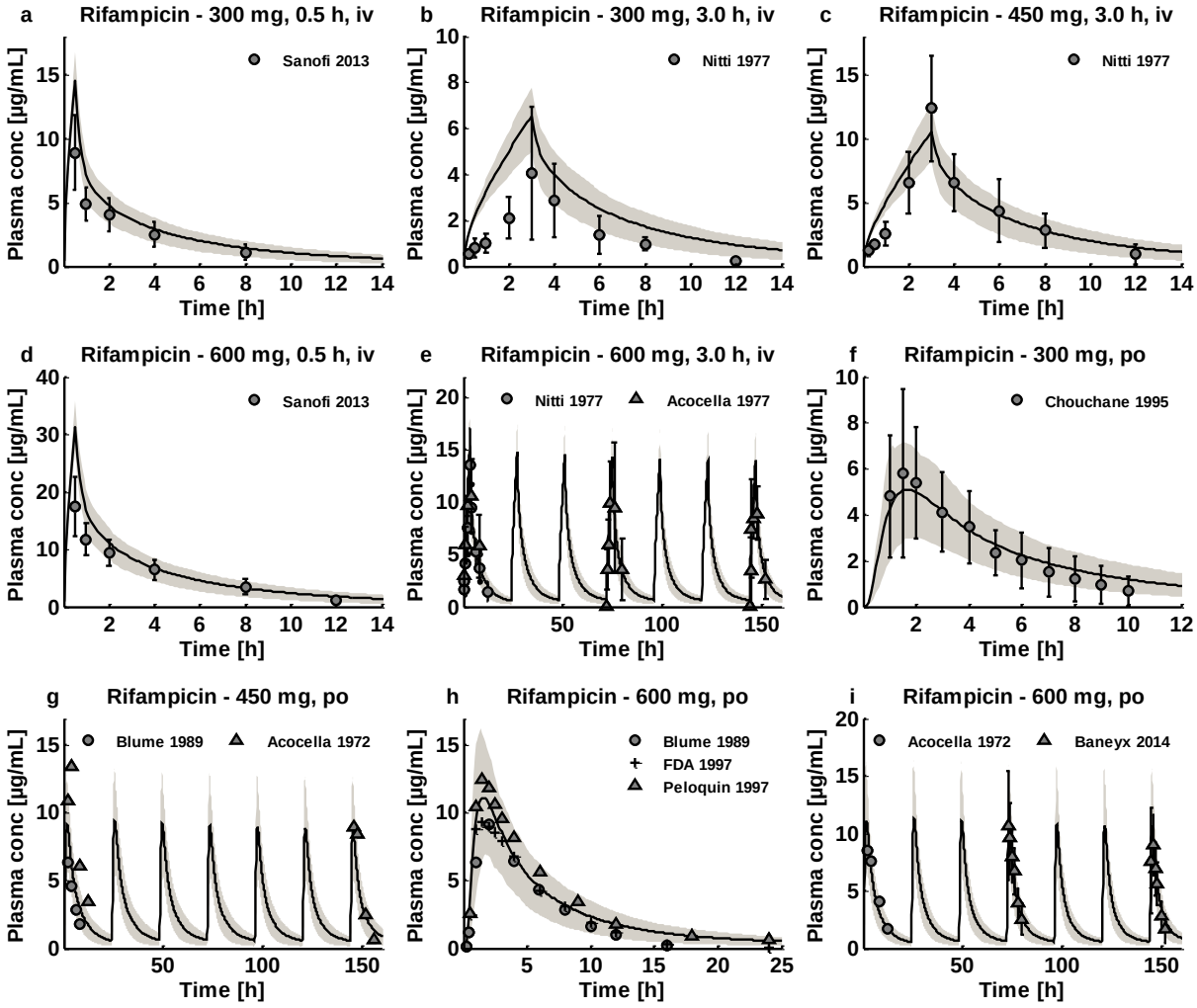

Figure S1d. Rifampicin (iv, po) linear. Population predictions of rifampicin plasma concentration-time profiles, compared to observed data. Observed data are shown as dots, triangles or crosses ± SD. Population simulation arithmetic means are shown as lines; the shaded areas illustrate the 68% population prediction intervals. Details on dosing regimens, study populations, predicted and observed PK parameters are summarized in Table S1a.

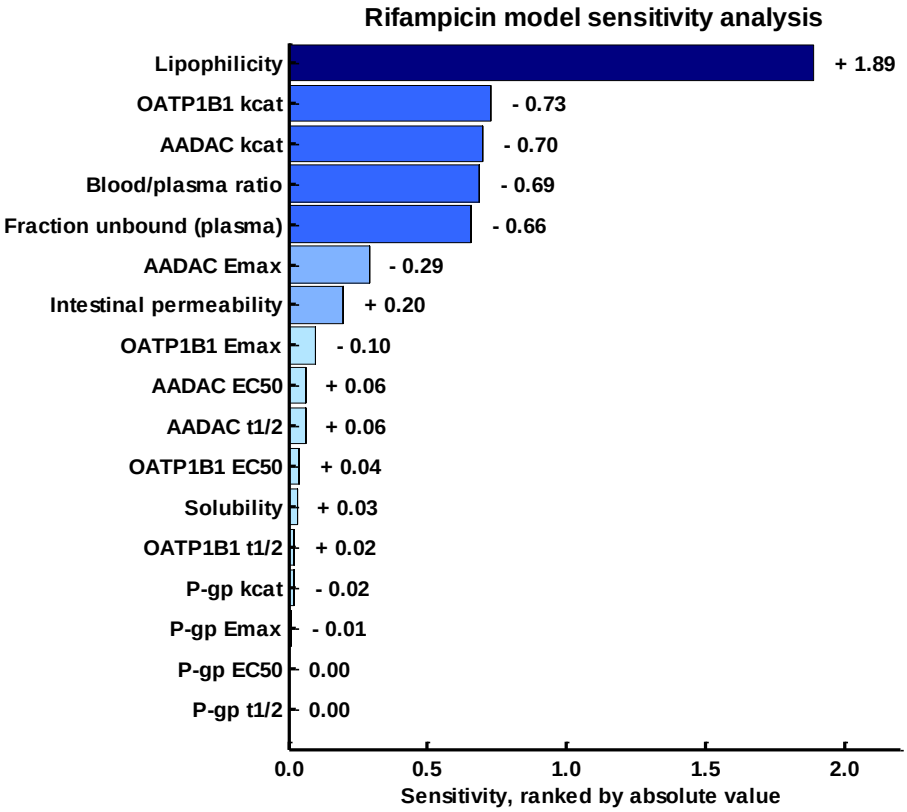

Figure S1e. Rifampicin model sensitivity analysis. Sensitivity of the model to single parameters, measured as change of the simulated AUC under steady-state conditions of a 600 mg once daily oral rifampicin regimen. A sensitivity value of + 1.0 signifies that a 10% increase of the examined parameter causes a 10% increase of the simulated AUC.

2.3 Itraconazole model establishment

Itraconazole is a triazole agent prescribed for the treatment of fungal infections. It is predominantly metabolized by CYP3A4, resulting in the sequential formation of several metabolites, starting with the major metabolite hydroxy-itraconazole, followed by keto-itraconazole and N-desalkyl-itraconazole. All three metabolites are further metabolized by CYP3A4 and parent and metabolites are reported to competitively inhibit CYP3A4 [34]. Therefore, the metabolites inhibit their own formation and itraconazole inhibits further conversion of its metabolites by CYP3A4. Itraconazole has been proposed as one of the most appropriate CYP3A4 inhibitors for clinical DDI studies, to replace the no longer recommended CYP3A4 inhibitor drug ketoconazole.

The itraconazole model was established using 27 clinical studies, covering a dosing range from 100 to 200 mg in different formulations, administered under fasted conditions or together with food (Table S2a). Although the plasma concentrations of keto-itraconazole and N-desalkyl-itraconazole are lower than those of itraconazole and hydroxy-itraconazole, N-desalkyl-itraconazole is reported to be a very potent inhibitor in vitro, and integration of the two further metabolites into the model with their inhibitory effects helped to describe the strong nonlinearity and plasma accumulation of itraconazole. The model applies sequential metabolism of itraconazole to hydroxy-itraconazole to keto-itraconazole to N-desalkyl-itraconazole by CYP3A4, including competitive inhibition of CYP3A4 by the parent drug and all three metabolites, and glomerular filtration (Table S2b).

The good descriptive and predictive performance is demonstrated in semilogarithmic (Figures S2c, S2f, S2h) as well as linear plots (Figures S2d, S2g, S2i) of population predicted compared to observed plasma concentration-time profiles of all clinical studies. In addition, predicted and observed AUC and C_{max} values of itraconazole with calculated GMFEs are presented in Table S2a.

Sensitivity analysis of a simulation of 200 mg itraconazole po QD, administered as solution in the fasted state, with a threshold of 0.5 reveals that the itraconazole model is sensitive to the values of itraconazole lipophilicity (optimized), hydroxy-itraconazole lipophilicity (optimized), itraconazole fraction unbound (optimized), itraconazole CYP3A4 catalytic rate constant (optimized), N-desalkyl-itraconazole lipophilicity (optimized) and itraconazole CYP3A4 Michaelis-Menten constant (optimized) (Figure S2e).

Table S2a. Clinical studies used for itraconazole model establishment

Dose [mg]	Route	n	Males [%]	Age [years]	Weight [kg]	Data set	Pred AUC	Obs AUC	Pred/Obs AUC	Pred C_{max}	Obs C_{max}	Pred/Obs C_{max}	Reference
Itraconazole							[h*µg/mL]	[h*µg/mL]		[µg/mL]	[µg/mL]		
100	iv (1 h)	6	100	-	-	e	4.8	4.6	1.04	1.40	0.66	2.10	Heykants 1989 [35]
200, QD	iv (2 h), LD	4	50	28.0 ± 8.1	68.3 ± 4.3	i	27.5 [a]	31.8 [a]	0.86	2.74	3.35	0.82	Mouton 2006 [36]
100	po (sol), fast	6	33	25.0 (19-33)	-	i	3.5	2.0	1.75	0.51	0.26	2.00	Templeton 2008 [37]
100	po (sol), fast	12	50	30.0 (21-40)	70.0 (54-103)	i	4.0	3.7	1.07	0.51	0.35	1.46	VanDeVelde 1996 [38]
100	po (sol), fast	6	100	30.0 (24-34)	71.0 (63-80)	i	4.0	1.9	2.07	0.51	0.22	2.29	VanPeer 1989 [39]
100, QD	po (sol), fast	6	33	25.0 (19-33)	-	i	5.4 [a]	5.1 [a]	1.05	0.65	0.81	0.80	Templeton 2008 [37]
200	po (sol), fast	27	100	18-45	-	i	6.6 [a]	4.5 [a]	1.46	1.03	0.55	1.89	Barone 1998a [40]
200, QD	po (sol), fast	27	100	18-45	-	i	32.6 [a]	29.3 [a]	1.11	2.18	1.97	1.11	Barone 1998a [40]
100	po (sol), fed	6	100	-	-	i °	3.6	2.5	1.46	0.31	0.13	2.41	Heykants 1989 [35]
100	po (sol), fed	12	50	30.0 (21-40)	70.0 (54-103)	i °	3.6	2.9	1.27	0.31	0.15	2.08	VanDeVelde 1996 [38]
200	po (sol), fed	27	100	18-45	-	i °	4.7 [a]	3.2 [a]	1.50	0.54	0.31	1.76	Barone 1998a [40]
200	po (sol), fed	30	100	24.0 (19-34)	75.7 (59-93)	i °	7.3	5.8	1.25	0.54	0.31	1.76	Barone 1998b [41]
200, QD	po (sol), fed	27	100	18-45	-	i °	21.5 [a]	22.7 [a]	0.94	1.30	1.43	0.91	Barone 1998a [40]
100	po (cap), fast	6	100	30.0 (24-34)	71.0 (63-80)	i *	1.5	0.7	2.10	0.09	0.04	2.25	VanPeer 1989 [39]
200	po (cap), fast	28	100	23.0 (20-32)	70.9 (57-90)	i *	3.0	2.1	1.45	0.18	0.14	1.27	Barone 1993 [42]
200, QD	po (cap), fast	9	22	19-26	52-85	i *	-	-	-	-	-	-	Olkkola 1994 [43]
100	po (cap), fed	5	100	23-42	65.1 ± 8.8	e	2.9	1.3	2.22	0.19	0.11	1.74	Hardin 1988 [44]
100	po (cap), fed	24	100	-	-	i *	3.0	2.0	1.51	0.19	0.15	1.28	Heykants 1989 [35]
100	po (cap), fed	6	100	30.0 (24-34)	71.0 (63-80)	i *	3.0	1.9	1.58	0.19	0.13	1.45	VanPeer 1989 [39]
100, QD	po (cap), fed	5	100	23-42	65.1 ± 8.8	e	4.7 [a]	5.3 [a]	0.89	0.33	0.41	0.81	Hardin 1988 [44]
100, QD	po (cap), fed	6	100	30.0 (24-34)	71.0 (63-80)	i *	-	-	-	-	-	-	VanPeer 1989 [39]
200	po (cap), fed	28	100	23.0 (20-32)	70.9 (57-90)	i *	4.9	3.4	1.43	0.27	0.24	1.13	Barone 1993 [42]
200	po (cap), fed	30	100	24.0 (19-34)	75.7 (59-93)	i *	4.9	4.5	1.09	0.27	0.31	0.85	Barone 1998b [41]
200	po (cap), fed	5	100	23-42	65.1 ± 8.8	e	4.9	4.2	1.17	0.27	0.27	0.99	Hardin 1988 [44]
200, QD	po (cap), fed	5	100	23-42	65.1 ± 8.8	i *	11.1 [a]	15.4 [a]	0.72	0.64	1.07	0.60	Hardin 1988 [44]
200, BID	po (cap), fed	28	100	23.0 (20-32)	70.9 (57-90)	i *	24.5 [b]	22.6 [b]	1.09	2.19	2.28	0.96	Barone 1993 [42]
200, BID	po (cap), fed	5	100	23-42	65.1 ± 8.8	e	42.7 [a]	39.3 [a]	1.09	1.99	1.98	1.01	Hardin 1988 [44]
							GMFE (range)		**1.34 (1.04-2.22)**			**1.49 (1.01-2.41)**	
							Pred/Obs within 2-fold		**22/25**			**19/25**	

° used only to fit solubility for sol, fed, * used only to fit solubility and capsule for cap, fasted or fed, [a]: AUC_{0-24}, [b]: AUC_{0-12}, AUC values are 0-∞ if not specified differently, BID: twice daily, cap: capsule, e: test dataset, i: training dataset, iv: intravenously, LD: study with loading dose, po: orally, QD: once daily, sol: solution, -: not given

Table S2b. Drug-dependent parameters of the final itraconazole PBPK model

Parameter	Unit	Itraconazole model	Itraconazole literature	OH-Itraconazole model	OH-Itraconazole literature	Description
Itraconazole						
MW	g/mol	705.633		721.633		Molecular weight
pKa		3.7 (base)	[35]	3.7 (base)	assumed	Acid dissociation constant
Solubility [pH]	mg/L	8.0 (FaSSIF) °	[45]			Solubility
logP		4.62	5.66 [35]	3.72	4.50 [46]	Lipophilicity
fu	%	0.6	0.2, 1.6, 3.6 [35,37,47,48]	1.7	[47]	Fraction unbound
CYP3A4 K_M	nmol/L	2.07	3.9 [34]	4.17	27.0 [34]	Michaelis-Menten constant
CYP3A4 k_{cat}	1/min	0.040	n.a.	0.020	n.a.	CYP3A4 catalytic rate constant
GFR fraction		1		1		Fraction of filtered drug reaching the urine
Inhibition K_i CYP3A4	nmol/L	1.3	[34]	14.4	[34]	Conc. for half-maximal inhibition
Inhibition K_i P-gp	nmol/L	8.0	[49]	-	n.a.	Conc. for half-maximal inhibition
Formulation		solution/capsule *				Formulation used in predictions
Cell permeabilities		calculated	PK-Sim [31]	calculated	PK-Sim [31]	Permeation across cell membranes
Partition coefficients		calculated	R + R [32,33]	calculated	R + R [32,33]	Organ-plasma partition coefficients
Specific intest. perm.	dm/min	5.33E-05	n.a.	1.52E-06	calculated	Normalized to surface area
Specific organ perm.	dm/min	1.44E-03	calculated	1.55E-04	calculated	Normalized to surface area
Parameter	**Unit**	**Keto-Itraconazole model**	**Keto-Itraconazole literature**	**ND-Itraconazole model**	**ND-Itraconazole literature**	**Description**
MW	g/mol	719.617		649.527		Molecular weight
pKa		3.7 (base)	assumed	3.7 (base)	assumed	Acid dissociation constant
logP		4.21	4.50 [50]	5.18	4.20 [51]	Lipophilicity
fu	%	1.0	[47]	1.1	[47]	Fraction unbound
CYP3A4 K_M	nmol/L	2.22	1.4 [34]	0.63	n.a.	Michaelis-Menten constant
CYP3A4 k_{cat}	1/min	0.393	n.a.	0.061	n.a.	CYP3A4 catalytic rate constant
GFR fraction		1		1		Fraction of filtered drug reaching the urine
Inhibition K_i CYP3A4	nmol/L	5.12 ^	[34]	0.32 ^	[34]	Conc. for half-maximal inhibition
Inhibition K_i P-gp	nmol/L	-	n.a.	-	n.a.	Conc. for half-maximal inhibition
Cell permeabilities		calculated	PK-Sim [31]	calculated	PK-Sim [31]	Permeation across cell membranes
Partition coefficients		calculated	R + R [32,33]	calculated	R + R [32,33]	Organ-plasma partition coefficients
Specific intest. perm.	dm/min	4.79E-06	calculated	7.37E-05	calculated	Normalized to surface area
Specific organ perm.	dm/min	4.92E-04	calculated	8.91E-03	calculated	Normalized to surface area

° solution fasted: 8.0 mg/L (literature value), solution fed: 1.58 mg/L (optimized), capsule fasted: 0.69 mg/L (optimized), capsule fed: 0.70 mg/L (optimized),* capsule fasted: Weibull function of 407 min dissolution time (50% dissolved) and shape 1.1 (optimized), capsule fed: Weibull function of 139 min dissolution time (50% dissolved) and shape 0.82 (optimized), ^: calculated from IC_{50} values via the Cheng-Prusoff equation [52], conc.: concentration, CYP3A4: cytochrome P450 3A4, FaSSIF: fasted state simulated intestinal fluid, GFR: glomerular filtration rate, intest.: intestinal, n.a.: not available, perm.: permeability, P-gp: P-glycoprotein, PK-Sim: PK-Sim Standard calculation method, R + R: Rodgers and Rowland calculation method

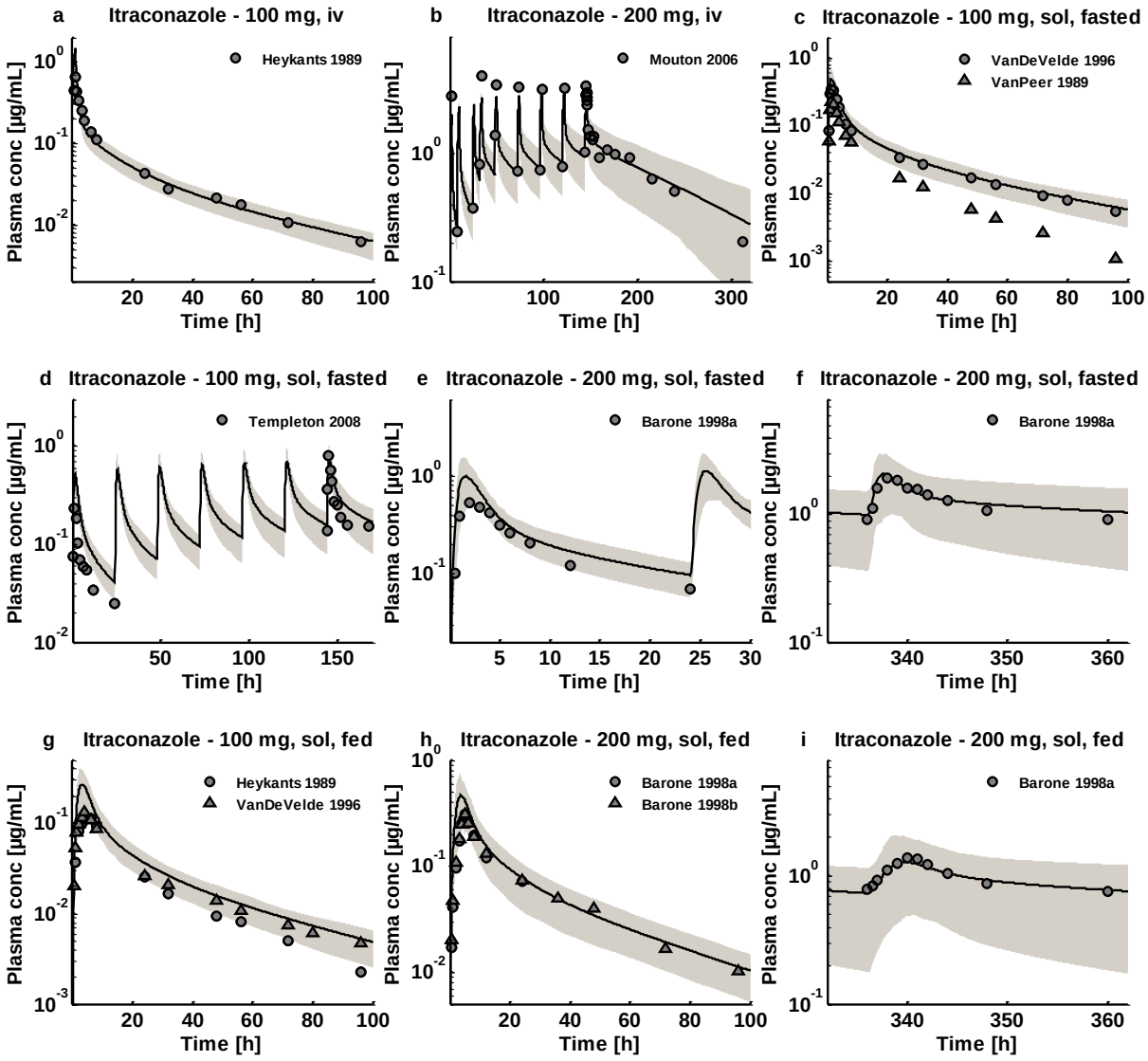
a Itraconazole - 100 mg, iv
Heykants 1989
b Itraconazole - 200 mg, iv
Mouton 2006
c Itraconazole - 100 mg, sol, fasted
VanDeVelde 1996
VanPeer 1989
d Itraconazole - 100 mg, sol, fasted
Templeton 2008
e Itraconazole - 200 mg, sol, fasted
Barone 1998a
f Itraconazole - 200 mg, sol, fasted
Barone 1998a
g Itraconazole - 100 mg, sol, fed
Heykants 1989
VanDeVelde 1996
h Itraconazole - 200 mg, sol, fed
Barone 1998a
Barone 1998b
i Itraconazole - 200 mg, sol, fed
Barone 1998a
Plasma conc [µg/mL]
Time [h]

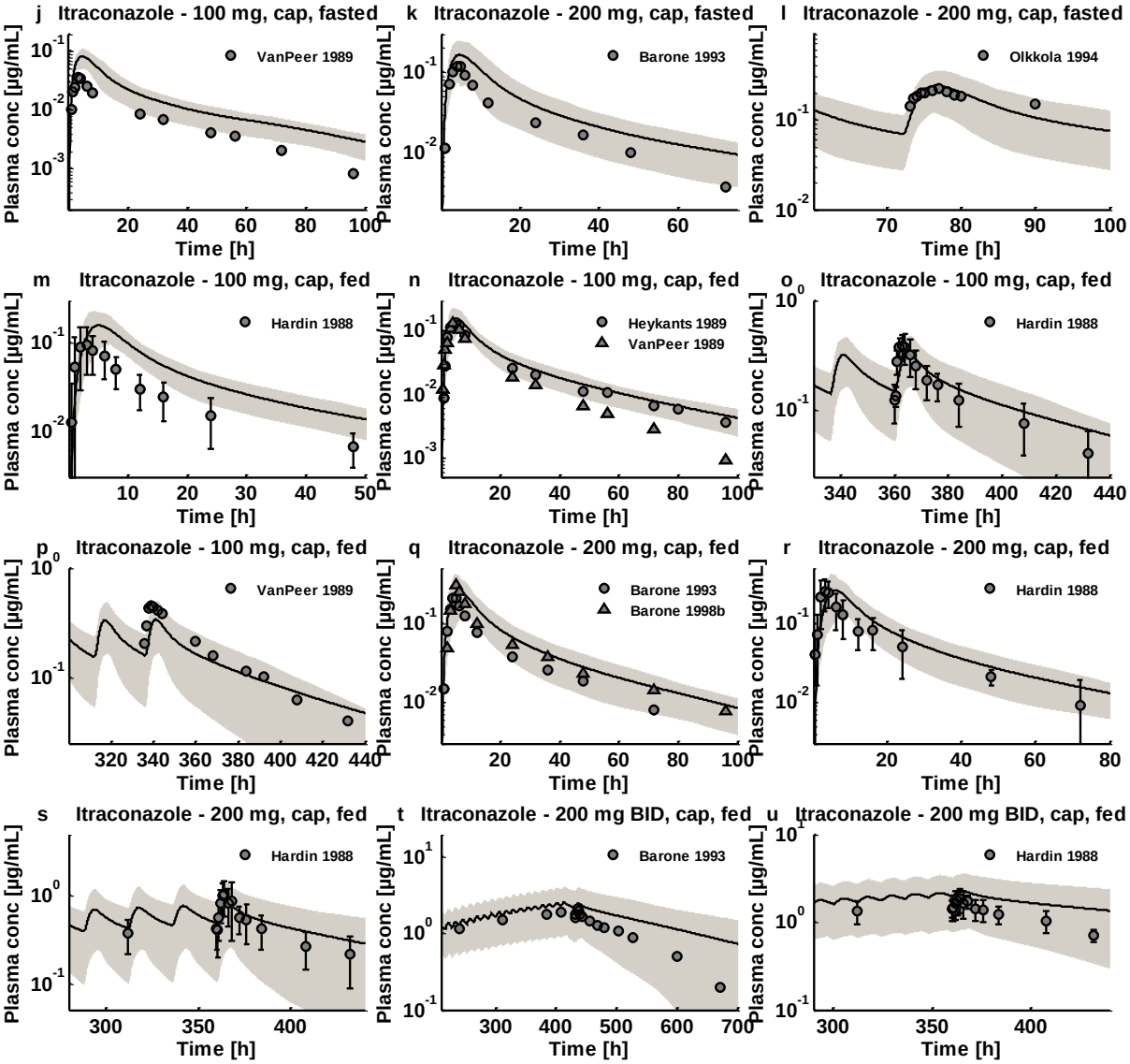

Figure S2c. Itraconazole (iv, po solution, po capsule) semilog. Population predictions of itraconazole plasma concentration-time profiles, compared to observed data. Observed data are shown as dots or triangles ± SD. Population simulation arithmetic means are shown as lines; the shaded areas illustrate the 68% population prediction intervals. (a, b) intravenous administration, (c - f) oral solution, fasted state administration, (g - i) oral solution, fed state administration, (j - l) oral capsule, fasted state administration, (m - s) oral capsule, fed state administration, (t, u) oral capsule, fed state, twice daily administration (all other multiple-dose regimens are once daily). Further details on dosing regimens, study populations, predicted and observed PK parameters are summarized in Table S2a.

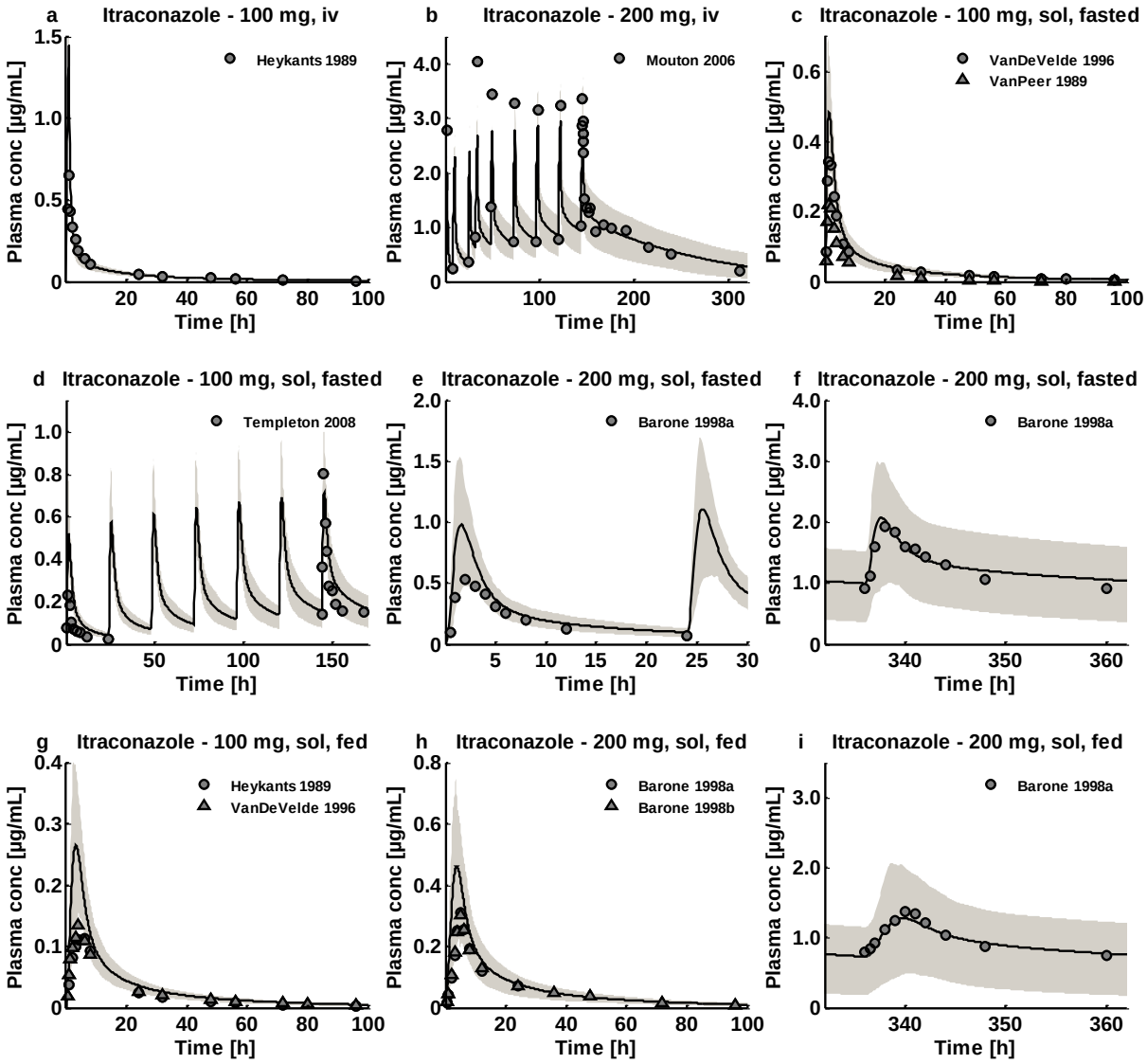
a Itraconazole - 100 mg, iv
Heykants 1989
b Itraconazole - 200 mg, iv
Mouton 2006
c Itraconazole - 100 mg, sol, fasted
VanDeVelde 1996
VanPeer 1989
d Itraconazole - 100 mg, sol, fasted
Templeton 2008
e Itraconazole - 200 mg, sol, fasted
Barone 1998a
f Itraconazole - 200 mg, sol, fasted
Barone 1998a
g Itraconazole - 100 mg, sol, fed
Heykants 1989
VanDeVelde 1996
h Itraconazole - 200 mg, sol, fed
Barone 1998a
Barone 1998b
i Itraconazole - 200 mg, sol, fed
Barone 1998a
Plasma conc [µg/mL]
Time [h]

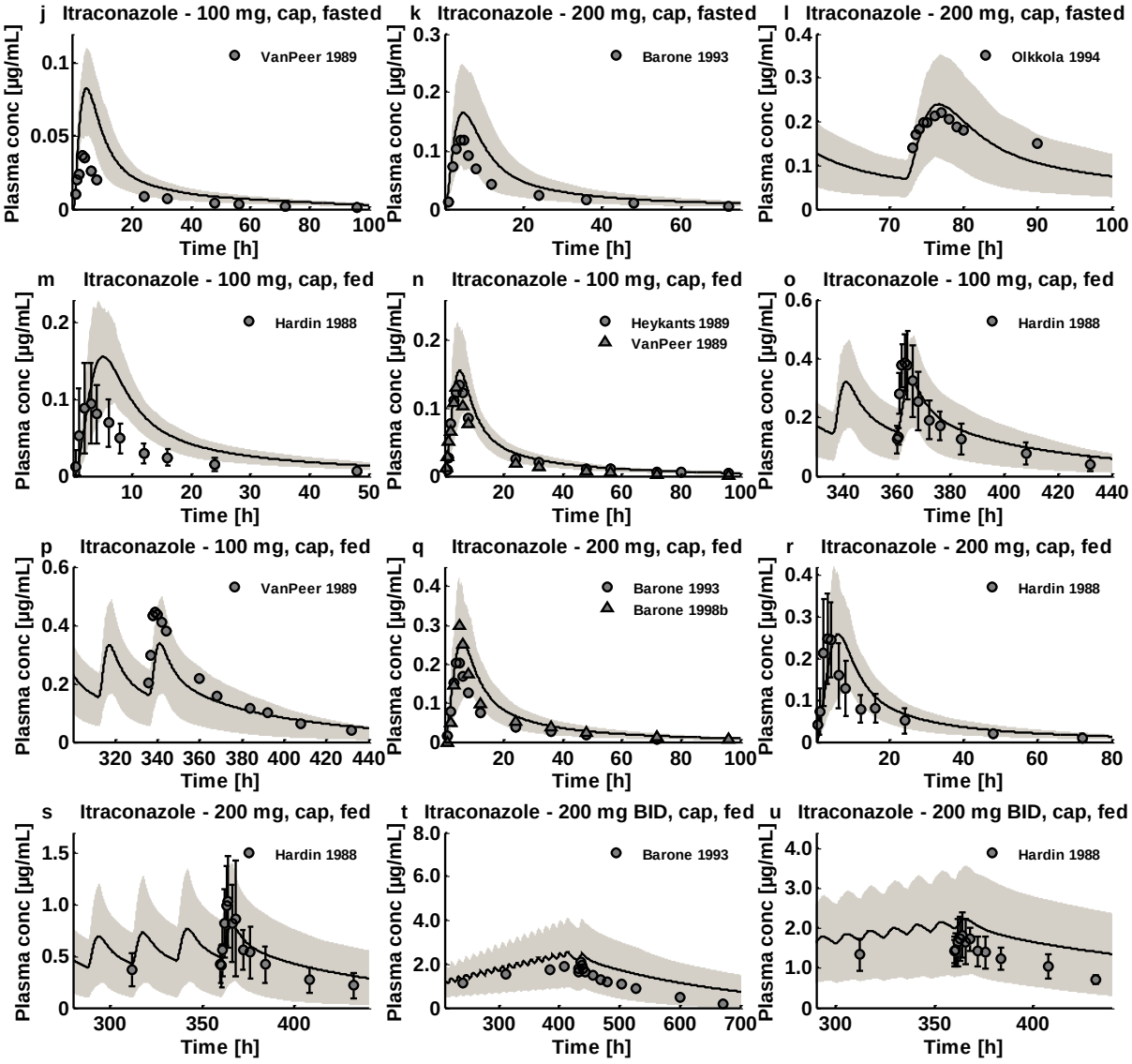

Figure S2d. Itraconazole (iv, po solution, po capsule) linear. Population predictions of itraconazole plasma concentration-time profiles, compared to observed data. Observed data are shown as dots or triangles ± SD. Population simulation arithmetic means are shown as lines; the shaded areas illustrate the 68% population prediction intervals. (a, b) intravenous administration, (c - f) oral solution, fasted state administration, (g - i) oral solution, fed state administration, (j - l) oral capsule, fasted state administration, (m - s) oral capsule, fed state administration, (t, u) oral capsule, fed state, twice daily administration (all other multiple-dose regimens are once daily). Further details on dosing regimens, study populations, predicted and observed PK parameters are summarized in Table S2a.

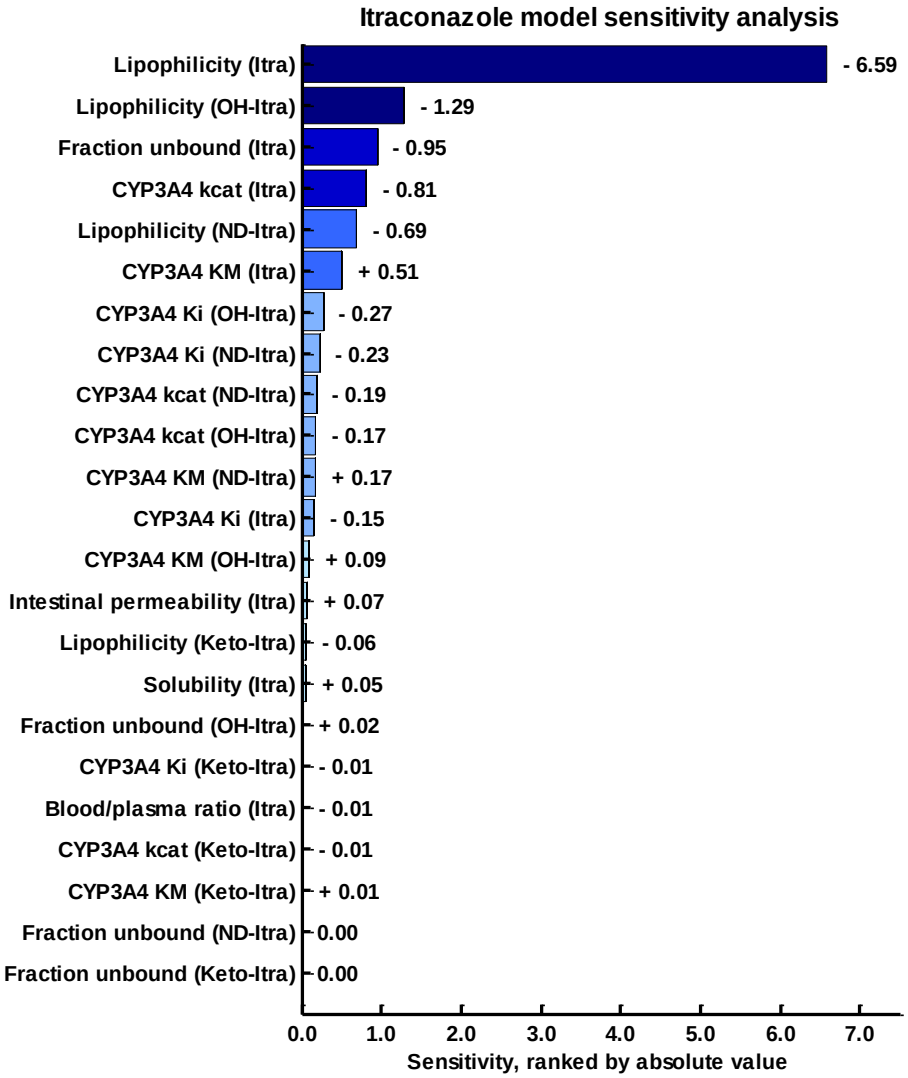

Figure S2e. Itraconazole model sensitivity analysis. Sensitivity of the model to single parameters, measured as change of the simulated AUC under steady-state conditions of a 200 mg once daily oral itraconazole regimen, administered as solution in the fasted state. A sensitivity value of + 1.0 signifies that a 10% increase of the examined parameter causes a 10% increase of the simulated AUC.

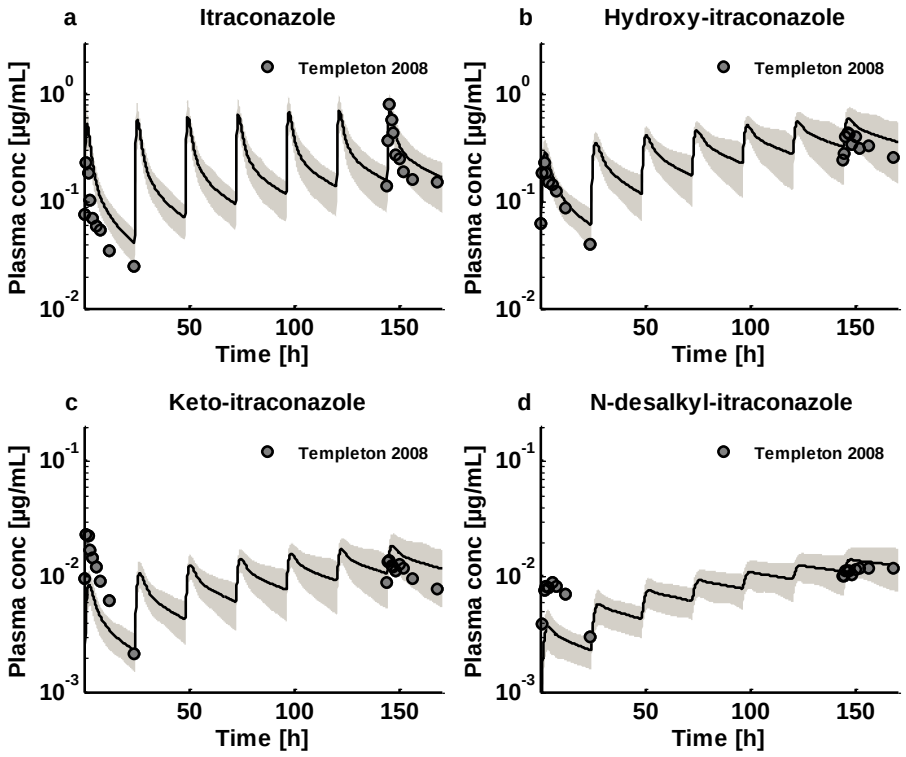

Figure S2f. Itraconazole, hydroxy-itraconazole, keto-itraconazole and N-desalkyl-itraconazole (administration of 100 mg itraconazole QD, solution, fasted) semilog. Population predictions of plasma concentration-time profiles, compared to observed data. Observed data are shown as dots. Population simulation arithmetic means are shown as lines; the shaded areas illustrate the 68% population prediction intervals. (a) itraconazole, (b) hydroxy-itraconazole, (c) keto-itraconazole, (d) N-desalkyl-itraconazole. Details on the study population are given in Table S2a.

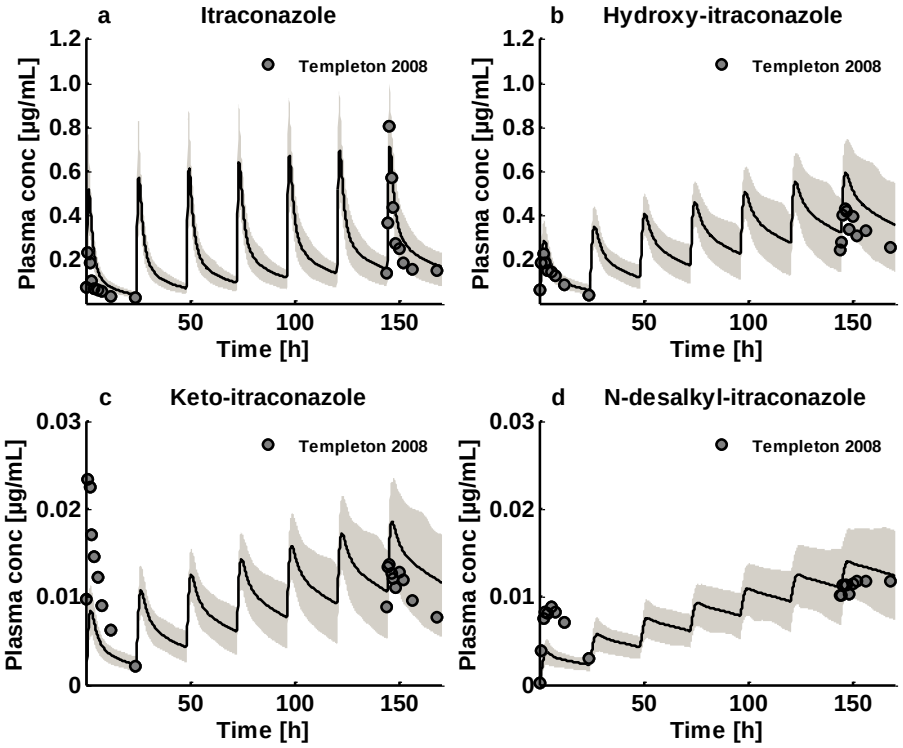

Figure S2g. Itraconazole, hydroxy-itraconazole, keto-itraconazole and N-desalkyl-itraconazole (administration of 100 mg itraconazole QD, solution, fasted) linear. Population predictions of plasma concentration-time profiles, compared to observed data. Observed data are shown as dots. Population simulation arithmetic means are shown as lines; the shaded areas illustrate the 68% population prediction intervals. (a) itraconazole, (b) hydroxy-itraconazole, (c) keto-itraconazole, (d) N-desalkyl-itraconazole. Details on the study population are given in Table S2a.

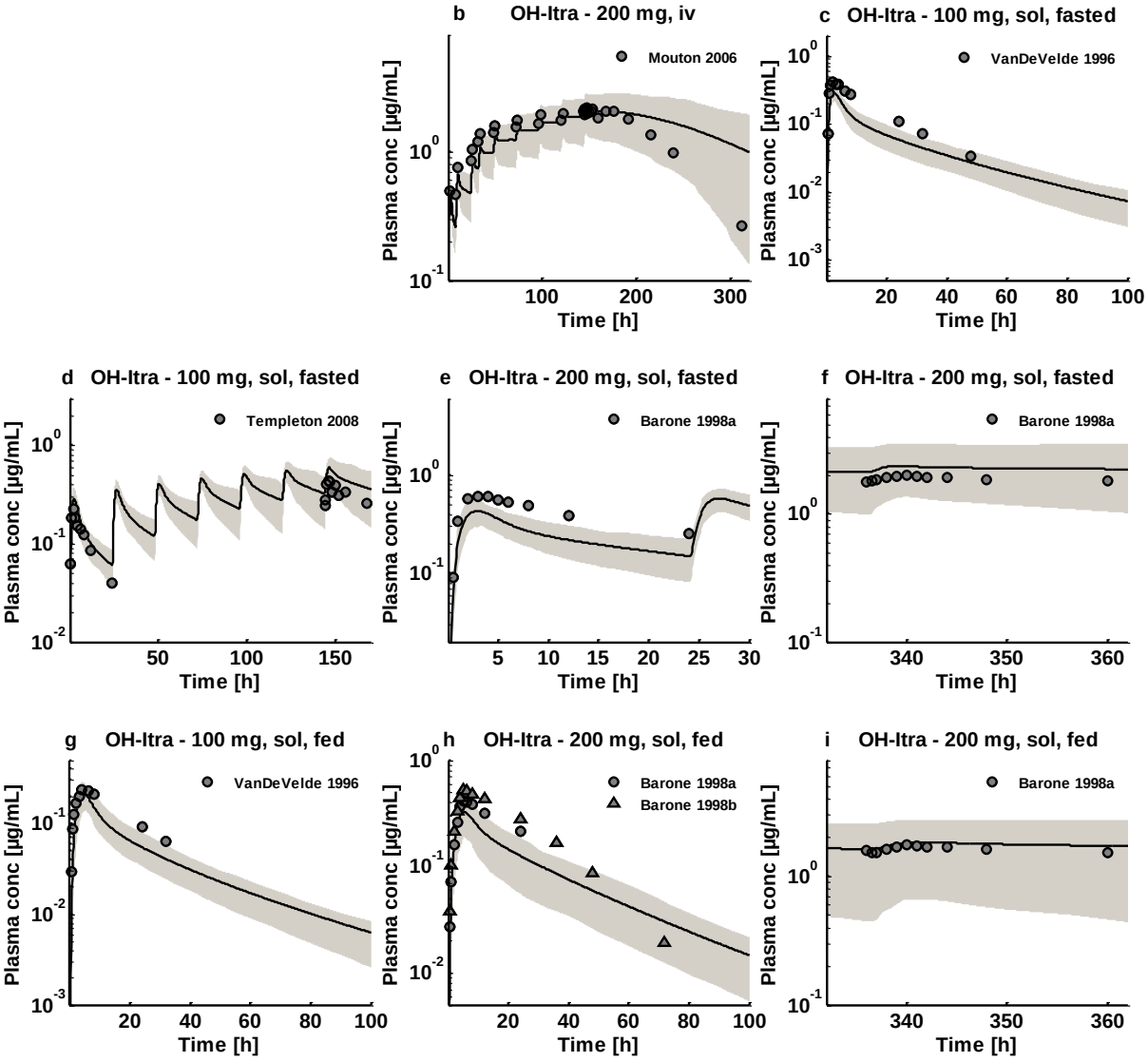
b OH-Itra - 200 mg, iv
Mouton 2006
c OH-Itra - 100 mg, sol, fasted
VanDeVelde 1996
d OH-Itra - 100 mg, sol, fasted
Templeton 2008
e OH-Itra - 200 mg, sol, fasted
Barone 1998a
f OH-Itra - 200 mg, sol, fasted
Barone 1998a
g OH-Itra - 100 mg, sol, fed
VanDeVelde 1996
h OH-Itra - 200 mg, sol, fed
Barone 1998a
Barone 1998b
i OH-Itra - 200 mg, sol, fed
Barone 1998a
Plasma conc [µg/mL]
Time [h]

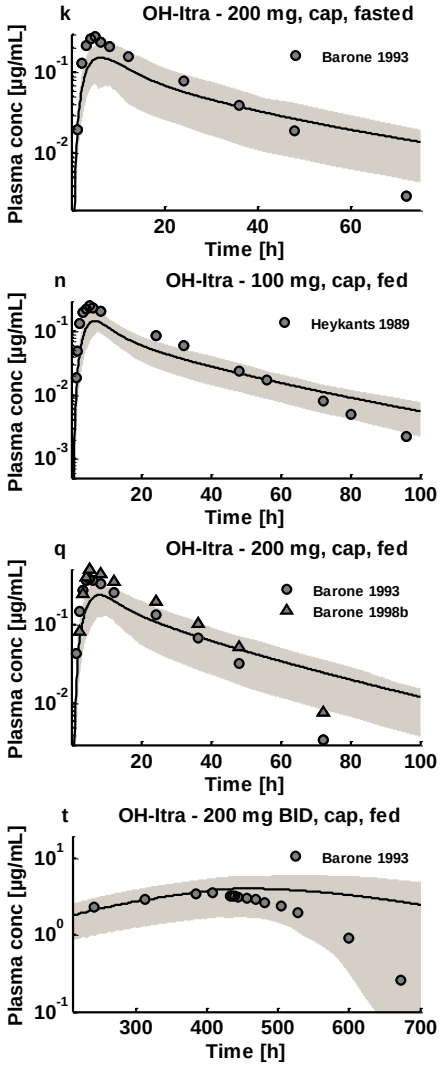

Figure S2h. Hydroxy-itraconazole (administration of itraconazole iv, po solution, po capsule) semilog. Population predictions of hydroxy-itraconazole plasma concentration-time profiles, compared to observed data. Observed data are shown as dots or triangles. Population simulation arithmetic means are shown as lines; the shaded areas illustrate the 68% population prediction intervals. Not all of the studies used for itraconazole model development report plasma concentrations of hydroxy-itraconazole. For quicker orientation and comparison, subplot names and zoom factors for the different studies are consistent with Figure S2c. (b) intravenous administration, (c - f) oral solution, fasted state administration, (g - i) oral solution, fed state administration, (k) oral capsule, fasted state administration, (n, q) oral capsule, fed state administration, (t) oral capsule, fed state, twice daily administration (all other multiple-dose regimens are once daily). Details on study populations are given in Table S2a.

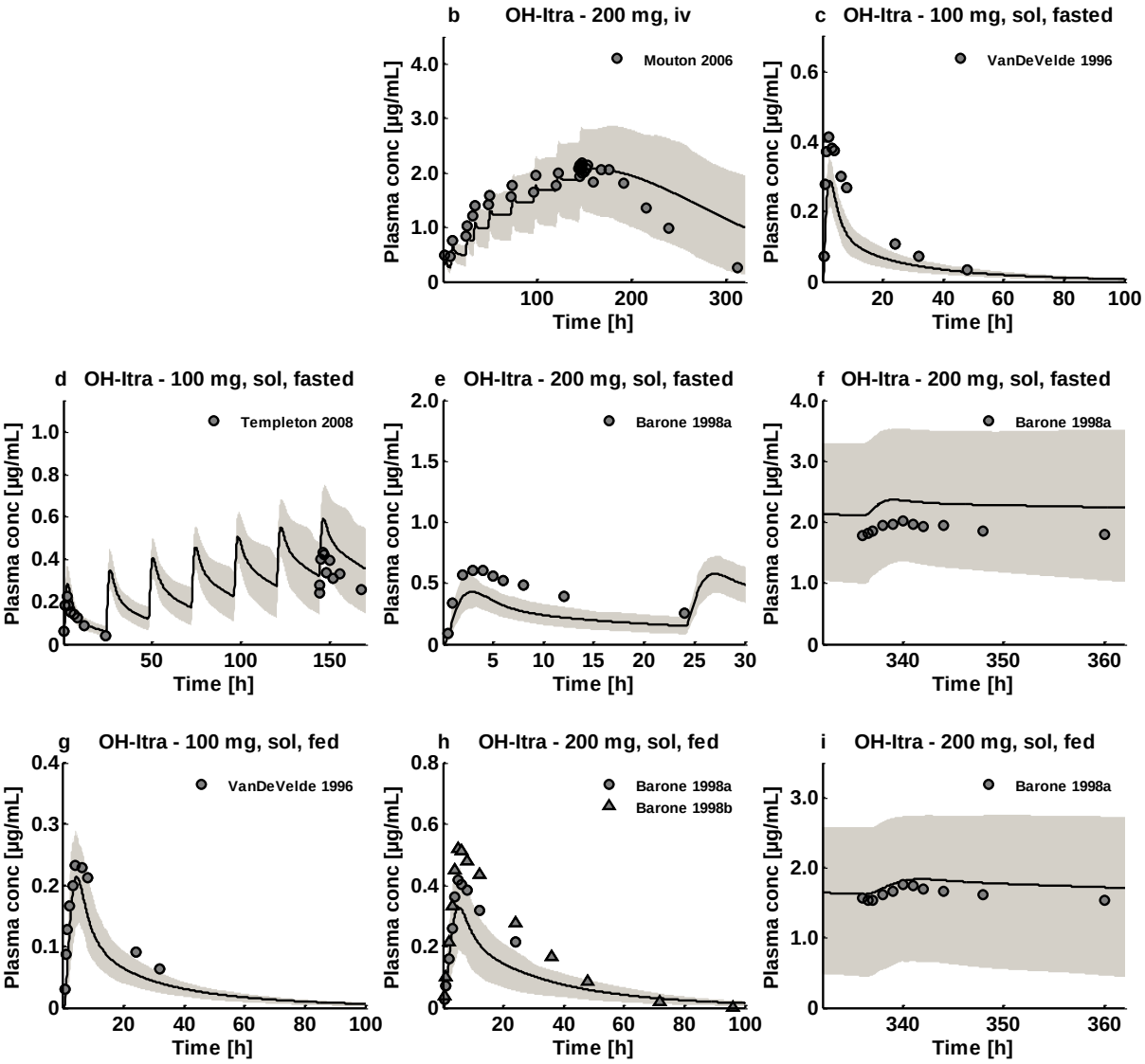
b OH-Itra - 200 mg, iv
Mouton 2006
Plasma conc [µg/mL]
Time [h]
c OH-Itra - 100 mg, sol, fasted
VanDeVelde 1996
Plasma conc [µg/mL]
Time [h]
d OH-Itra - 100 mg, sol, fasted
Templeton 2008
Plasma conc [µg/mL]
Time [h]
e OH-Itra - 200 mg, sol, fasted
Barone 1998a
Plasma conc [µg/mL]
Time [h]
f OH-Itra - 200 mg, sol, fasted
Barone 1998a
Plasma conc [µg/mL]
Time [h]
g OH-Itra - 100 mg, sol, fed
VanDeVelde 1996
Plasma conc [µg/mL]
Time [h]
h OH-Itra - 200 mg, sol, fed
Barone 1998a
Barone 1998b
Plasma conc [µg/mL]
Time [h]
i OH-Itra - 200 mg, sol, fed
Barone 1998a
Plasma conc [µg/mL]
Time [h]

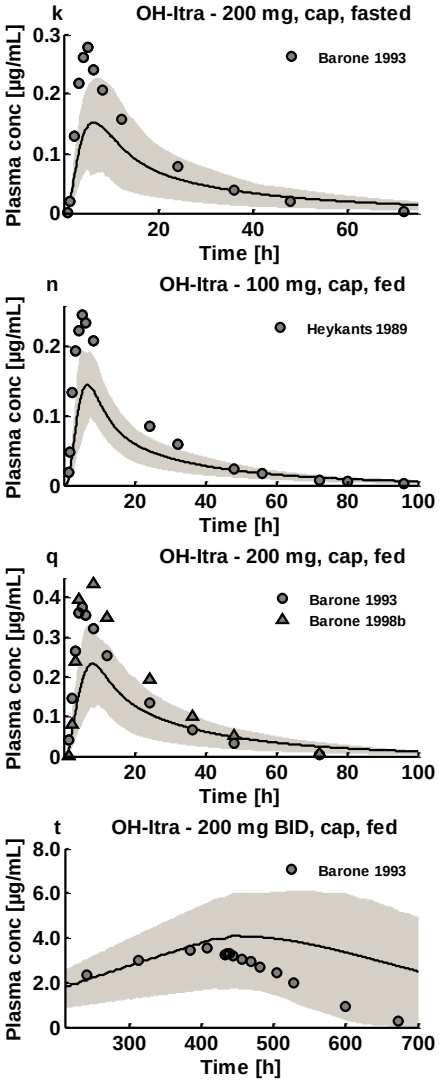

Figure S2i. Hydroxy-itraconazole (administration of itraconazole iv, po solution, po capsule) linear. Population predictions of hydroxy-itraconazole plasma concentration-time profiles, compared to observed data. Observed data are shown as dots or triangles. Population simulation arithmetic means are shown as lines; the shaded areas illustrate the 68% population prediction intervals. Not all of the studies used for itraconazole model development report plasma concentrations of hydroxy-itraconazole. For quicker orientation and comparison, subplot names and zoom factors for the different studies are consistent with Figure S2d. (b) intravenous administration, (c - f) oral solution, fasted state administration, (g - i) oral solution, fed state administration, (k) oral capsule, fasted state administration, (n, q) oral capsule, fed state administration, (t) oral capsule, fed state, twice daily administration (all other multiple-dose regimens are once daily). Details on study populations are given in Table S2a.

2.4 Clarithromycin model establishment

Clarithromycin is a widely prescribed macrolide antibiotic and a substrate and mechanism-based inactivator of CYP3A4. Furthermore, clarithromycin is a substrate and inhibitor of P-gp and an inhibitor of OATP1B1 and OATP1B3 [53,54]. Like itraconazole, clarithromycin has been proposed as one of the best alternative CYP3A4 inhibitors for clinical DDI studies to avoid further use of ketoconazole.

The clarithromycin model was established and described by Moj et al. [55]. As different models can only be coupled using the same individual, this clarithromycin model was adapted from its original literature-based CYP3A4 expression profile to the CYP3A4 RT-PCR expression profile [56] used in the other models (see Table S7). Furthermore, transport by OATP1B3 was removed, according to literature [57], and the values for pKa, logP, fu and CYP3A4 K_M were fixed to literature values.

The clarithromycin model was revised using 17 clinical studies, covering a dosing range from 100 to 1200 mg (Table S3a). The model applies partitioning into blood cells, metabolism by CYP3A4 including mechanism-based auto-inactivation and a renal clearance (Table S3b).

The good descriptive and predictive performance is demonstrated in semilogarithmic (Figures S3c) as well as linear plots (Figures S3d) of population predicted compared to observed plasma concentration-time profiles of all clinical studies. In addition, predicted and observed AUC and C_{max} values of clarithromycin with calculated GMFEs are presented in Table S3a.

Sensitivity analysis of a simulation of 500 mg clarithromycin po BID with a threshold of 0.5 reveals that the clarithromycin model is sensitive to the values of lipophilicity (literature value) and fraction unbound (literature value) (Figure S3e).

Table S3a. Clinical studies used for clarithromycin model establishment

Dose [mg]	Route	n	Males [%]	Age [years]	Weight [kg]	Data set	Pred AUC	Obs AUC	Pred/Obs AUC	Pred C_{max}	Obs C_{max}	Pred/Obs C_{max}	Reference
Clarithromycin							[h*µg/mL]	[h*µg/mL]		[µg/mL]	[µg/mL]		
250	iv (0.75 h)	19	100	29.0 (18-40)	71.5 (58-88)	i	8.3	8.6	0.97	2.67	2.78	0.96	Chu 1992 [58]
100	po (-)	6	100	25.3 (19-36) °	71.4 (56-97) °	e	2.0	1.7	1.18	0.33	0.35	0.94	Chu 1992 [59]
200	po (-)	8	100	25.3 (19-36) °	71.4 (56-97) °	e	4.6	3.0	1.53	0.74	0.60	1.23	Chu 1992 [59]
250	po (tab)	17	100	29.0 (18-40)	70.8 (58-88)	i	6.0	4.4	1.36	0.96	0.78	1.23	Chu 1993 [60]
250	po (tab)	12	100	26.5 (24-38)	79.5 (65-88)	e	5.9	5.8	1.02	0.96	0.94	1.02	Kees 1995 [61]
250, BID	po (tab)	17	100	29.0 (18-40)	70.8 (58-88)	i	7.9 [b]	6.9 [b]	1.14	1.30	1.14	1.14	Chu 1993 [60]
250, BID	po (tab)	12	100	26.5 (24-38)	79.5 (65-88)	e	8.0 [b]	7.9 [b]	1.01	1.32	1.23	1.07	Kees 1995 [61]
250, BID	po (tab)	12	100	28.0 (21-39)	80.0 (68-98)	e	-	-	-	-	-	-	Rengelshausen 2003 [62]
400	po (-)	8	100	25.3 (19-36) °	71.4 (56-97) °	e	10.4	8.6	1.21	1.60	1.13	1.42	Chu 1992 [59]
500	po (tab)	17	100	31.0 (20-39)	72.2 (64-87)	i	13.4	14.1	0.95	2.02	2.12	0.95	Chu 1993 [60]
500	po (tab)	12	100	26.5 (24-38)	79.5 (65-88)	e	13.4	15.6	0.86	2.02	2.10	0.96	Kees 1995 [61]
500, QD	po (tab)	12	100	26.5 (24-38)	79.5 (65-88)	e	16.1 [a]	18.3 [a]	0.88	2.29	2.33	0.98	Kees 1995 [61]
500, BID	po (susp)	12	58	28.0 (19-41)	66.5 (45-86)	e	-	-	-	-	-	-	Abduljalil 2009 [63]
500, BID	po (tab)	17	100	31.0 (20-39)	72.2 (64-87)	i	17.3 [b]	20.8 [b]	0.83	2.74	2.85	0.96	Chu 1993 [60]
600	po (-)	8	100	25.3 (19-36) °	71.4 (56-97) °	e	16.4	15.4	1.06	2.39	2.03	1.18	Chu 1992 [59]
800	po (-)	8	100	25.3 (19-36) °	71.4 (56-97) °	e	22.5	24.7	0.91	3.07	2.63	1.17	Chu 1992 [59]
1200	po (-)	8	100	25.3 (19-36) °	71.4 (56-97) °	e	35.1	44.6	0.79	3.98	3.97	1.00	Chu 1992 [59]
							GMFE (range)		**1.16 (1.01-1.53)**			**1.11 (1.00-1.42)**	
							Pred/Obs within 2-fold		**15/15**			**15/15**	

°: demographics of whole study population (n = 36), [a]: AUC_{0-24}, [b]: AUC_{0-12}, AUC values are 0-∞ if not specified differently**,** BID: twice daily, e: test dataset, i: training dataset, iv: intravenously, po: orally, QD: once daily, susp: suspension, tab: tablet, -: not given

Table S3b. Drug-dependent parameters of the final clarithromycin PBPK model

Parameter	Unit	Clarithromycin model	Clarithromycin literature	Description
Clarithromycin				
MW	g/mol	747.95		Molecular weight
pKa		8.99 (base)	[64]	Acid dissociation constant
Solubility (pH)	mg/L	12170 (2.4)	[65]	Solubility
logP		2.3	[66]	Lipophilicity
fu	%	30.0	28.0, 30.0, 40.0 [67–69]	Fraction unbound
CYP3A4 K_M	µmol/L	48.7	[70]	Michaelis-Menten constant
CYP3A4 k_{cat}	1/min	76.5	n.a.	CYP3A4 catalytic rate constant
CL_{Ren}	mL/min	100	111 - 213 [71]	Renal plasma clearance
Inhibition K_I CYP3A4	µmol/L	6.04	2.25, 4.12, 5.49, 29.5, 39.2 [72–75]	Conc. for half-maximal inactivation
Inhibition k_{inact} CYP3A4	1/min	0.04	0.04, 0.04, 0.05, 0.07, 0.23 [72–75]	Maximum inactivation rate
Inhibition K_i P-gp	µmol/L	4.1	[53]	Conc. for half-maximal inhibition
Formulation		tablet °		Formulation used in predictions
Cell permeabilities		calculated	PK-Sim [31]	Permeation across cell membranes
Partition coefficients		calculated	R + R [32,33]	Organ-plasma partition coefficients
Specific intest. perm.	dm/min	1.23E-06	n.a.	Normalized to surface area
Specific organ perm.	dm/min	3.28E-06	calculated	Normalized to surface area
Perm. into blood cells	dm/min	3.62E-05	n.a.	Plasma to blood cells permeability
Perm. out of blood cells	dm/min	1.04E-06	n.a.	Blood cells to plasma permeability

CL: clearance, conc.: concentration, CYP3A4: cytochrome P450 3A4, intest.: intestinal, n.a.: not available, perm.: permeability, P-gp: P-glycoprotein, PK-Sim: PK-Sim Standard calculation method, R + R: Rodgers and Rowland calculation method, °: tablets with a Weibull function of 5.0 min dissolution time (50% dissolved) and shape 2.9 [55]

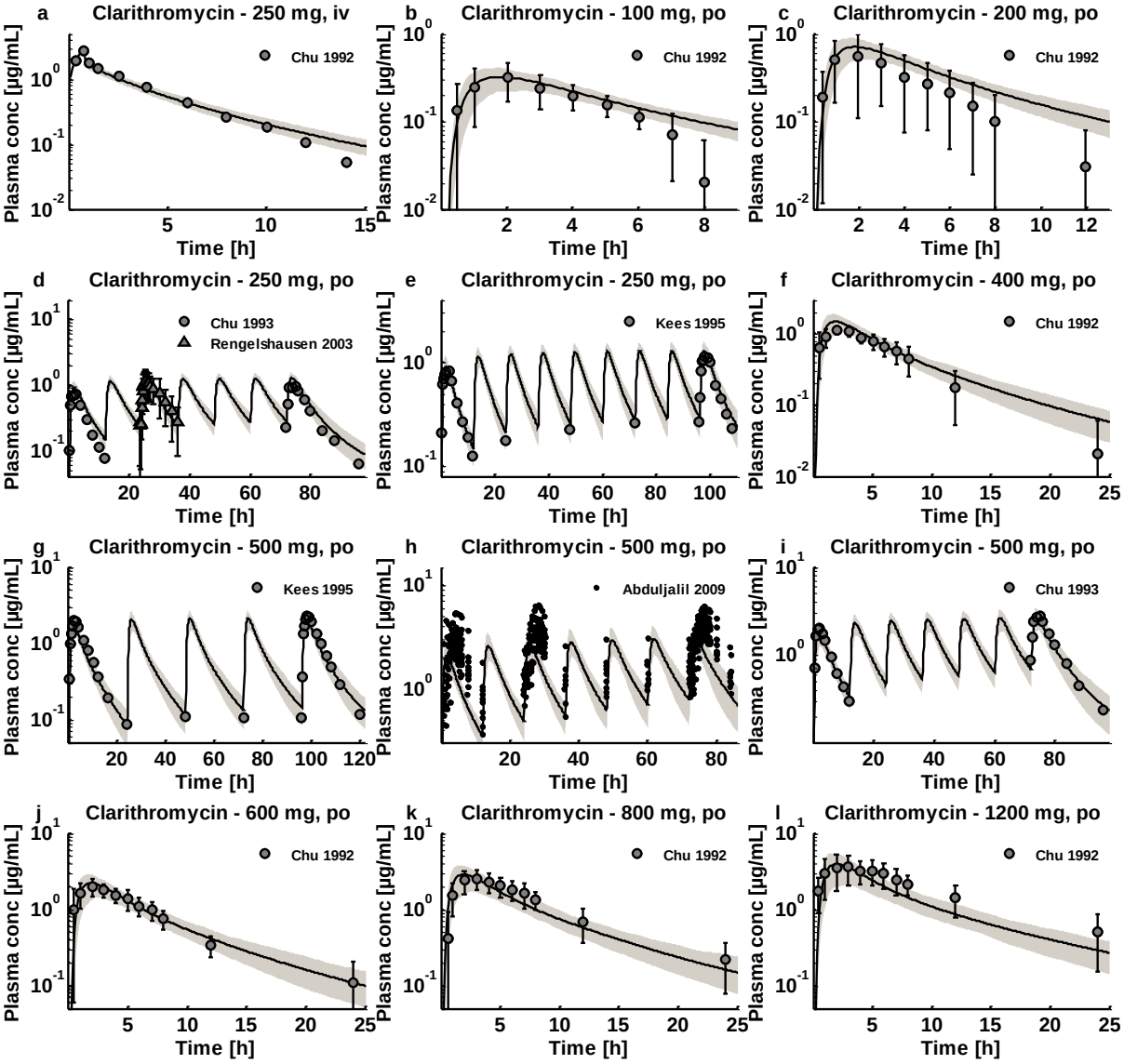

Figure S3c. Clarithromycin (iv, po) semilog. Population predictions of clarithromycin plasma concentration-time profiles, compared to observed data. Observed data are shown as dots or triangles ± SD. Population simulation arithmetic means are shown as lines; the shaded areas illustrate the 68% population prediction intervals. Details on dosing regimens, study populations, predicted and observed PK parameters are summarized in Table S3a.

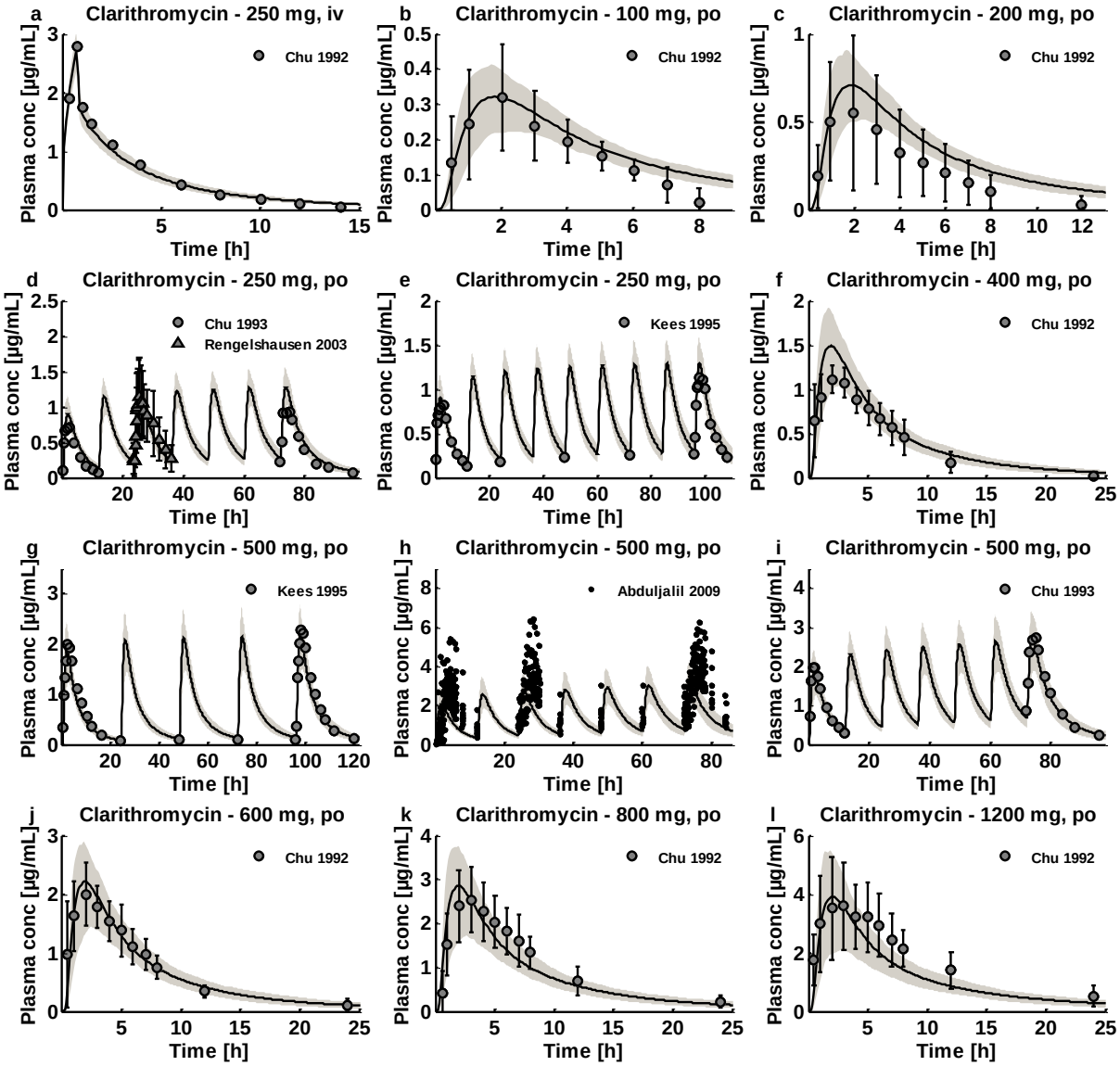

Figure S3d. Clarithromycin (iv, po) linear. Population predictions of clarithromycin plasma concentration-time profiles, compared to observed data. Observed data are shown as dots or triangles ± SD. Population simulation arithmetic means are shown as lines; the shaded areas illustrate the 68% population prediction intervals. Details on dosing regimens, study populations, predicted and observed PK parameters are summarized in Table S3a.

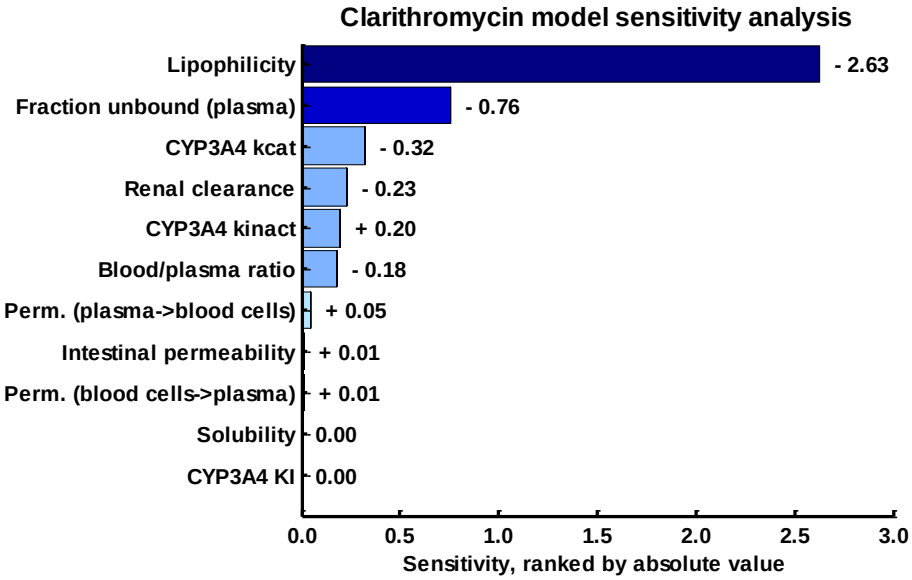

Figure S3e. Clarithromycin model sensitivity analysis. Sensitivity of the model to single parameters, measured as change of the simulated AUC under steady-state conditions of a 500 mg twice daily oral clarithromycin regimen. A sensitivity value of + 1.0 signifies that a 10% increase of the examined parameter causes a 10% increase of the simulated AUC. Perm.: permeability.

2.5 Midazolam model establishment

Midazolam is a widely-used sedative, approved as premedication before surgical interventions. It is almost exclusively metabolized by CYP3A4, turning it into a sensitive probe and victim drug for the investigation of in vivo CYP3A4 activity. For the same reason it shows substantial first pass metabolism, resulting in a bioavailability of under 50%. Less than 1% of a midazolam dose is excreted unchanged in urine.

The midazolam model was established using 7 clinical studies, covering a dosing range from 0.05 mg/kg to 20 mg (Table S4a). The final midazolam model applies metabolism by CYP3A4 and glomerular filtration (Table S4b).

The good descriptive and predictive performance is demonstrated in semilogarithmic (Figures S4c) as well as linear plots (Figures S4d) of population predicted compared to observed plasma concentration-time profiles of all clinical studies. In addition, predicted and observed AUC and C_{max} values of midazolam with calculated GMFEs are presented in Table S4a.

Sensitivity analysis of a simulation of 20 mg midazolam po SD with a threshold of 0.5 reveals that the midazolam model is sensitive to the values of CYP3A4 catalytic rate constant (optimized), fraction unbound (literature value) and lipophilicity (optimized) (Figure S4e).

Table S4a. Clinical studies used for midazolam model establishment

Dose [mg]	Route	n	Males [%]	Age [years]	Weight [kg]	Data set	Pred AUC	Obs AUC	Pred/Obs AUC	Pred C_{max}	Obs C_{max}	Pred/Obs C_{max}	Reference
Midazolam							[h*ng/mL]	[h*ng/mL]		[ng/mL]	[ng/mL]		
0.05 /kg	iv (0.5 h)	16	50	31.5 (20-40)	71.5 (45-100)	e	132.8	127.0	1.05	-	-	-	Gorski 1998 [76]
5.0	iv (bol)	6	83	21.5 (21-22)	72.5 (66-78)	e	165.1	190.3	0.87	179.3	112.6	1.59	Smith 1981 [77]
0.15 /kg	iv (bol)	6	-	22-27	55-77	i	362.0	550.0	0.66	-	-	-	Heizmann 1983 [78]
0.075 /kg	po (syr)	19	47	38.7	73.4	e	67.0	49.0	1.37	27.0	23.0	1.17	Chung 2006 [79]
10.0	po (sol)	6	83	21.5 (21-22)	72.5 (66-78)	i	133.1	135.6	0.98	52.7	60.0	0.88	Smith 1981 [77]
10.0	po (tab)	4	-	22-27	55-77	e	130.9	188.0	0.70	52.7	137.8	0.38	Heizmann 1983 [78]
20.0	po (tab)	6	-	22-27	55-77	e	293.6	437.0	0.67	115.2	263.8	0.44	Heizmann 1983 [78]
							GMFE (range)		**1.27 (1.02-1.52)**			**1.66 (1.14-2.61)**	
							Pred/Obs within 2-fold		**7/7**			**3/5**	

AUC values are 0-∞, bol: bolus, e: test dataset, i: training dataset, iv: intravenously, po: orally, sol: solution, syr: syrup, tab: tablet, -: not given

Table S4b. Drug-dependent parameters of the final midazolam PBPK model

Parameter	Unit	Midazolam model	Midazolam literature	Description
Midazolam				
MW	g/mol	325.77		Molecular weight
pKa		6.15 (base)	[80]	Acid dissociation constant
Solubility (pH)	mg/L	49.0 (6.5)	[81]	Solubility
logP		3.13	2.9, 3.9 [82,83]	Lipophilicity
fu	%	1.6	1.6, 2.4 [82,84]	Fraction unbound
CYP3A4 K_M	µmol/L	2.73	[85]	Michaelis-Menten constant
CYP3A4 k_{cat}	1/min	13.0	n.a.	CYP3A4 catalytic rate constant
GFR fraction		1		Fraction of filtered drug reaching the urine
Formulation		solution		Formulation used in predictions
Cell permeabilities		calculated	PK-Sim [31]	Permeation across cell membranes
Partition coefficients		calculated	R + R [32,33]	Organ-plasma partition coefficients
Specific intest. perm.	dm/min	2.00E-06	n.a.	Normalized to surface area
Specific organ perm.	dm/min	7.00E-03	calculated	Normalized to surface area

CYP3A4: cytochrome P450 3A4, GFR: glomerular filtration rate, intest.: intestinal, n.a.: not available, perm.: permeability, PK-Sim: PK-Sim Standard calculation method, R + R: Rodgers and Rowland calculation method

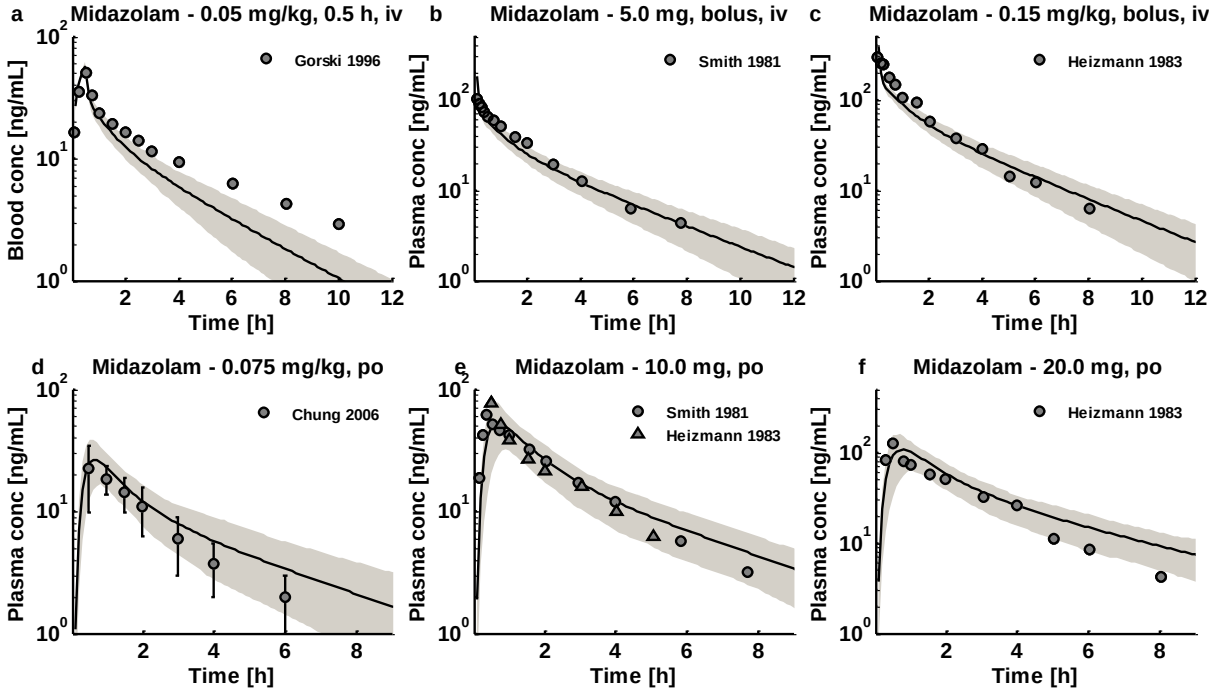

Figure S4c. Midazolam (iv, po) semilog. Population predictions of midazolam blood (a) or plasma (b - f) concentration-time profiles, compared to observed data. Observed data are shown as dots or triangles ± SD. Population simulation arithmetic means are shown as lines; the shaded areas illustrate the 68% population prediction intervals. Details on dosing regimens, study populations, predicted and observed PK parameters are summarized in Table S4a.

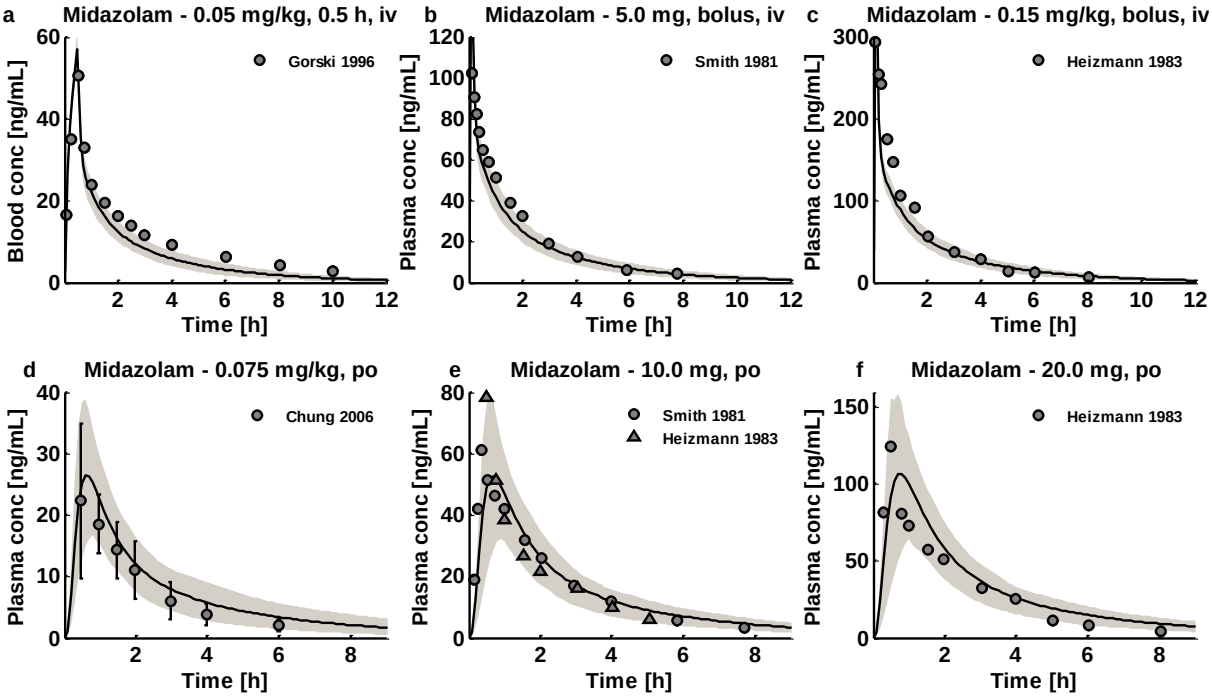

Figure S4d. Midazolam (iv, po) linear. Population predictions of midazolam blood (a) or plasma (b - f) concentration-time profiles, compared to observed data. Observed data are shown as dots or triangles ± SD. Population simulation arithmetic means are shown as lines; the shaded areas illustrate the 68% population prediction intervals. Details on dosing regimens, study populations, predicted and observed PK parameters are summarized in Table S4a.

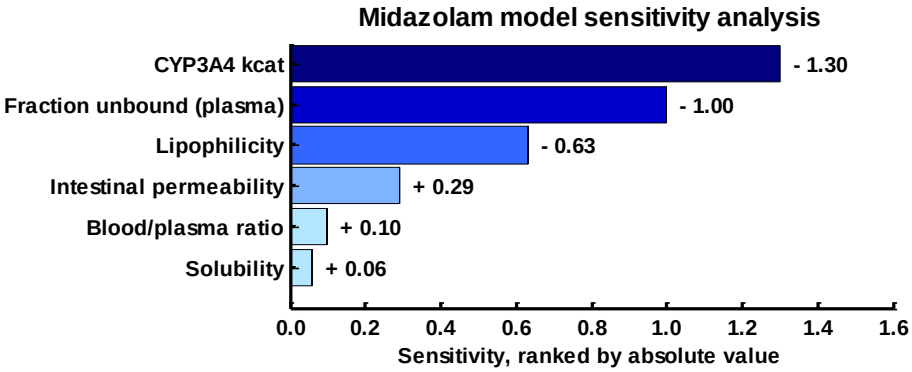

Figure S4e. Midazolam model sensitivity analysis. Sensitivity of the model to single parameters, measured as change of the simulated AUC extrapolated to infinity of a 15 mg single-dose oral midazolam administration. A sensitivity value of + 1.0 signifies that a 10% increase of the examined parameter causes a 10% increase of the simulated AUC.

2.6 Alfentanil model establishment

Alfentanil is a potent analgesic synthetic opioid. It is fast but short-acting and used for anesthesia during surgery. Alfentanil is metabolized solely by CYP3A4 [86]. Like midazolam, alfentanil is not a substrate for P-gp [87] and less than 1% of an alfentanil dose is excreted unchanged in urine [88].

The alfentanil model was established using 7 clinical studies, covering a dosing range from 0.015 to 0.075 mg/kg (Table S5a). The model applies metabolism by CYP3A4 and glomerular filtration (Table S5b). Although in clinical use alfentanil is always administered intravenously, some DDI studies published plasma concentration-time profiles of alfentanil following oral ingestion. Colonic absorption was disabled in the model, as late absorption after oral administration is not consistent with the reported concentration time-profiles.

The good descriptive and predictive performance is demonstrated in semilogarithmic (Figures S5c) as well as linear plots (Figures S5d) of population predicted compared to observed plasma concentration-time profiles of all clinical studies. In addition, predicted and observed AUC and C_{max} values of alfentanil with calculated GMFEs are presented in Table S5a.

Sensitivity analysis of a simulation of 0.015 mg/kg alfentanil iv SD with a threshold of 0.5 reveals that the alfentanil model is sensitive to the values of fraction unbound (literature value), CYP3A4 catalytic rate constant (optimized) and lipophilicity (optimized) (Figure S5e).

Table S5a. Clinical studies used for alfentanil model establishment

Dose [mg]	Route	n	Males [%]	Age [years]	Weight [kg]	Data set	Pred AUC	Obs AUC	Pred/Obs AUC	Pred C_{max}	Obs C_{max}	Pred/Obs C_{max}	Reference
Alfentanil							[h*ng/mL]	[h*ng/mL]		[ng/mL]	[ng/mL]		
0.015 /kg	iv (bol)	12	67	25.0 (18-38)	74.0 (55-108)	i	82.8	78.0	1.06	109.8	102.0	1.08	Kharasch 2011 [89]
0.015 /kg	iv (bol)	10	50	27.0 (20-39)	74.0 (53-96)	e	79.9	64.8	1.23	97.3	90.2	1.08	Kharasch 2004 [90]
0.015 /kg	iv (bol)	6	50	19-26	77.0 (70-85)	e	79.8	111.3	0.72	-	-	-	Phimmasone 2001 [86]
0.02 /kg	iv (bol)	9	100	29.0 (20-43)	74.0 (67-80)	e	106.5	62.9	1.69	-	-	-	Kharasch 1997 [91]
0.05 /kg	iv (bol)	10	-	45.0 (24-66)	59.0 (34-84)	e	276.0	268.8	1.03	-	-	-	Ferrier 1985 [92]
0.06 /kg	po (sol)	10	50	27.0 (20-39)	74.0 (53-96)	i	106.5	103.0	1.03	40.5	45.0	0.90	Kharasch 2004 [90]
0.075 /kg	po (sol)	12	67	25.0 (18-38)	74.0 (55-108)	i	133.1	146.0	0.91	50.7	51.0	0.99	Kharasch 2011 [89]
							GMFE (range)		**1.20 (1.03-1.69)**			**1.07 (1.01-1.11)**	
							Pred/Obs within 2-fold		**7/7**			**4/4**	

AUC values are 0-∞, bol: bolus, e: test dataset, i: training dataset, iv: intravenously, po: orally, sol: solution, -: not given

Table S5b. Drug-dependent parameters of the final alfentanil PBPK model

Parameter	Unit	Alfentanil model	Alfentanil literature	Description
Alfentanil				
MW	g/mol	416.52		Molecular weight
pKa		6.5 (base)	[93]	Acid dissociation constant
Solubility (pH)	mg/L	992.0 (6.5)	[3]	Solubility
logP		1.75	2.1, 2.2 [3,93]	Lipophilicity
fu	%	10.0	8.6, 10.0, 12.0 [3,94,95]	Fraction unbound
CYP3A4 K_M	µmol/L	1st order CL	-	Michaelis-Menten constant
CYP3A4 k_{cat}	1/min	0.32	n.a.	CYP3A4 catalytic rate constant
GFR fraction		0.06		Fraction of filtered drug reaching the urine
Formulation		solution		Formulation used in predictions
Cell permeabilities		calculated	PK-Sim [31]	Permeation across cell membranes
Partition coefficients		calculated	R + R [32,33]	Organ-plasma partition coefficients
Specific intest. perm.	dm/min	3.48E-07	n.a.	Normalized to surface area
Specific organ perm.	dm/min	3.10E-05	calculated	Normalized to surface area

CYP3A4: cytochrome P450 3A4, GFR: glomerular filtration rate, intest.: intestinal, n.a.: not available, perm.: permeability, PK-Sim: PK-Sim Standard calculation method, R + R: Rodgers and Rowland calculation method

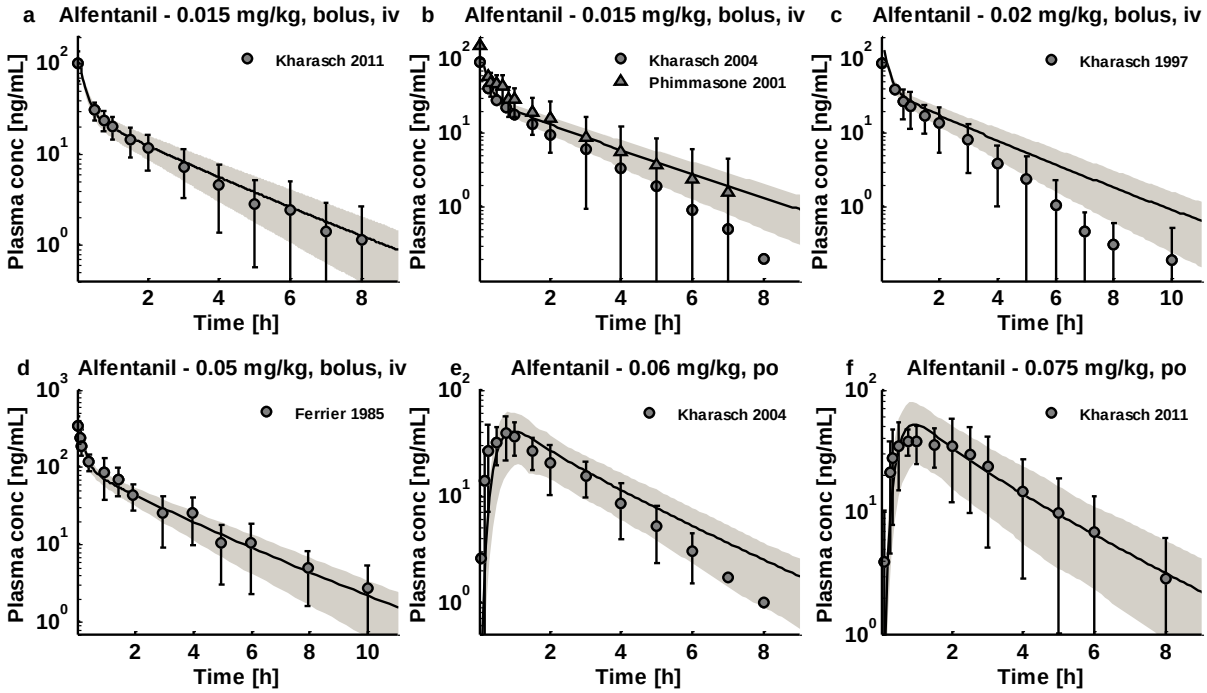

Figure S5c. Alfentanil (iv, po) semilog. Population predictions of alfentanil plasma concentration-time profiles, compared to observed data. Observed data are shown as dots or triangles ± SD. Population simulation arithmetic means are shown as lines; the shaded areas illustrate the 68% population prediction intervals. Details on dosing regimens, study populations, predicted and observed PK parameters are summarized in Table S5a.

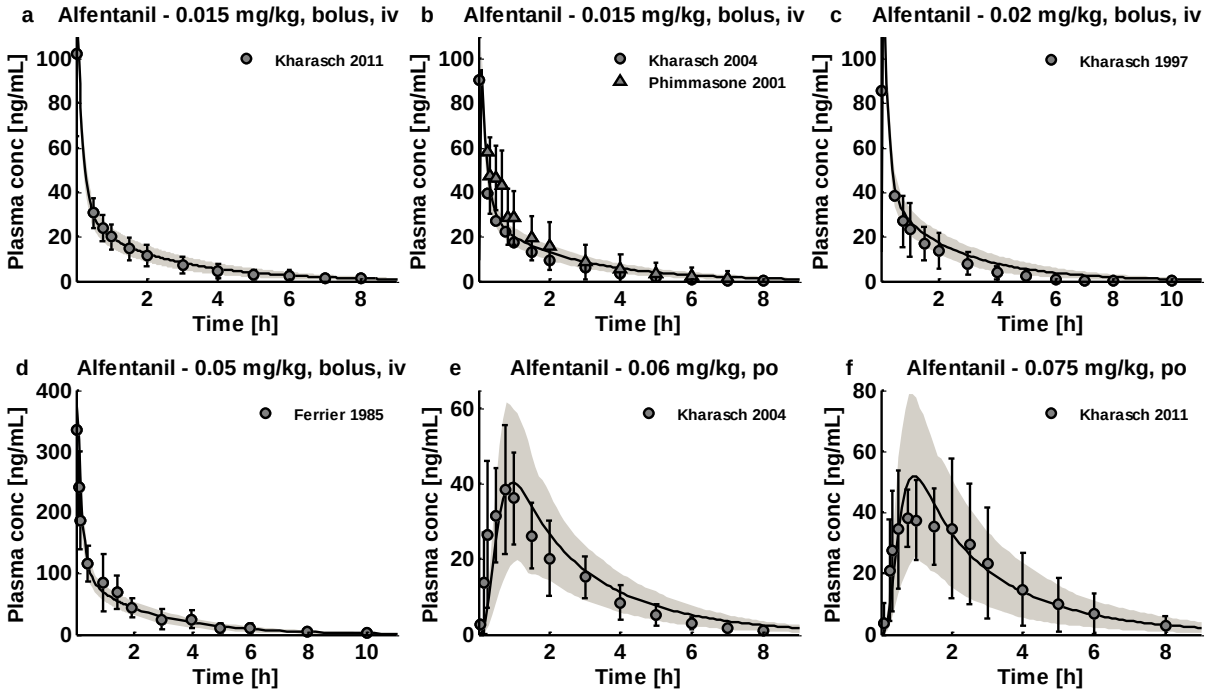

Figure S5d. Alfentanil (iv, po) linear. Population predictions of alfentanil plasma concentration-time profiles, compared to observed data. Observed data are shown as dots or triangles ± SD. Population simulation arithmetic means are shown as lines; the shaded areas illustrate the 68% population prediction intervals. Details on dosing regimens, study populations, predicted and observed PK parameters are summarized in Table S5a.

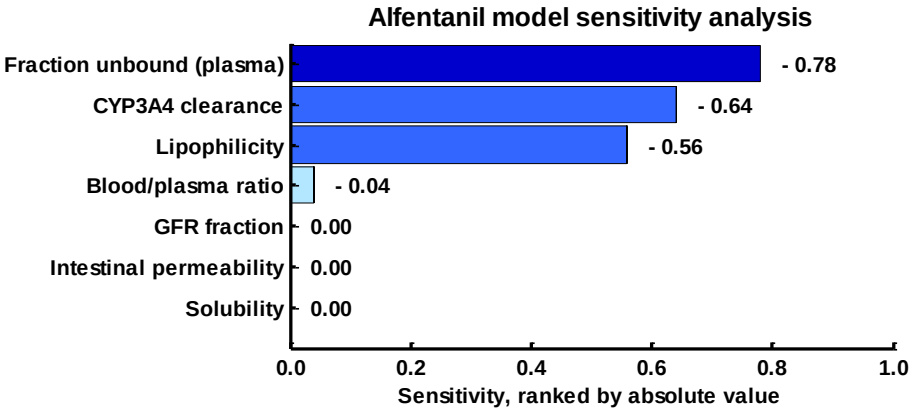

Figure S5e. Alfentanil model sensitivity analysis. Sensitivity of the model to single parameters, measured as change of the simulated AUC extrapolated to infinity of a 0.015 mg/kg single-dose intravenous alfentanil bolus administration. A sensitivity value of + 1.0 signifies that a 10% increase of the examined parameter causes a 10% increase of the simulated AUC.

2.7 Digoxin model establishment

Digoxin is a cardiac glycoside used to treat atrial fibrillation, atrial flutter and heart failure. Digoxin is transported by P-gp and mainly excreted unchanged via the kidneys with a small fraction eliminated via biliary excretion and only a very low degree of hepatic metabolism [5,96]. Many other substrates of P-gp are metabolized by CYP3A4, setting digoxin apart as an exception and thereby turning it into a model victim drug of P-gp-mediated DDIs. The narrow therapeutic window of digoxin demands close monitoring of digoxin plasma concentrations, as small increases in exposure can already cause adverse events. This results in safety concerns when co-treatment with a P-gp inhibitor is initiated or co-treatment with a P-gp inducer is stopped.

The digoxin model was established using 38 clinical studies, covering a dosing range from 0.125 to 1.5 mg (Table S6a). Digoxin is reported to have a large volume of distribution due to extensive tissue binding and to be mainly excreted unchanged to urine (50 - 70%) while the remainder of a dose is eliminated by hepatic metabolism and biliary excretion [96,97]. The final digoxin model applies target-binding, transport by P-gp in various organs including gut, liver and kidney, an unspecific hepatic metabolic clearance and glomerular filtration (Table S6b). Implementation of target-binding to the ATPase Na+/K+ transporting subunit alpha 2 (ATP1A2) was crucial, to mechanistically describe the large volume of distribution and the long plasma half-life of digoxin. To accurately predict the digoxin plasma concentrations following intravenous and oral administration, the relative expression of P-gp in the intestinal mucosa was increased (3.57-fold) compared to the PK-Sim database RT-PCR expression profile (see Table S7). This factor has been identified in an optimization that included digoxin plasma concentrations and fraction excreted to urine data following intravenous and oral administration plus digoxin excreted to duodenum measurements after intravenous administration [98]. The optimized P-gp expression profile shows highest expression in small intestinal mucosa (1.41 µmol/L), followed by kidney (1.00 µmol/L), large intestinal mucosa (0.56 µmol/L), liver (0.27 µmol/L) and tissues of lower expression. Implementation of transport by OATP (4C1) did not improve the model performance and was not used in the final model.

The good descriptive and predictive performance is demonstrated in semilogarithmic (Figures S6c) as well as linear plots (Figures S6d) of population predicted compared to observed plasma concentration-time profiles of all clinical studies. In addition, predicted and observed AUC and C_{max} values of digoxin with calculated GMFEs are presented in Table S6a.

Sensitivity analysis of a simulation of 0.5 mg digoxin po QD with a threshold of 0.5 reveals that the digoxin model is sensitive to the values of fraction unbound (literature value), intestinal permeability (optimized), P-gp catalytic rate constant (optimized) and lipophilicity (optimized) (Figure S6e).

Table S6a. Clinical studies used for digoxin model establishment

Dose [mg]	Route	n	Males [%]	Age [years]	Weight [kg]	Data set	Pred AUC	Obs AUC	Pred/Obs AUC	Pred C_{max}	Obs C_{max}	Pred/Obs C_{max}	Reference
Digoxin							[h*ng/mL]	[h*ng/mL]		[ng/mL]	[ng/mL]		
0.5	iv (bol)	6	100	-	66-96	i	30.0 [g]	65.7 [g]	0.46	-	-	-	Wagner 1981 [99]
0.5	iv (5 min)	12	100	28.0	74.0	e	33.3	22.0	1.51	-	-	-	Ding 2004 [100]
0.5	iv (1 h)	9	100	31.3 (23-37)	77.7 (69-90)	e	33.4	45.1	0.74	-	-	-	Ochs 1978 [96]
0.5	iv (1 h)	9	100	27.9	66.6	e	24.4	60.0	0.41	8.7	9.1	0.96	Tsutsumi 2002 [101]
0.5	iv (1 h)	6	100	-	66-96	e	31.1 [f]	53.7 [f]	0.58	-	-	-	Wagner 1981 [99]
0.5	iv (3 h)	6	100	-	66-96	e	31.2 [d]	47.5 [d]	0.66	-	-	-	Wagner 1981 [99]
0.01 /kg	iv (bol)	3	100	28.0 (21-39)	80.0 (68-98)	e	31.4 [a]	27.0 [a]	1.16	-	-	-	Rengelshausen 2003 [62]
0.01 /kg	iv (5 min)	10	50	29.2 (23-40)	69.5 (48-95)	e	48.5	57.4	0.84	-	-	-	Lalonde 1985 [102]
0.01 /kg°	iv (5 min)	10	50	29.2 (23-40)	69.5 (48-95)	e	33.9	38.9	0.87	-	-	-	Lalonde 1985 [102]
0.75	iv (1 h)	1	100	-	-	e	49.9	53.8	0.93	-	-	-	Koup 1975 [103]
1.0	iv (bol)	12	100	-	72.4	e	64.7	63.9	1.01	-	-	-	Kramer 1979 [104]
1.0	iv (0.5 h)	8	100	29.0	84.0	i	65.3 [c]	87.3 [c]	0.75	27.1	24.7	1.10	Greiner 1999 [5]
1.0	iv (1 h)	9	100	31.3 (23-37)	77.7 (69-90)	e	66.8	80.9	0.83	-	-	-	Ochs 1978 [96]
0.015 /kg	iv (bol)	6	50	24.0 (22-29)	-	e	-	-	-	-	-	-	Steiness 1982 [105]
1.5	iv (1 h)	9	100	31.3 (23-37)	77.7 (69-90)	e	100.0	128.7	0.78	-	-	-	Ochs 1978 [96]
0.125, QD	po (-)	12	100	37.8 (24-49)	87.8 (70-95)	e	6.5 [a]	7.0 [a]	0.93	0.8	0.6	1.33	Qiu 2010 [106]
0.25	po (-)	16	69	39.0 (20-43)	72.5	e	17.8	17.0	1.05	1.3	1.5	0.87	Eckermann 2012 [107]
0.25	po (-)	18	50	30.0	77.5	i	6.6 [a]	8.1 [a]	0.81	1.3	1.3	1.00	Gurley 2008b [108]
0.25, QD	po (tab)	19	100	23.9 (18-39)	68.0 (60-77)	e	12.9 [a]	7.7 [a]	1.68	1.6	1.0	1.60	FDA 2009 [109]
0.25, QD	po (tab)	20	45	23-49	74.8	e	12.9 [a]	15.4 [a]	0.84	1.6	1.8	0.89	Friedrich 2011 [110]
0.25, QD	po (tab)	20	73	30.2 (19-38)	80.4	e	12.9 [a]	14.9 [a]	0.87	1.6	1.4	1.14	Vaidyanathan 2008 [111]
0.25, QD	po (-), LD	12	50	26.0 (22-33)	69.0 (50-100)	e	13.0 [a]	17.2 [a]	0.76	1.6	1.9	0.84	Johne 1999 [112]
0.25, BID	po (tab)	10	100	30.3 (23-40)	77.6 (62-94)	e	12.9 [b]	15.7 [b]	0.82	2.1	2.5	0.84	Rodin 1988 [113]
0.25, BID	po (-), LD	7	100	24.9	75.1 (65-88)	e	12.8 [b]	10.2 [b]	1.25	2.1	2.1	1.00	Kirch 1986 [114]

continued...

continued...

Dose [mg]	Route	n	Males [%]	Age [years]	Weight [kg]	Data set	Pred AUC	Obs AUC	Pred/Obs AUC	Pred C_{max}	Obs C_{max}	Pred/Obs C_{max}	Reference
Digoxin							[h*ng/mL]	[h*ng/mL]		[ng/mL]	[ng/mL]		
0.5	po (sol)	1	-	24-34	53-115	e	13.1 [a]	12.8 [a]	1.02	2.6	1.6	1.63	Larsen 2007 [115]
0.5	po (sol)	6	100	-	66-96	e	23.4 [g]	29.0 [g]	0.81	2.6	2.4	1.08	Wagner 1981 [99]
0.5	po (-)	12	58	26.0 (19-35)	-	i	18.7 [k]	20.2 [k]	0.93	2.6	2.2	1.18	Becquemont 2001 [116]
0.5	po (tab)	10	10	22.0 (19-25)	60.2 (53-80)	e	19.0 [h]	22.7 [h]	0.84	2.6	2.7	0.96	Jalava 1997 [117]
0.5	po (tab)	18	56	22.0 (19-36)	-	e	39.7	28.3	1.40	2.6	2.5	1.04	Ragueneau 1999 [118]
0.5	po (-)	-	-	-	-	e	-	-	-	-	-	-	Reitman 2011 [29]
0.5	po (tab)	12	100	26.0 (21-31)	77.0 (64-100)	e	7.9 [m]	5.3 [m]	1.50	2.6	2.0	1.30	Tayrouz 2003 [119]
0.5	po (tab)	12	92	26.0 (22-35)	-	e	18.7 [k]	27.2 [k]	0.69	2.6	3.0	0.87	Verstuyft 2003 [120]
0.5	po (tab)	10	50	23-30	60-90	e	19.0 [h]	23.0 [h]	0.83	2.6	1.9	1.37	Westphal 2000 [121]
0.6	po (cap)	12	100	31.0 (24-39)	78.8 (60-102)	e	30.8	32.6	0.94	3.1	2.5	1.24	Martin 1997 [122]
0.75	po (tab)	12	100	28.0 (21-39)	80.0 (68-98)	e	19.6 [a]	14.0 [a]	1.40	3.9	3.6	1.08	Rengelshausen 2003 [62]
1.0	po (-)	8	100	29.0	84.0	e	26.5 [c]	54.8 [c]	0.48	5.1	5.4	0.94	Greiner 1999 [5]
1.0	po (tab)	5	100	26.0 (23-32)	72.0 (60-83)	e	14.8 [n]	14.9 [n]	0.99	5.1	5.4	0.94	Hayward 1978 [123]
1.0	po (ir)	10	100	24.0 (19-27)	73.0 (61-92)	i	26.5 [g]	49.7 [g]	0.53	5.1	4.0	1.28	Oosterhuis 1991 [124]
							GMFE (range)		**1.32 (1.01-2.46)**			**1.17 (1.00-1.63)**	
							Pred/Obs within 2-fold		**33/36**			**24/24**	

°: iv digoxin study with po charcoal administration, [a]: AUC_{0-24}, [b]: AUC_{0-12}, [c]: AUC_{0-144}, [d]: AUC_{0-99}, [f]: AUC_{0-97}, [g]: AUC_{0-96}, [h]: AUC_{0-72}, [k]: AUC_{0-48}, [m]: AUC_{0-9}, [n]: AUC_{0-8}, AUC values are 0-∞ if not specified differently, BID: twice daily, bol: bolus, cap: capsule, e: test dataset, i: training dataset, ir: immediate release tablet, iv: intravenously, LD: study with loading dose, po: orally, QD: once daily, sol: solution, tab: tablet, -: not given

Table S6b. Drug-dependent parameters of the final digoxin PBPK model

Parameter	Unit	Digoxin model	Digoxin literature	Description
Digoxin				
MW	g/mol	780.93		Molecular weight
pKa		-		Acid dissociation constant
Solubility (pH)	mg/L	64.8 (water)	17.0 (FaSSIF), 30.0 (6.5), 64.8 (water) [125,126]	Solubility
logP		1.40	1.22, 1.62, 1.67 [125,127,128]	Lipophilicity
fu	%	71.0	70.0, 71.0, 77.7 [127,129,130]	Fraction unbound
ATP1A2 K_D	µmol/L	0.0256	[131]	Dissociation constant
ATP1A2 k_{off}	1/min	9.89E-04	n.a.	Dissociation rate constant
P-gp K_M	µmol/L	177.0	73.0, 177.0 [28,132]	Michaelis-Menten constant
P-gp k_{cat}	1/min	71.2	n.a.	P-gp catalytic rate constant
CL_{Hep}	mL/min	41.1	n.a.	Hepatic plasma clearance
GFR fraction		1		Fraction of filtered drug reaching the urine
Formulation		solution		Formulation used in predictions
Cell permeabilities		calculated	PK-Sim [31]	Permeation across cell membranes
Partition coefficients		calculated	R + R [32,33]	Organ-plasma partition coefficients
Specific intest. perm.	dm/min	2.76E-07	n.a.	Normalized to surface area
Specific organ perm.	dm/min	1.01E-05	n.a.	Normalized to surface area

ATP1A2: ATPase Na+/K+ transporting subunit alpha 2, CL: clearance, GFR: glomerular filtration rate, intest.: intestinal, n.a.: not available, perm.: permeability, P-gp: P-glycoprotein, PK-Sim: PK-Sim Standard calculation method, R + R: Rodgers and Rowland calculation method

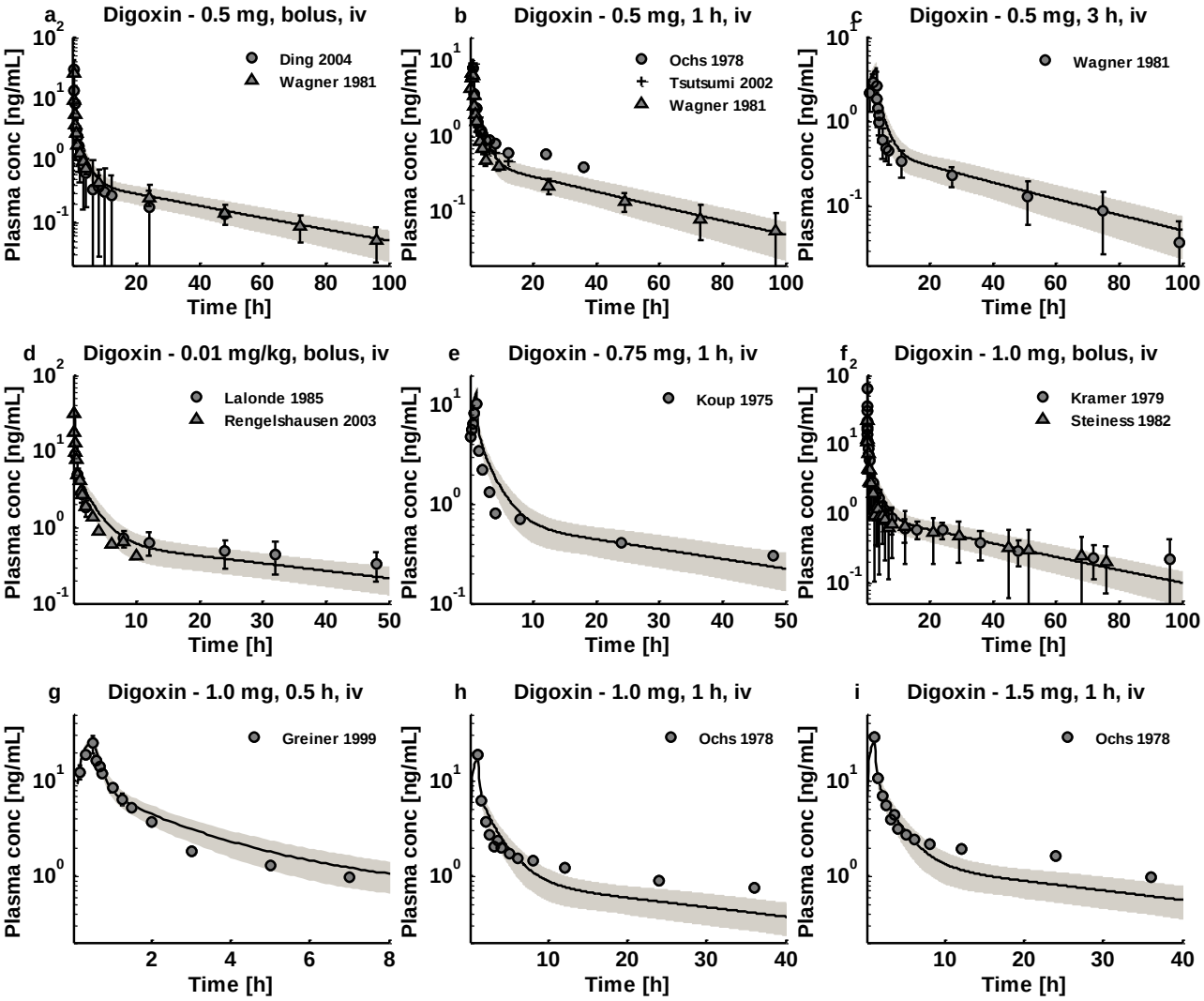
a
Digoxin - 0.5 mg, bolus, iv
Ding 2004
Wagner 1981
b
Digoxin - 0.5 mg, 1 h, iv
Ochs 1978
Tsutsumi 2002
Wagner 1981
c
Digoxin - 0.5 mg, 3 h, iv
Wagner 1981
d
Digoxin - 0.01 mg/kg, bolus, iv
Lalonde 1985
Rengelshausen 2003
e
Digoxin - 0.75 mg, 1 h, iv
Koup 1975
f
Digoxin - 1.0 mg, bolus, iv
Kramer 1979
Steiness 1982
g
Digoxin - 1.0 mg, 0.5 h, iv
Greiner 1999
h
Digoxin - 1.0 mg, 1 h, iv
Ochs 1978
i
Digoxin - 1.5 mg, 1 h, iv
Ochs 1978
Plasma conc [ng/mL]
Time [h]

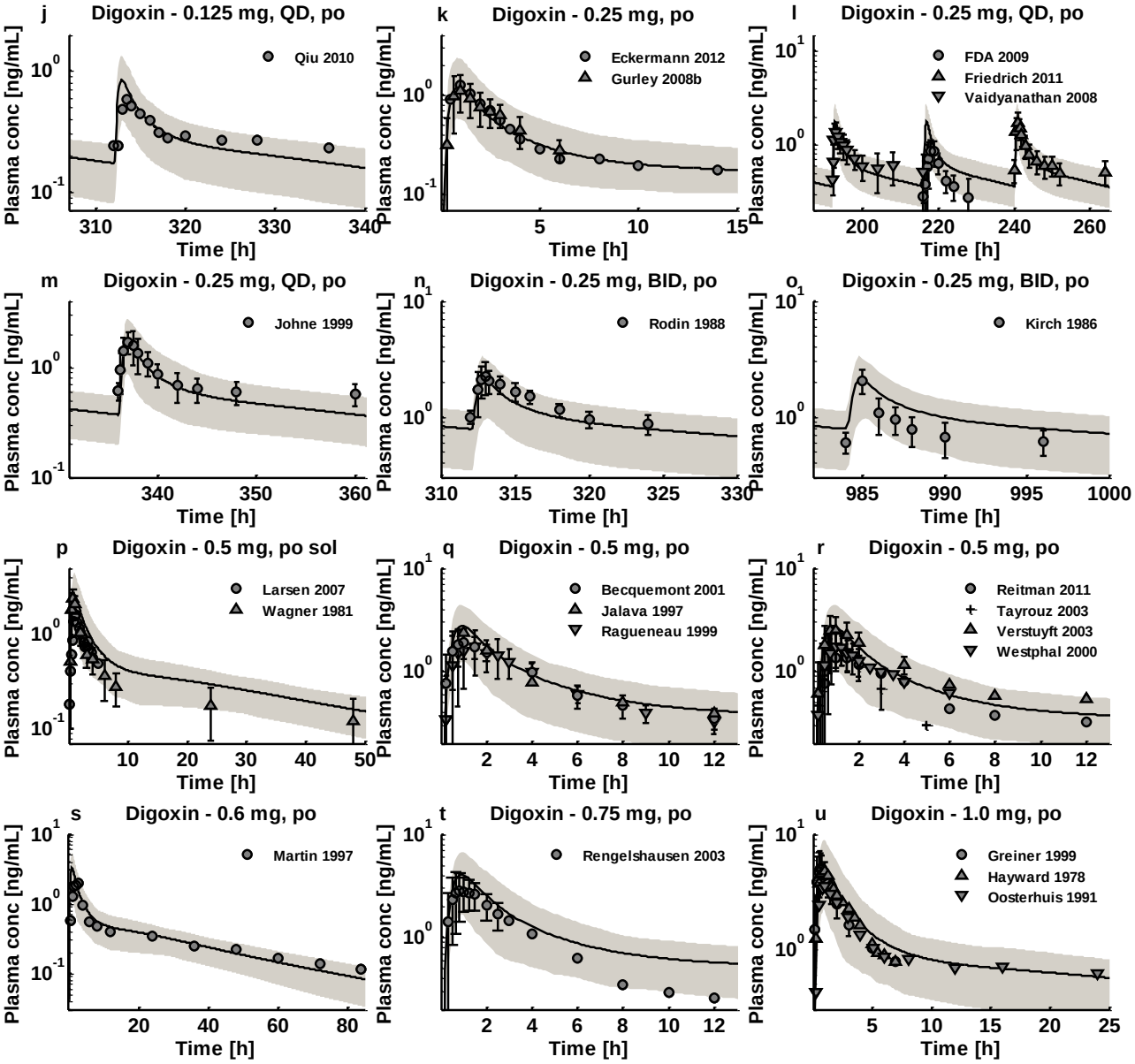

Figure S6c. Digoxin (iv, po) semilog. Population predictions of digoxin plasma concentration-time profiles, compared to observed data. Observed data are shown as dots, triangles or crosses ± SD. Population simulation arithmetic means are shown as lines; the shaded areas illustrate the 68% population prediction intervals. Details on dosing regimens, study populations, predicted and observed PK parameters are summarized in Table S6a.

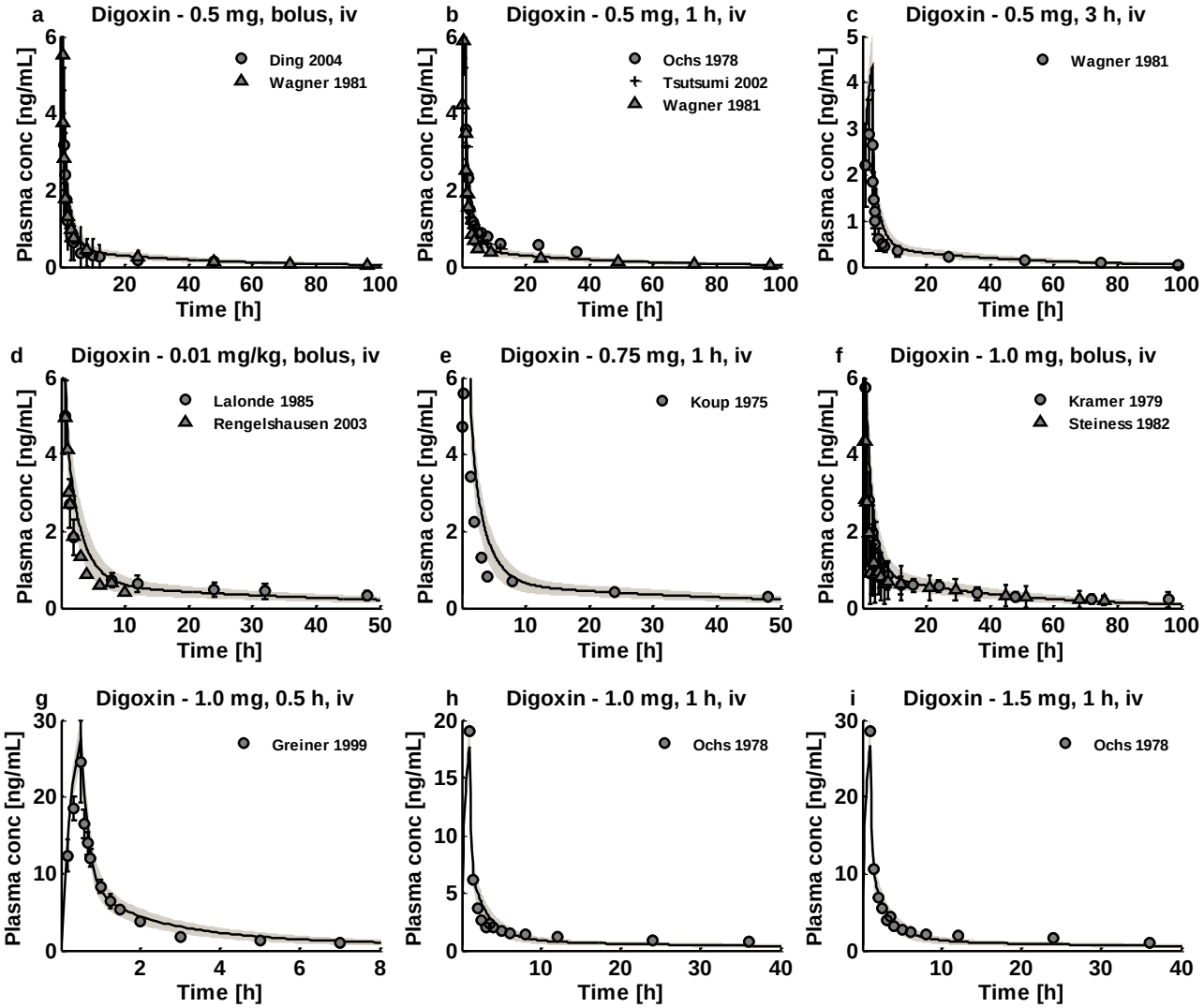
a
Digoxin - 0.5 mg, bolus, iv
Ding 2004
Wagner 1981
b
Digoxin - 0.5 mg, 1 h, iv
Ochs 1978
Tsutsumi 2002
Wagner 1981
c
Digoxin - 0.5 mg, 3 h, iv
Wagner 1981
d
Digoxin - 0.01 mg/kg, bolus, iv
Lalonde 1985
Rengelshausen 2003
e
Digoxin - 0.75 mg, 1 h, iv
Koup 1975
f
Digoxin - 1.0 mg, bolus, iv
Kramer 1979
Steiness 1982
g
Digoxin - 1.0 mg, 0.5 h, iv
Greiner 1999
h
Digoxin - 1.0 mg, 1 h, iv
Ochs 1978
i
Digoxin - 1.5 mg, 1 h, iv
Ochs 1978
Plasma conc [ng/mL]
Time [h]

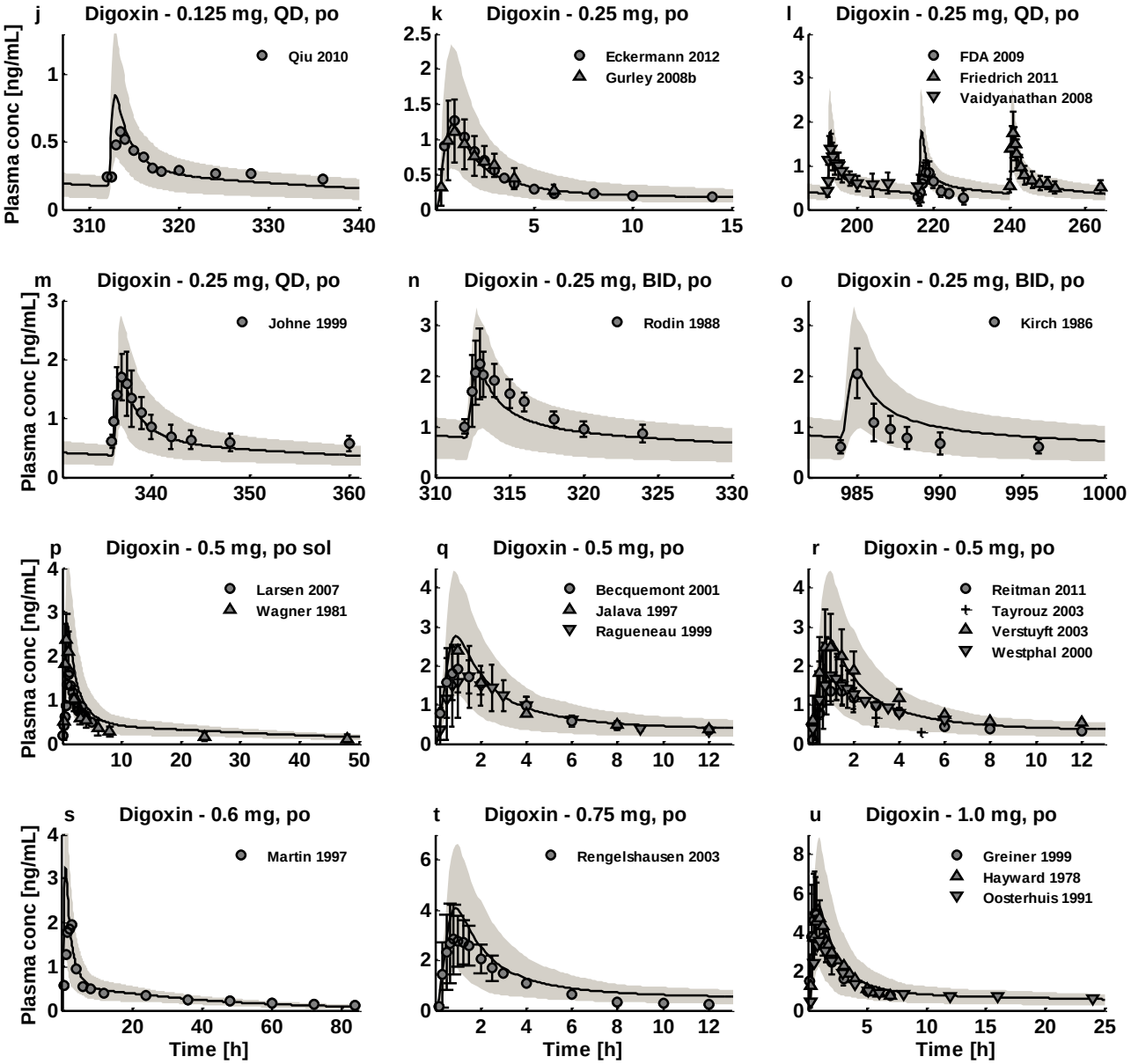

Figure S6d. Digoxin (iv, po) linear. Population predictions of digoxin plasma concentration-time profiles, compared to observed data. Observed data are shown as dots, triangles or crosses ± SD. Population simulation arithmetic means are shown as lines; the shaded areas illustrate the 68% population prediction intervals. Details on dosing regimens, study populations, predicted and observed PK parameters are summarized in Table S6a.

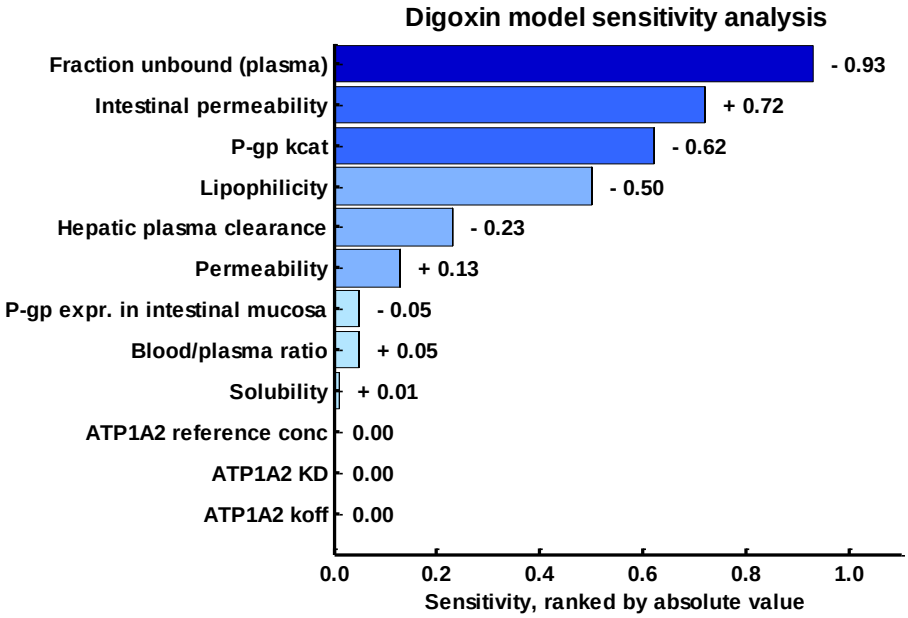

Figure S6e. Digoxin model sensitivity analysis. Sensitivity of the model to single parameters, measured as change of the simulated AUC under steady-state conditions of a 0.5 mg once daily oral digoxin regimen. A sensitivity value of + 1.0 signifies that a 10% increase of the examined parameter causes a 10% increase of the simulated AUC. Expr.: expression.

2.8 System-dependent parameters

System-dependent parameters, such as reference concentrations and tissue expression profiles of metabolizing enzymes, transporters and binding partners, are listed in Table S7.

Table S7. System-dependent parameters, expression of ADME relevant proteins

Protein	Mean reference concentration [µmol protein/L in the tissue of highest expression]	Geometric standard deviation of reference concentration	Relative expression in the different organs (PK-Sim expression database profile)	Half-life liver [h]	Half-life intestine [h]
AADAC	1.0 [133]	1.40 [a]	RT-PCR [134]	36	23
ATP1A2	0.48 optimized	1.40 [a]	Affymetrix Chip U133A E-GEOD-2361	36	23
CYP3A4	4.32 [135]	1.18 liver, 1.46 intestine [136]	RT-PCR [56]	36 [137]	23 [138]
OATP1B1	1.0 [133]	1.54 [139]	RT-PCR [140]	36	23
P-gp (efflux)	1.41 optimized	1.60 [139]	RT-PCR [140], with the relative expression in intestinal mucosa increased by factor 3.57 (optimized)	36	23
EHC continuous fraction: Fraction of biliary secreted compound directly entering the duodenum = 1					

[a]: CV of 35% assumed, AADAC: arylacetamide deacetylase, ATP1A2: ATPase Na^+/K^+ transporting subunit alpha 2, CYP3A4: cytochrome P450 3A4, EHC: enterohepatic circulation, OATP1B1: organic anion transporting polypeptide 1B1, P-gp: P-glycoprotein. If no information on reference concentration was available, it was set to 1.0 µmol/L and the catalytic rate constant (k_{cat}) was optimized according to [133]

3 DDI prediction

3.1 DDI modeling – general

All DDI simulations are pure predictions, in the sense that no drug interaction studies were used during the parameter optimization phase of the perpetrator and victim drug model development. Some values needed for auto-induction or auto-inactivation (auto-induction of AADAC and OATP1B1 by rifampicin and mechanism-based auto-inactivation of CYP3A4 by clarithromycin) were optimized during the perpetrator model development using the available multiple-dose studies to inform these "self-interaction" parameters (optimized without the use of DDI studies), as no experimental values for these parameters could be found. All further interaction parameters necessary to model the DDIs were taken directly from literature. The aim of this approach was to evaluate the models not only by their performance during the prediction of test datasets, but also by prediction of DDI studies.

Plots of population predicted compared to observed plasma concentration-time profiles (or predicted compared to observed DDI AUC ratios for the rifampicin-itraconazole DDI) during the **rifampicin-midazolam**, **rifampicin-alfentanil**, **rifampicin-itraconazole**, **itraconazole-midazolam**, **clarithromycin-midazolam**, **rifampicin-digoxin**, **itraconazole-digoxin** and **clarithromycin-digoxin** DDIs of all clinical DDI studies obtained from literature are shown in this supplementary document. Details on the clinical studies are summarized in Table 1 of the main document, together with predicted and observed DDI AUC ratios, C_{max} ratios and calculated GMFEs.

3.2 Rifampicin-midazolam DDI

To predict the rifampicin-midazolam DDI, induction of CYP3A4 by rifampicin was modeled using the reported mean $EC_{50,total}$ = 0.80 µmol/L and E_{max} = 9 estimates, based on induction of CYP3A4 activity in primary human hepatocytes [24]. Similar values for $EC_{50,total}$ (0.77, 0.80 µmol/L) and E_{max} (7, 9, 10) have been reported by other groups [141–143]. The in vitro $EC_{50,total}$ = 0.80 µmol/L was corrected for rifampicin binding in hepatocytes, to obtain the EC_{50} of unbound rifampicin: EC_{50} = 0.80 µmol/L * 0.42 = 0.34 µmol/L [3,25]. Furthermore, simultaneous competitive inhibition of CYP3A4 by rifampicin was integrated with CYP3A4 K_i = 18.5 µmol/L, determined in human liver microsomes [30]. No correction of this value to account for rifampicin binding in the assay was attempted, as only 0.1 mg/mL human liver microsomal protein were used, suggesting an unbound fraction of approx. 100% [144].

Plots of population predicted compared to observed midazolam plasma concentration-time profiles of all rifampicin-midazolam DDI studies obtained from literature are shown in Figures S8a (semilogarithmic plot) and S8b (linear plot).

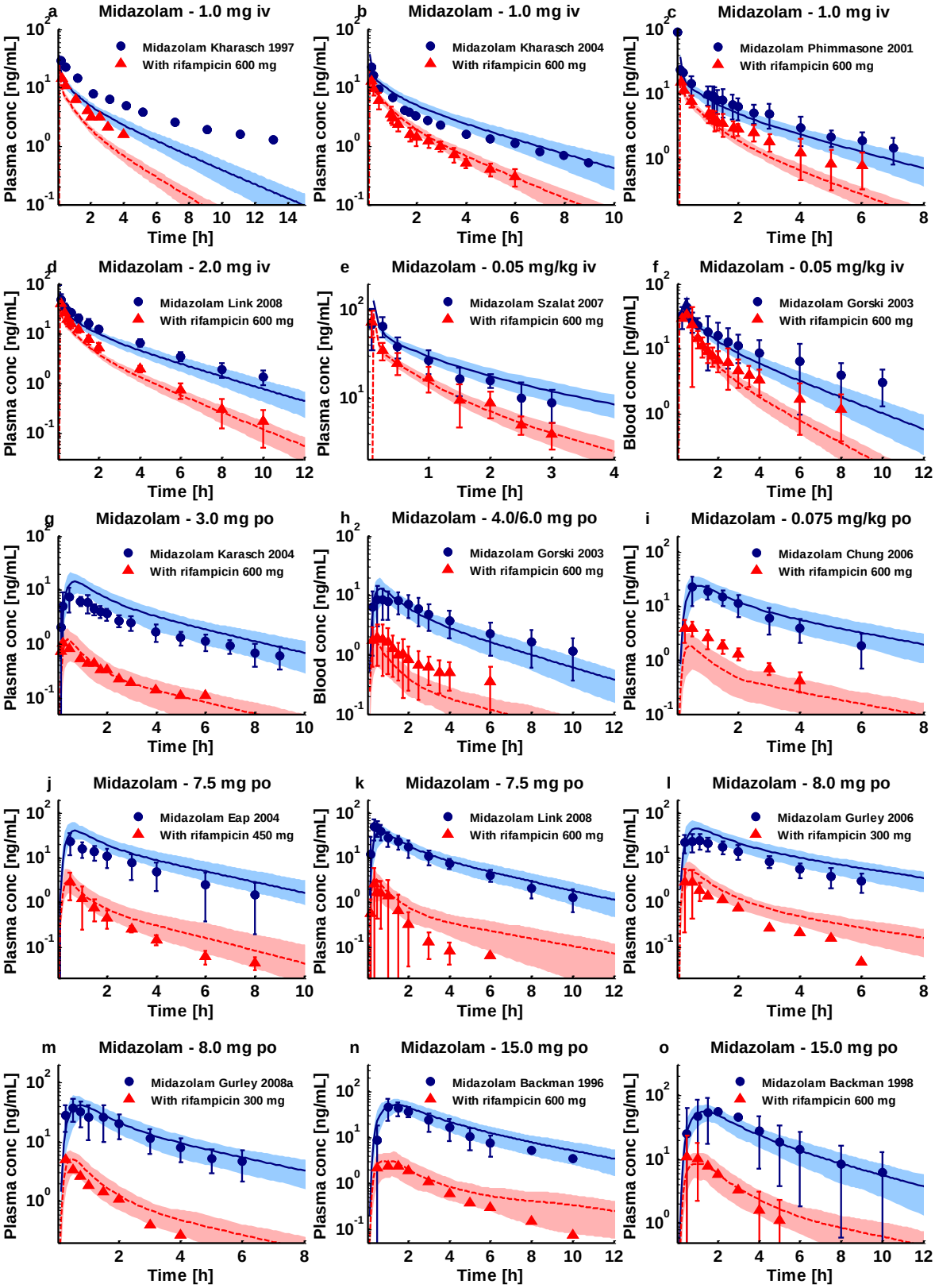

Figure S8a. Rifampicin-midazolam DDI (iv, po) semilog. Population predictions of midazolam plasma or blood (f, h) concentration-time profiles, before and during rifampicin treatment, compared to observed data. Observed data are shown as blue dots (control) or red triangles (DDI) ± SD. Population simulation arithmetic means are shown as solid blue lines (control) or dashed red lines (DDI); the shaded areas illustrate the respective 68% population prediction intervals. (e) shows CTX patient data. Details on dosing regimens, study populations, predicted and observed DDI AUC ratios and C_{max} ratios are summarized in Table 1 of the main document.

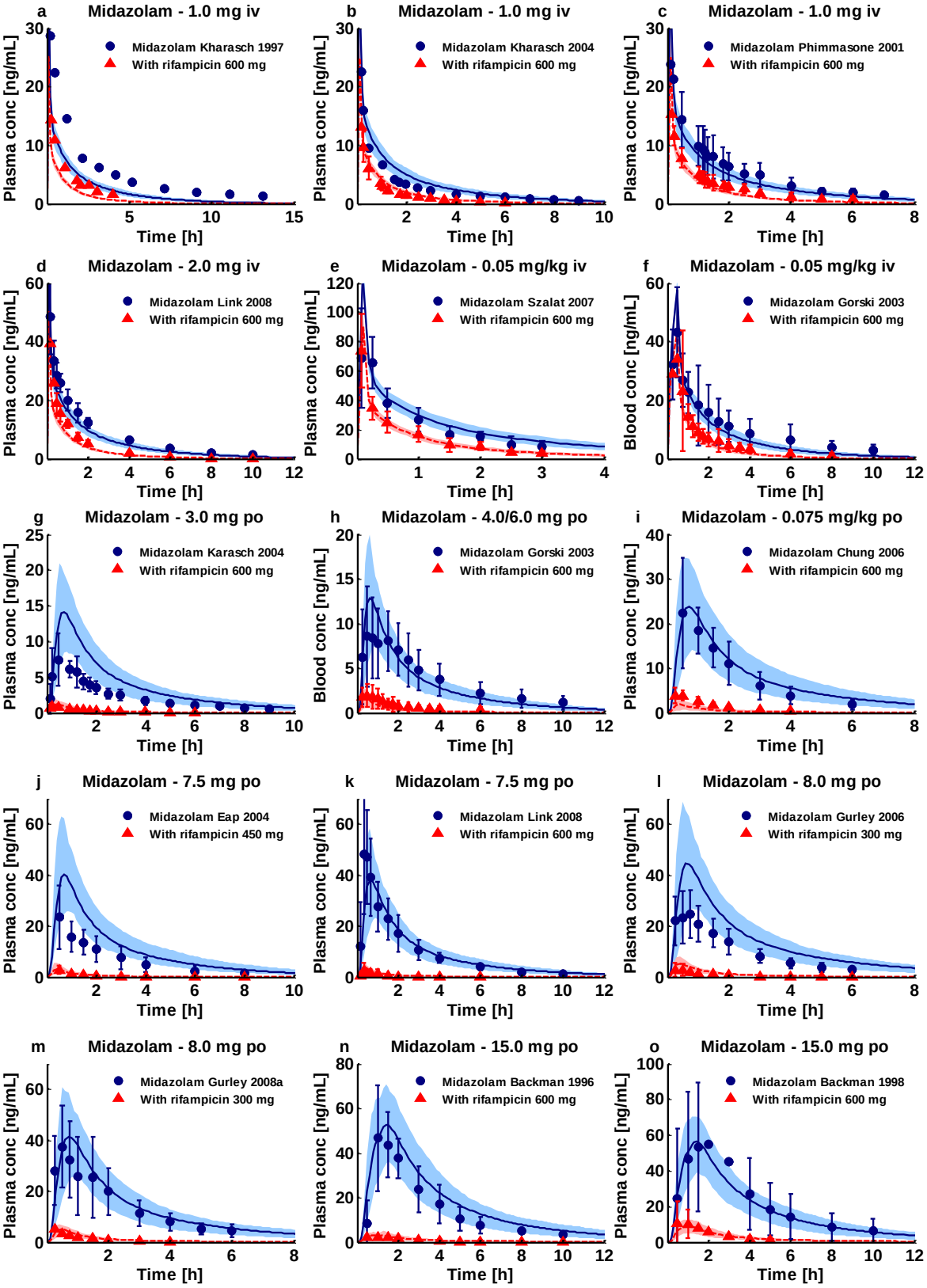

Figure S8b. Rifampicin-midazolam DDI (iv, po) linear. Population predictions of midazolam plasma or blood (f, h) concentration-time profiles, before and during rifampicin treatment, compared to observed data. Observed data are shown as blue dots (control) or red triangles (DDI) ± SD. Population simulation arithmetic means are shown as solid blue lines (control) or dashed red lines (DDI); the shaded areas illustrate the respective 68% population prediction intervals. (e) shows CTX patient data. Details on dosing regimens, study populations, predicted and observed DDI AUC ratios and C_{max} ratios are summarized in Table 1 of the main document.

3.3 Rifampicin-alfentanil DDI

To predict the rifampicin-alfentanil DDI, induction of CYP3A4 by rifampicin with simultaneous competitive inhibition was modeled using the same parameters as for the rifampicin-midazolam DDI (induction of CYP3A4 with EC_{50} = 0.34 µmol/L and E_{max} = 9 [3,24,25], simultaneous competitive inhibition of CYP3A4 with CYP3A4 K_i = 18.5 µmol/L [30]).

Plots of population predicted compared to observed alfentanil plasma concentration-time profiles of all rifampicin-alfentanil DDI studies obtained from literature are shown in Figures S9a (semilogarithmic plot) and S9b (linear plot).

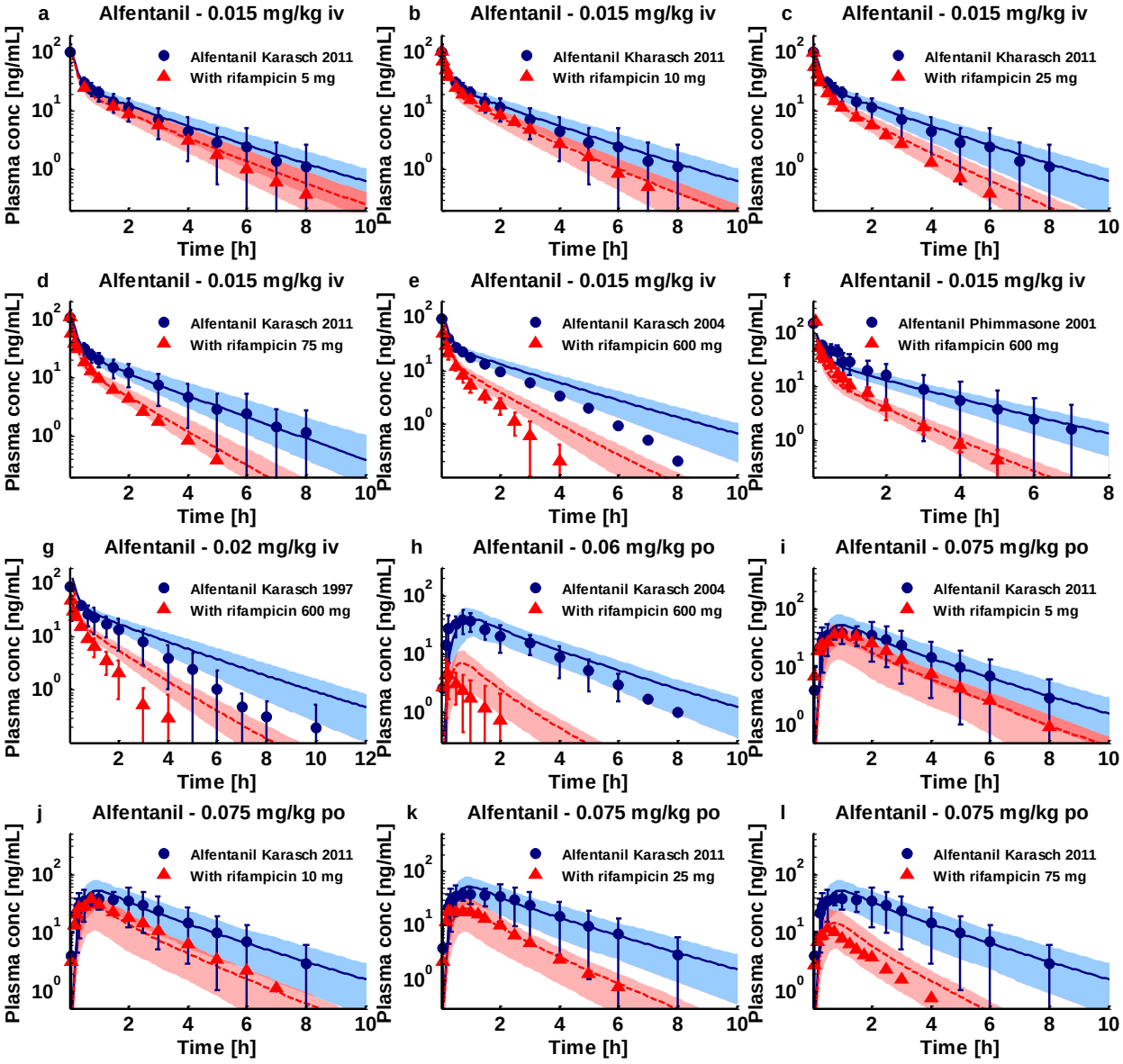

Figure S9a. Rifampicin-alfentanil DDI (iv, po) semilog. Population predictions of alfentanil plasma concentration-time profiles, before and during rifampicin treatment, compared to observed data. Observed data are shown as blue dots (control) or red triangles (DDI) ± SD. Population simulation arithmetic means are shown as solid blue lines (control) or dashed red lines (DDI); the shaded areas illustrate the respective 68% population prediction intervals. Details on dosing regimens, study populations, predicted and observed DDI AUC ratios and C_{max} ratios are summarized in Table 1 of the main document.

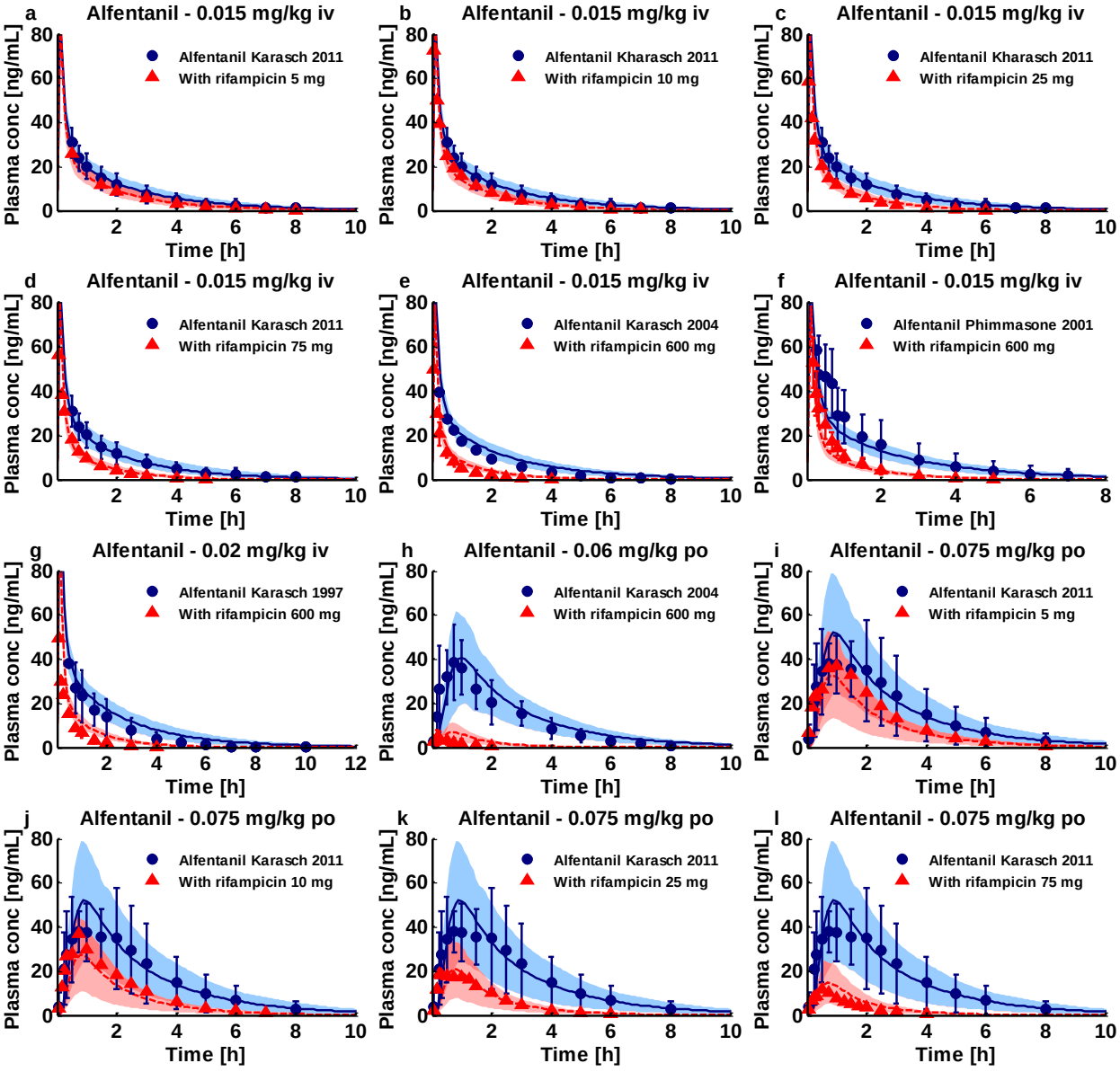

Figure S9b. Rifampicin-alfentanil DDI (iv, po) linear. Population predictions of alfentanil plasma concentration-time profiles, before and during rifampicin treatment, compared to observed data. Observed data are shown as blue dots (control) or red triangles (DDI) ± SD. Population simulation arithmetic means are shown as solid blue lines (control) or dashed red lines (DDI); the shaded areas illustrate the respective 68% population prediction intervals. Details on dosing regimens, study populations, predicted and observed DDI AUC ratios and C_{max} ratios are summarized in Table 1 of the main document.

3.4 Rifampicin-itraconazole DDI

To predict the rifampicin-itraconazole DDI, induction of CYP3A4 by rifampicin with simultaneous competitive inhibition was modeled using the same parameters as for the rifampicin-midazolam DDI (induction of CYP3A4 with EC_{50} = 0.34 µmol/L and E_{max} = 9 [3,24,25], simultaneous competitive inhibition of CYP3A4 with CYP3A4 K_i = 18.5 µmol/L [30]). In addition, inhibition of P-gp by itraconazole has been taken into account for this DDI, as described for the itraconazole-digoxin DDI (itraconazole P-gp K_i = 8.0 nmol/L).

The only available report of rifampicin-itraconazole co-administration [145] contains individual data of two coccidioidomycosis patients, showing that the itraconazole AUC during treatment with rifampicin is close to zero. The individual itraconazole concentration-time profiles before and during co-treatment with rifampicin are also presented, however, these concentrations were determined on *Candida pseudotropicalis* inoculated agar plates by measurements of zones of inhibition, and the reported trough concentrations during itraconazole mono-therapy are in the range of 10 µg/mL, while other clinical studies of 200 mg itraconazole BID find trough concentrations of approximately 2 µg/mL (see Figure S2d, subplots t and u, determined by HPLC). Nevertheless, the reported DDI AUC ratios are in good agreement with model predictions.

Table S10. Two case reports of rifampicin-itraconazole co-treatment

Perpetrator [mg]	Victim [mg]	Patient [M/F]	Age [years]	Pred AUC_{ratio}	Obs AUC_{ratio}	Pred/Obs AUC_{ratio}	Reference
Rifampicin	**Itraconazole**						
600 po, QD	200 po, BID (cap) fed	#7, M	38		0.035		Tucker 1992 [145]
600 po, QD	200 po, BID (cap) fed	#8, M	53		0.000		Tucker 1992 [145]
			$\bar{x}$	**0.0145**	**0.0175**	**0.83**	

Itraconazole AUC values are 0-12 h of day 14, #: patient ID, BID: twice daily, cap: capsule, F: female, M: male, po: orally, QD: once daily, $\bar{x}$: sample mean

3.5 Itraconazole-midazolam DDI

Competitive inhibition of midazolam metabolism by itraconazole and its metabolites was modeled with the same unbound K_i values as used to describe the auto-inhibition within the itraconazole model. These values are taken from in vitro measurements by Isoherranen et al.: itraconazole CYP3A4 K_i = 1.3 nmol/L, hydroxy-itraconazole CYP3A4 K_i = 14.4 nmol/L, keto-itraconazole CYP3A4 K_i = 5.12 nmol/L and N-desalkyl-itraconazole CYP3A4 K_i = 0.32 nmol/L [34].

Plots of population predicted compared to observed midazolam plasma concentration-time profiles of all itraconazole-midazolam DDI studies obtained from literature are shown in Figures S11a (semilogarithmic plot) and S11b (linear plot).

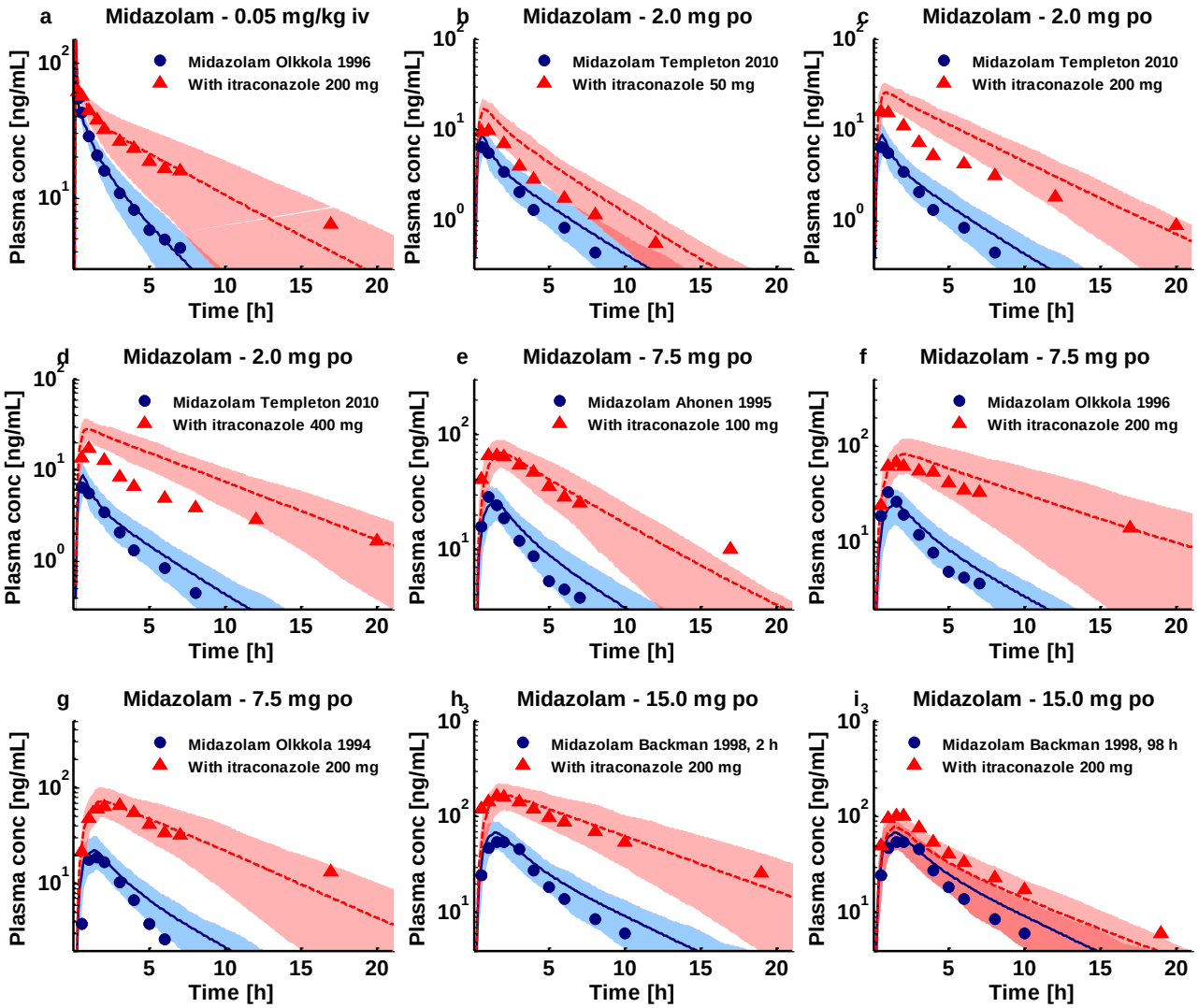

Figure S11a. Itraconazole-midazolam DDI (iv, po) semilog. Population predictions of midazolam plasma concentration-time profiles, before and during itraconazole treatment, compared to observed data. Observed data are shown as blue dots (control) or red triangles (DDI). Population simulation arithmetic means are shown as solid blue lines (control) or dashed red lines (DDI); the shaded areas illustrate the respective 68% population prediction intervals. Details on dosing regimens, study populations, predicted and observed DDI AUC ratios and C_{max} ratios are summarized in Table 1 of the main document.

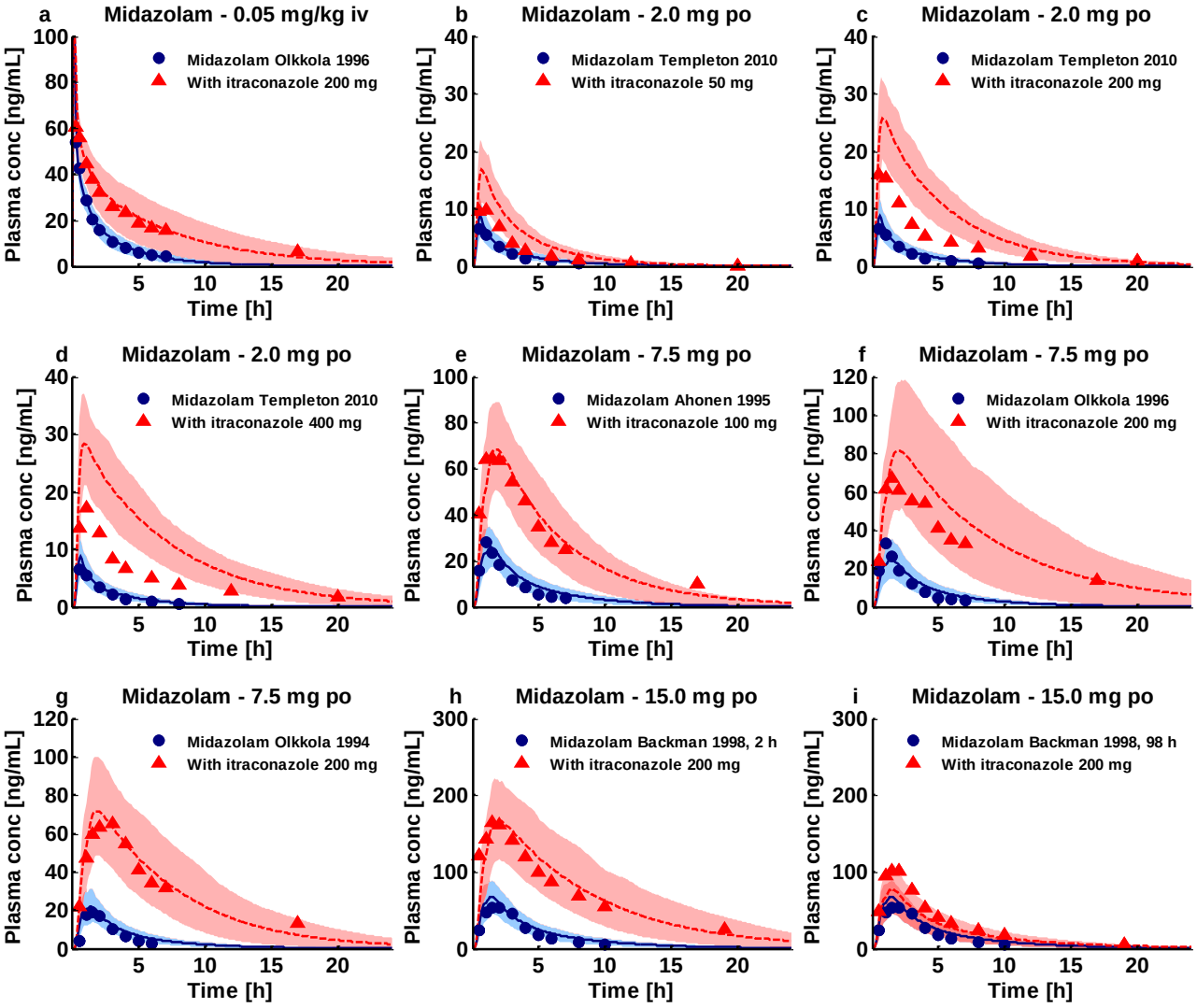

Figure S11b. Itraconazole-midazolam DDI (iv, po) linear. Population predictions of midazolam plasma concentration-time profiles, before and during itraconazole treatment, compared to observed data. Observed data are shown as blue dots (control) or red triangles (DDI). Population simulation arithmetic means are shown as solid blue lines (control) or dashed red lines (DDI); the shaded areas illustrate the respective 68% population prediction intervals. Details on dosing regimens, study populations, predicted and observed DDI AUC ratios and C_{max} ratios are summarized in Table 1 of the main document.

3.6 Clarithromycin-midazolam DDI

Mechanism-based inactivation of midazolam metabolism by clarithromycin was modeled with the K_I and k_{inact} values identified for auto-inactivation of CYP3A4 by clarithromycin during the clarithromycin model development: CYP3A4 K_I = 6.04 µmol/L and CYP3A4 k_{inact} = 0.04 1/min. Please see Table S3b for literature ranges and references regarding these two parameters.

Plots of population predicted compared to observed midazolam plasma concentration-time profiles of all clarithromycin-midazolam DDI studies obtained from literature are shown in Figures S12a (semilogarithmic plot) and S12b (linear plot).

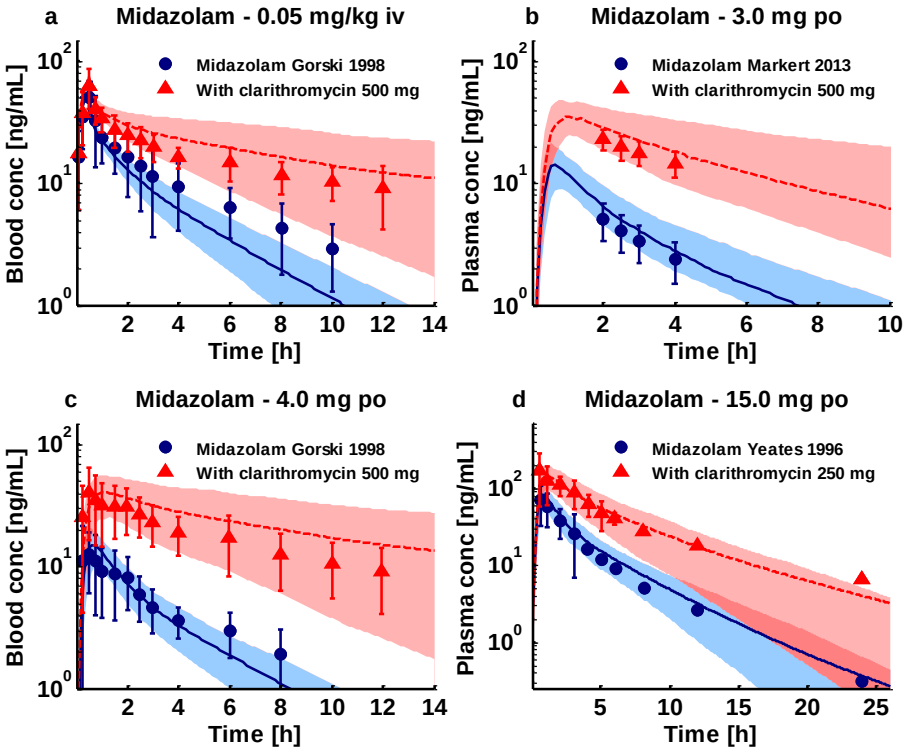

Figure S12a. Clarithromycin-midazolam DDI (iv, po) semilog. Population predictions of midazolam blood (a, c) or plasma (b, d) concentration-time profiles, before and during clarithromycin treatment, compared to observed data. Observed data are shown as blue dots (control) or red triangles (DDI) ± SD. Population simulation arithmetic means are shown as solid blue lines (control) or dashed red lines (DDI); the shaded areas illustrate the respective 68% population prediction intervals. Details on dosing regimens, study populations, predicted and observed DDI AUC ratios and C_{max} ratios are summarized in Table 1 of the main document.

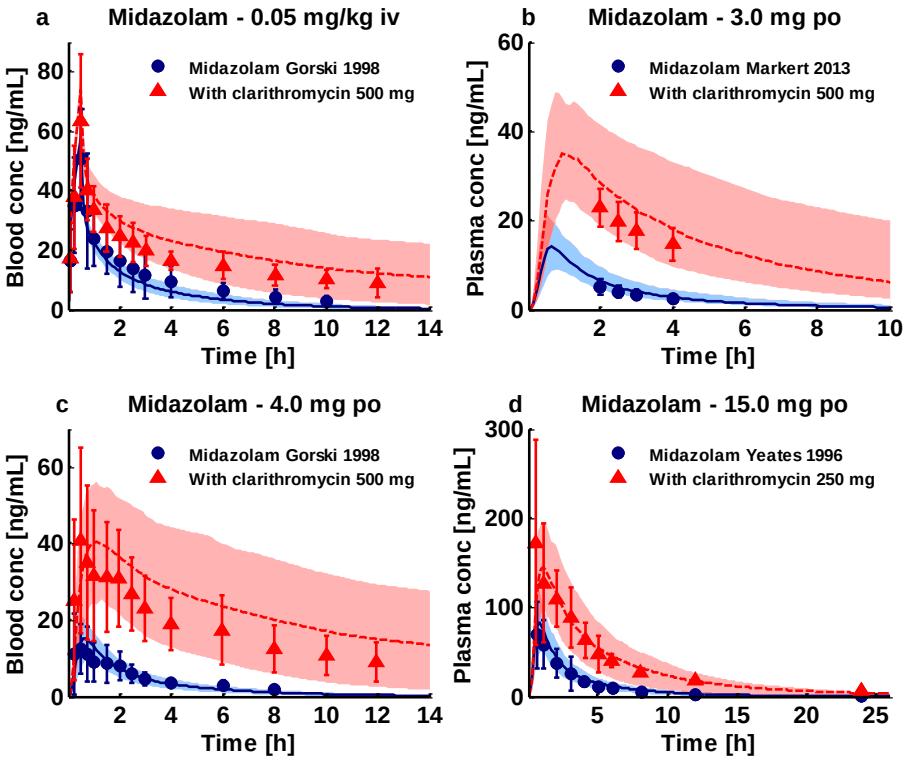

Figure S12b. Clarithromycin-midazolam DDI (iv, po) linear. Population predictions of midazolam blood (a, c) or plasma (b, d) concentration-time profiles, before and during clarithromycin treatment, compared to observed data. Observed data are shown as blue dots (control) or red triangles (DDI) ± SD. Population simulation arithmetic means are shown as solid blue lines (control) or dashed red lines (DDI); the shaded areas illustrate the respective 68% population prediction intervals. Details on dosing regimens, study populations, predicted and observed DDI AUC ratios and C_{max} ratios are summarized in Table 1 of the main document.

3.7 Rifampicin-digoxin DDI

Induction of P-gp by rifampicin was modeled with the same EC_{50} = 0.34 µmol/L as the induction of CYP3A4. This assumption is based on the knowledge that the co-induction of CYP3A4 and P-gp by rifampicin is mediated via binding of rifampicin to the same nuclear receptor (pregnane X receptor (PXR)) [4]. The E_{max} = 2.5 for induction of P-gp has been experimentally determined in a clinical study using human duodenal biopsies [5]. Simultaneous competitive inhibition of P-gp by rifampicin was modeled with a P-gp K_i = 169 µmol/L, quantified in LLC-MDR1 cell monolayers [29]. For lack of information on binding of rifampicin in this assay, fraction unbound was assumed to be 1.

Plots of population predicted compared to observed digoxin plasma concentration-time profiles of all rifampicin-digoxin DDI studies obtained from literature are shown in Figures S13a (semilogarithmic plot) and S13b (linear plot).

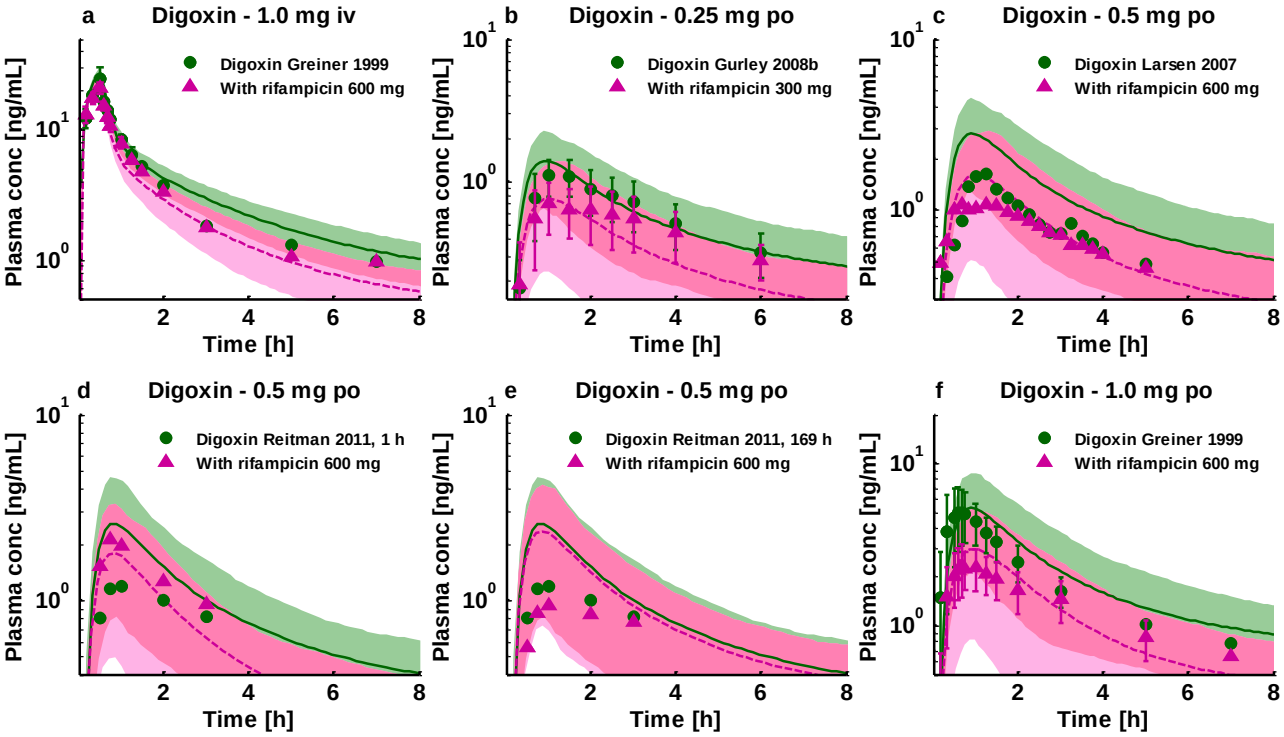

Figure S13a. Rifampicin-digoxin DDI (iv, po) semilog. Population predictions of digoxin plasma concentration-time profiles, before and during rifampicin treatment, compared to observed data. Observed data are shown as green dots (control) or pink triangles (DDI) ± SD. Population simulation arithmetic means are shown as solid green lines (control) or dashed pink lines (DDI); the shaded areas illustrate the respective 68% population prediction intervals. Details on dosing regimens, study populations, predicted and observed DDI AUC ratios and C_{max} ratios are summarized in Table 1 of the main document.

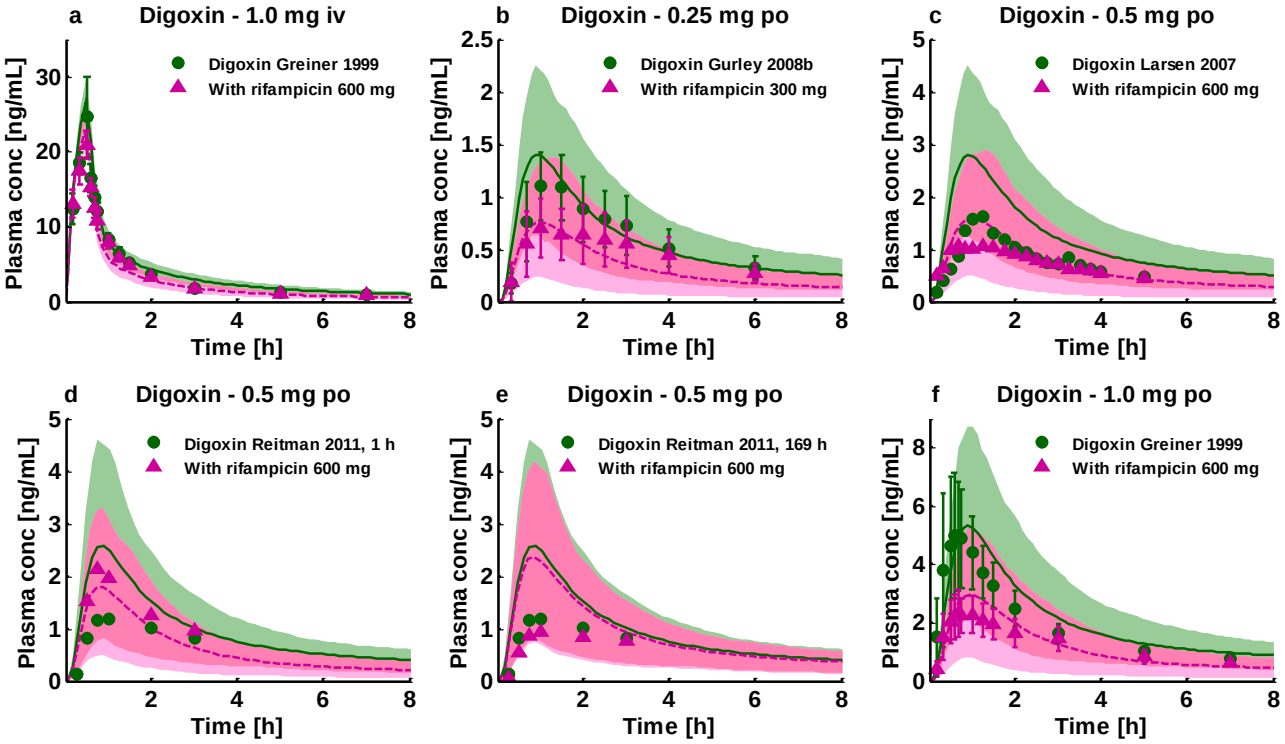

Figure S13b. Rifampicin-digoxin DDI (iv, po) linear. Population predictions of digoxin plasma concentration-time profiles, before and during rifampicin treatment, compared to observed data. Observed data are shown as green dots (control) or pink triangles (DDI) ± SD. Population simulation arithmetic means are shown as solid green lines (control) or dashed pink lines (DDI); the shaded areas illustrate the respective 68% population prediction intervals. Details on dosing regimens, study populations, predicted and observed DDI AUC ratios and C_{max} ratios are summarized in Table 1 of the main document.

3.8 Itraconazole-digoxin DDI

Competitive inhibition of P-gp by itraconazole was modeled using the unbound itraconazole P-gp K_i = 8.0 nmol/L reported by Shityakov and Förster [49]. P-gp inhibition by hydroxy-itraconazole, keto-itraconazole or N-desalkyl-itraconazole was not taken into account.

Plots of population predicted compared to observed digoxin plasma concentration-time profiles during the itraconazole-digoxin DDI are shown in Figures S14a (semilogarithmic plot) and S14b (linear plot).

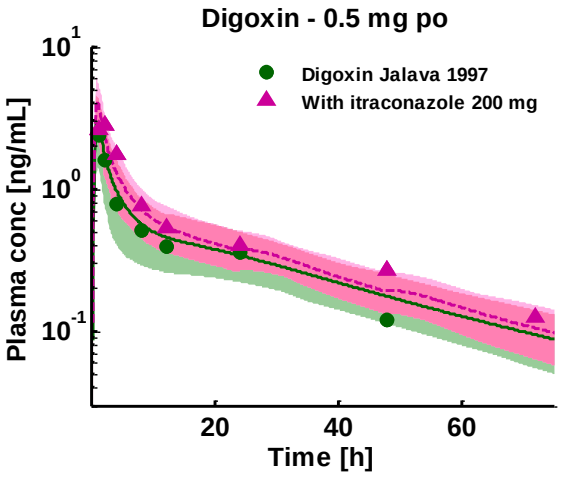

Figure S14a. Itraconazole-digoxin DDI (po) semilog. Population predictions of digoxin plasma concentration-time profiles, before and during itraconazole treatment, compared to observed data. Observed data are shown as green dots (control) or pink triangles (DDI). Population simulation arithmetic means are shown as solid green lines (control) or dashed pink lines (DDI); the shaded areas illustrate the respective 68% population prediction intervals. Details on dosing regimens, study populations, predicted and observed DDI AUC ratios and C_{max} ratios are summarized in Table 1 of the main document.

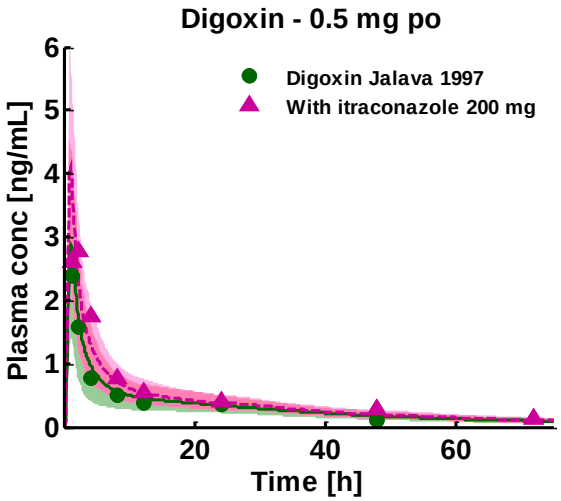

Figure S14b. Itraconazole-digoxin DDI (po) linear. Population predictions of digoxin plasma concentration-time profiles, before and during itraconazole treatment, compared to observed data. Observed data are shown as green dots (control) or pink triangles (DDI). Population simulation arithmetic means are shown as solid green lines (control) or dashed pink lines (DDI); the shaded areas illustrate the respective 68% population prediction intervals. Details on dosing regimens, study populations, predicted and observed DDI AUC ratios and C_{max} ratios are summarized in Table 1 of the main document.

3.9 Clarithromycin-digoxin DDI

Competitive inhibition of P-gp by clarithromycin was modeled using a P-gp K_i = 4.1 µmol/L determined in Caco-2 cells [53]. No correction of this in vitro value to account for binding in the assay was applied, as the fraction unbound of clarithromycin in hepatocytes was reported to be 0.98 and similar binding in colon cells and hepatocytes was assumed [146].

Plots of population predicted compared to observed digoxin plasma concentration-time profiles of all clarithromycin-digoxin DDI studies obtained from literature are shown in Figures S15a (semilogarithmic plot) and S15b (linear plot).

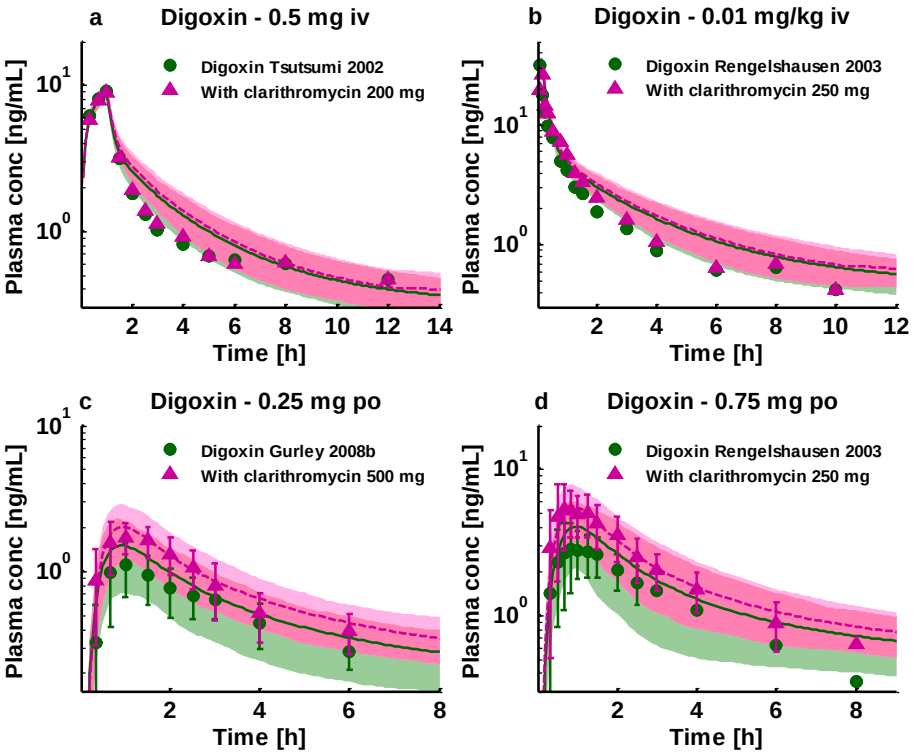

Figure S15a. Clarithromycin-digoxin DDI (iv, po) semilog. Population predictions of digoxin plasma concentration-time profiles, before and during clarithromycin treatment, compared to observed data. Observed data are shown as green dots (control) or pink triangles (DDI) ± SD. Population simulation arithmetic means are shown as solid green lines (control) or dashed pink lines (DDI); the shaded areas illustrate the respective 68% population prediction intervals. Details on dosing regimens, study populations, predicted and observed DDI AUC ratios and C_{max} ratios are summarized in Table 1 of the main document.

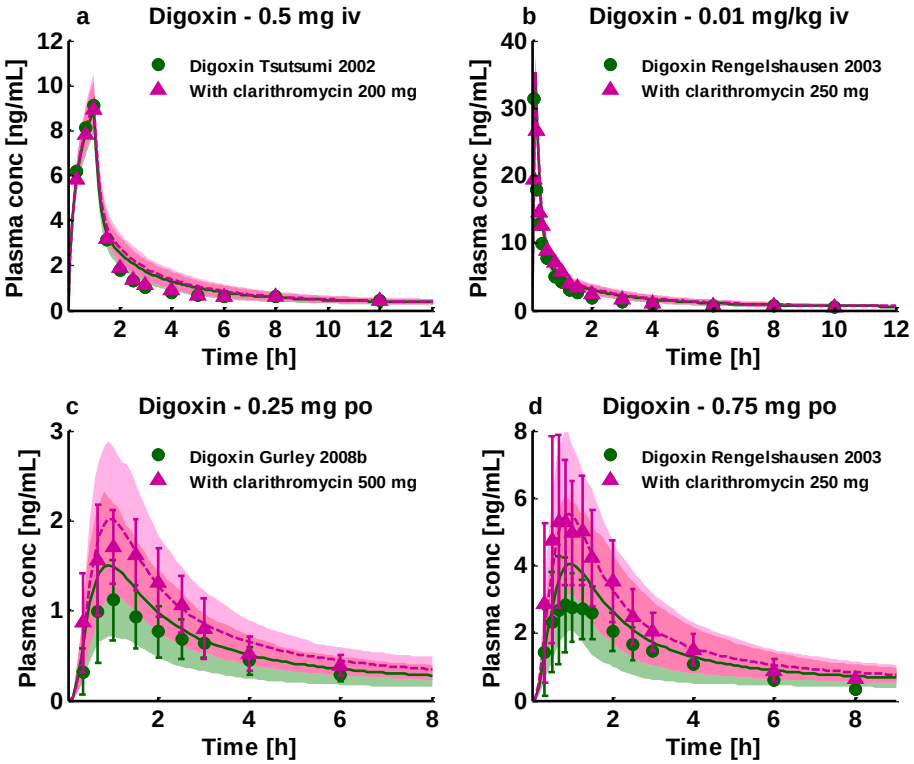

Figure S15b. Clarithromycin-digoxin DDI (iv, po) linear. Population predictions of digoxin plasma concentration-time profiles, before and during clarithromycin treatment, compared to observed data. Observed data are shown as green dots (control) or pink triangles (DDI) ± SD. Population simulation arithmetic means are shown as solid green lines (control) or dashed pink lines (DDI); the shaded areas illustrate the respective 68% population prediction intervals. Details on dosing regimens, study populations, predicted and observed DDI AUC ratios and C_{max} ratios are summarized in Table 1 of the main document.

4 References

1. U.S. Food and Drug Administration. *Drug Interaction Studies - Study Design, Data Analysis, Implications for Dosing, and Labeling Recommendations. Draft Guidance for Industry*. (2012).
2. Nakajima, A. *et al.* Human arylacetamide deacetylase is responsible for deacetylation of rifamycins: rifampicin, rifabutin, and rifapentine. *Biochem. Pharmacol.* **82**, 1747–56 (2011).
3. Baneyx, G., Parrott, N., Meille, C., Iliadis, A. & Lavé, T. Physiologically based pharmacokinetic modeling of CYP3A4 induction by rifampicin in human: influence of time between substrate and inducer administration. *Eur. J. Pharm. Sci.* **56**, 1–15 (2014).
4. Geick, A., Eichelbaum, M. & Burk, O. Nuclear receptor response elements mediate induction of intestinal MDR1 by rifampin. *J. Biol. Chem.* **276**, 14581–7 (2001).
5. Greiner, B. *et al.* The role of intestinal P-glycoprotein in the interaction of digoxin and rifampin. *J. Clin. Invest.* **104**, 147–53 (1999).
6. Dixit, V. *et al.* Cytochrome P450 enzymes and transporters induced by anti-human immunodeficiency virus protease inhibitors in human hepatocytes: implications for predicting clinical drug interactions. *Drug Metab. Dispos.* **35**, 1853–9 (2007).
7. Williamson, B., Dooley, K.E., Zhang, Y., Back, D.J. & Owen, A. Induction of influx and efflux transporters and cytochrome P450 3A4 in primary human hepatocytes by rifampin, rifabutin, and rifapentine. *Antimicrob. Agents Chemother.* **57**, 6366–9 (2013).
8. Staudinger, J.L., Xu, C., Cui, Y.J. & Klaassen, C.D. Nuclear receptor-mediated regulation of carboxylesterase expression and activity. *Expert Opin. drug Metab. Toxicol.* **6**, 261–71 (2010).
9. Smythe, W. *et al.* A semimechanistic pharmacokinetic-enzyme turnover model for rifampin autoinduction in adult tuberculosis patients. *Antimicrob. Agents Chemother.* **56**, 2091–8 (2012).
10. LLC, S.-A.U.S. RIFADIN® (rifampin capsules USP) and RIFADIN® IV (rifampin for injection USP). *Revis. labeling information, Ref. ID 3261635* (2013).
11. Nitti, V., Virgilio, R., Patricolo, M.R. & Iuliano, A. Pharmacokinetic study of intravenous rifampicin. *Chemotherapy* **23**, 1–6 (1977).
12. Acocella, G., Bonollo, L., Mainardi, M., Margaroli, P. & Tenconi, L.T. Serum and urine concentrations of rifampicin administered by intravenous infusion in man. *Arzneimittelforschung.* **27**, 1221–6 (1977).
13. Chouchane, N., Barre, J., Toumi, A., Tillement, J.P. & Benakis, A. Bioequivalence study of two pharmaceutical forms of rifampicin capsules in man. *Eur. J. Drug Metab. Pharmacokinet.* **20**, 315–20 (1995).
14. Blume, H. & Mutschler, E. *Bioäquivalenz: Qualitätsbewertung wirkstoffgleicher Fertigarzneimittel: Anleitung, Methoden, Materialien*. (1989).
15. Acocella, G., Lamarina, A., Nicolis, F.B., Pagani, V. & Segre, G. Kinetic studies on rifampicin II. Multicompartmental analysis of the serum, urine and bile concentrations in subjects treated for one week. *Eur. J. Clin. Pharmacol.* **5**, 111–115 (1972).
16. Acocella, G. *et al.* Kinetics of rifampicin and isoniazid administered alone and in combination to normal subjects and patients with liver disease. *Gut* **13**, 47–53 (1972).
17. U.S. Food and Drug Administration. *Rifampin Review Package - FDA 064150*. (1997). http://www.accessdata.fda.gov/drugsatfda_docs/anda/97/064150review.pdf
18. Peloquin, C.A. *et al.* Population pharmacokinetic modeling of isoniazid, rifampin, and pyrazinamide. *Antimicrob. Agents Chemother.* **41**, 2670–9 (1997).
19. The Merck Index 14th edition: Rifampin. p 8217 (2006).
20. Panchagnula, R., Gulati, I., Varma, M. & Raj, Y.A. Dissolution methodology for evaluation of rifampicin-containing fixed-dose combinations using biopharmaceutic classification sytem based approach. *Clin. Res. Regul. Aff.* **24**, 61–76 (2007).

21. Agrawal, S. & Panchagnula, R. Implication of biopharmaceutics and pharmacokinetics of rifampicin in variable bioavailability from solid oral dosage forms. *Biopharm. drug Dispos.* **26**, 321–34 (2005).
22. Boman, G. & Ringberger, V.A. Binding of rifampicin by human plasma proteins. *Eur. J. Clin. Pharmacol.* **7**, 369–73 (1974).
23. Wishart, D.S. *et al.* DrugBank: a comprehensive resource for in silico drug discovery and exploration. *Nucleic Acids Res.* **34**, D668-72 (2006).
24. Templeton, I.E., Houston, J.B. & Galetin, A. Predictive utility of in vitro rifampin induction data generated in fresh and cryopreserved human hepatocytes, Fa2N-4, and HepaRG cells. *Drug Metab. Dispos.* **39**, 1921–9 (2011).
25. Shou, M. *et al.* Modeling, prediction, and in vitro in vivo correlation of CYP3A4 induction. *Drug Metab. Dispos.* **36**, 2355–70 (2008).
26. Loos, U. *et al.* Pharmacokinetics of oral and intravenous rifampicin during chronic administration. *Klin. Wochenschr.* **63**, 1205–11 (1985).
27. Tirona, R.G., Leake, B.F., Wolkoff, A.W. & Kim, R.B. Human organic anion transporting polypeptide-C (SLC21A6) is a major determinant of rifampin-mediated pregnane X receptor activation. *J. Pharmacol. Exp. Ther.* **304**, 223–8 (2003).
28. Collett, A., Tanianis-Hughes, J., Hallifax, D. & Warhurst, G. Predicting P-glycoprotein effects on oral absorption: correlation of transport in Caco-2 with drug pharmacokinetics in wild-type and mdr1a(-/-) mice in vivo. *Pharm. Res.* **21**, 819–26 (2004).
29. Reitman, M.L. *et al.* Rifampin's acute inhibitory and chronic inductive drug interactions: experimental and model-based approaches to drug-drug interaction trial design. *Clin. Pharmacol. Ther.* **89**, 234–42 (2011).
30. Kajosaari, L.I., Laitila, J., Neuvonen, P.J. & Backman, J.T. Metabolism of repaglinide by CYP2C8 and CYP3A4 in vitro: effect of fibrates and rifampicin. *Basic Clin. Pharmacol. Toxicol.* **97**, 249–56 (2005).
31. Kawai, R. *et al.* Physiologically based pharmacokinetic study on a cyclosporin derivative, SDZ IMM 125. *J. Pharmacokinet. Biopharm.* **22**, 327–65 (1994).
32. Rodgers, T., Leahy, D. & Rowland, M. Physiologically based pharmacokinetic modeling 1: predicting the tissue distribution of moderate-to-strong bases. *J. Pharm. Sci.* **94**, 1259–76 (2005).
33. Taylor, M.J., Tanna, S. & Sahota, T. In vivo study of a polymeric glucose-sensitive insulin delivery system using a rat model. *J. Pharm. Sci.* **99**, 4215–27 (2010).
34. Isoherranen, N., Kunze, K.L., Allen, K.E., Nelson, W.L. & Thummel, K.E. Role of itraconazole metabolites in CYP3A4 inhibition. *Drug Metab. Dispos.* **32**, 1121–31 (2004).
35. Heykants, J. *et al.* The clinical pharmacokinetics of itraconazole: an overview. *Mycoses* **32 Suppl 1**, 67–87 (1989).
36. Mouton, J.W. *et al.* Pharmacokinetics of itraconazole and hydroxyitraconazole in healthy subjects after single and multiple doses of a novel formulation. *Antimicrob. Agents Chemother.* **50**, 4096–102 (2006).
37. Templeton, I.E. *et al.* Contribution of itraconazole metabolites to inhibition of CYP3A4 in vivo. *Clin. Pharmacol. Ther.* **83**, 77–85 (2008).
38. Velde, V.J. Van de *et al.* Effect of food on the pharmacokinetics of a new hydroxypropyl-beta-cyclodextrin formulation of itraconazole. *Pharmacotherapy* **16**, 424–8 (1996).
39. Peer, A. Van, Woestenborghs, R., Heykants, J., Gasparini, R. & Gauwenbergh, G. The effects of food and dose on the oral systemic availability of itraconazole in healthy subjects. *Eur. J. Clin. Pharmacol.* **36**, 423–6 (1989).
40. Barone, J.A. *et al.* Food interaction and steady-state pharmacokinetics of itraconazole oral solution in healthy volunteers. *Pharmacotherapy* **18**, 295–301 (1998).

41. Barone, J.A. *et al.* Enhanced bioavailability of itraconazole in hydroxypropyl-beta-cyclodextrin solution versus capsules in healthy volunteers. *Antimicrob. Agents Chemother.* **42**, 1862–5 (1998).
42. Barone, J.A. *et al.* Food interaction and steady-state pharmacokinetics of itraconazole capsules in healthy male volunteers. *Antimicrob. Agents Chemother.* **37**, 778–84 (1993).
43. Olkkola, K.T., Backman, J.T. & Neuvonen, P.J. Midazolam should be avoided in patients receiving the systemic antimycotics ketoconazole or itraconazole. *Clin. Pharmacol. Ther.* **55**, 481–5 (1994).
44. Hardin, T.C. *et al.* Pharmacokinetics of itraconazole following oral administration to normal volunteers. *Antimicrob. Agents Chemother.* **32**, 1310–3 (1988).
45. Taupitz, T., Dressman, J.B., Buchanan, C.M. & Klein, S. Cyclodextrin-water soluble polymer ternary complexes enhance the solubility and dissolution behaviour of poorly soluble drugs. Case example: itraconazole. *Eur. J. Pharm. Biopharm.* **83**, 378–87 (2013).
46. National Center for Biotechnology Information Hydroxy-itraconazole - PubChem Identifier: CID 108222. *PubChem Database.* https://pubchem.ncbi.nlm.nih.gov/compound/108222
47. Riccardi, K. *et al.* Plasma protein binding of challenging compounds. *J. Pharm. Sci.* **104**, 2627–36 (2015).
48. Ishigam, M. *et al.* Inhibition of in vitro metabolism of simvastatin by itraconazole in humans and prediction of in vivo drug-drug interactions. *Pharm. Res.* **18**, 622–31 (2001).
49. Shityakov, S. & Förster, C. In silico structure-based screening of versatile P-glycoprotein inhibitors using polynomial empirical scoring functions. *Adv. Appl. Bioinforma. Chem. AABC* **7**, 1–9 (2014).
50. National Center for Biotechnology Information Keto-itraconazole - PubChem Identifier: CID 45039625. *PubChem Database.* https://pubchem.ncbi.nlm.nih.gov/compound/45039625
51. National Center for Biotechnology Information N-Desalkyl-itraconazole - PubChem Identifier: CID 53789808. *PubChem Database.*https://pubchem.ncbi.nlm.nih.gov/compound/53789808
52. Cheng, Y.-C. & Prusoff, W.H. Relationship between the inhibition constant (K1) and the concentration of inhibitor which causes 50 per cent inhibition (I50) of an enzymatic reaction. *Biochem. Pharmacol.* **22**, 3099–108 (1973).
53. Eberl, S. *et al.* Role of p-glycoprotein inhibition for drug interactions: evidence from in vitro and pharmacoepidemiological studies. *Clin. Pharmacokinet.* **46**, 1039–49 (2007).
54. Seithel, A. *et al.* The influence of macrolide antibiotics on the uptake of organic anions and drugs mediated by OATP1B1 and OATP1B3. *Drug Metab. Dispos.* **35**, 779–86 (2007).
55. Moj, D. *et al.* Clarithromycin, midazolam, and digoxin: application of PBPK modeling to gain new insights into drug-drug interactions and co-medication regimens. *AAPS J.* **19**, 298–312 (2017).
56. Nishimura, M., Yaguti, H., Yoshitsugu, H., Naito, S. & Satoh, T. Tissue distribution of mRNA expression of human cytochrome P450 isoforms assessed by high-sensitivity real-time reverse transcription PCR. *J. Pharm. Soc. Japan* **123**, 369–75 (2003).
57. Higgins, J.W., Ke, A.B. & Zamek-Gliszczynski, M.J. Clinical CYP3A inhibitor alternatives to ketoconazole, clarithromycin and itraconazole, are not transported into the liver by hepatic organic anion transporting polypeptides and organic cation transporter 1. *Drug Metab. Dispos.* **42**, 1780–4 (2014).
58. Chu, S.Y., Deaton, R. & Cavanaugh, J. Absolute bioavailability of clarithromycin after oral administration in humans. *Antimicrob. Agents Chemother.* **36**, 1147–50 (1992).
59. Chu, S.Y. *et al.* Pharmacokinetics of clarithromycin, a new macrolide, after single ascending oral doses. *Antimicrob. Agents Chemother.* **36**, 2447–53 (1992).
60. Chu, S. *et al.* Single- and multiple-dose pharmacokinetics of clarithromycin, a new macrolide antimicrobial. *J. Clin. Pharmacol.* **33**, 719–26 (1993).

61. Kees, F., Wellenhofer, M. & Grobecker, H. Serum and cellular pharmacokinetics of clarithromycin 500 mg q.d. and 250 mg b.i.d. in volunteers. *Infection* **23**, 168–72 (1995).
62. Rengelshausen, J. *et al.* Contribution of increased oral bioavailability and reduced nonglomerular renal clearance of digoxin to the digoxin-clarithromycin interaction. *Br. J. Clin. Pharmacol.* **56**, 32–8 (2003).
63. Abduljalil, K. *et al.* Modeling the autoinhibition of clarithromycin metabolism during repeated oral administration. *Antimicrob. Agents Chemother.* **53**, 2892–901 (2009).
64. McFarland, J.W. *et al.* Quantitative structure-activity relationships among macrolide antibacterial agents: in vitro and in vivo potency against Pasteurella multocida. *J. Med. Chem.* **40**, 1340–6 (1997).
65. Salem, I.I. & Düzgünes, N. Efficacies of cyclodextrin-complexed and liposome-encapsulated clarithromycin against Mycobacterium avium complex infection in human macrophages. *Int. J. Pharm.* **250**, 403–14 (2003).
66. Lappin, G. *et al.* Comparative pharmacokinetics between a microdose and therapeutic dose for clarithromycin, sumatriptan, propafenone, paracetamol (acetaminophen), and phenobarbital in human volunteers. *Eur. J. Pharm. Sci.* **43**, 141–50 (2011).
67. Davey, P.G. The pharmacokinetics of clarithromycin and its 14-OH metabolite. *J. Hosp. Infect.* **19 Suppl A**, 29–37 (1991).
68. Chu, S.Y. *et al.* Effect of moderate or severe hepatic impairment on clarithromycin pharmacokinetics. *J. Clin. Pharmacol.* **33**, 480–5 (1993).
69. Noreddin, A.M. *et al.* Pharmacodynamic modeling of clarithromycin against macrolide-resistant [PCR-positive mef(A) or erm(B)] Streptococcus pneumoniae simulating clinically achievable serum and epithelial lining fluid free-drug concentrations. *Antimicrob. Agents Chemother.* **46**, 4029–34 (2002).
70. Rodrigues, A.D., Roberts, E.M., Mulford, D.J., Yao, Y. & Ouellet, D. Oxidative metabolism of clarithromycin in the presence of human liver microsomes. Major role for the cytochrome P4503A (CYP3A) subfamily. *Drug Metab. Dispos.* **25**, 623–30 (1997).
71. Rodvold, K.A. Clinical pharmacokinetics of clarithromycin. *Clin. Pharmacokinet.* **37**, 385–98 (1999).
72. Polasek, T.M. & Miners, J.O. Quantitative prediction of macrolide drug-drug interaction potential from in vitro studies using testosterone as the human cytochrome P4503A substrate. *Eur. J. Clin. Pharmacol.* **62**, 203–8 (2006).
73. Jones, D.R., Ekins, S., Li, L. & Hall, S.D. Computational approaches that predict metabolic intermediate complex formation with CYP3A4 (+b5). *Drug Metab. Dispos.* **35**, 1466–75 (2007).
74. Mayhew, B.S., Jones, D.R. & Hall, S.D. An in vitro model for predicting in vivo inhibition of cytochrome P450 3A4 by metabolic intermediate complex formation. *Drug Metab. Dispos.* **28**, 1031–7 (2000).
75. Ito, K., Ogihara, K., Kanamitsu, S.-I. & Itoh, T. Prediction of the in vivo interaction between midazolam and macrolides based on in vitro studies using human liver microsomes. *Drug Metab. Dispos.* **31**, 945–54 (2003).
76. Gorski, J.C. *et al.* The contribution of intestinal and hepatic CYP3A to the interaction between midazolam and clarithromycin. *Clin. Pharmacol. Ther.* **64**, 133–43 (1998).
77. Smith, M.T., Eadie, M.J. & Brophy, T.O. The pharmacokinetics of midazolam in man. *Eur. J. Clin. Pharmacol.* **19**, 271–8 (1981).
78. Heizmann, P., Eckert, M. & Ziegler, W.H. Pharmacokinetics and bioavailability of midazolam in man. *Br. J. Clin. Pharmacol.* **16 Suppl 1**, 43S–49S (1983).
79. Chung, E., Nafziger, A.N., Kazierad, D.J. & Bertino, J.S. Comparison of midazolam and simvastatin as cytochrome P450 3A probes. *Clin. Pharmacol. Ther.* **79**, 350–61 (2006).

80. Walser, A. *et al.* Quinazolines and 1, 4-benzodiazepines. 84. Synthesis and reactions of imidazo [1, 5-a][1, 4] benzodiazepines. *J. Org. Chem.* **43**, 936–944 (1978).
81. Heikkinen, A.T., Baneyx, G., Caruso, A. & Parrott, N. Application of PBPK modeling to predict human intestinal metabolism of CYP3A substrates - an evaluation and case study using GastroPlus. *Eur. J. Pharm. Sci.* **47**, 375–86 (2012).
82. Vossen, M. *et al.* Dynamically simulating the interaction of midazolam and the CYP3A4 inhibitor itraconazole using individual coupled whole-body physiologically-based pharmacokinetic (WB-PBPK) models. *Theor. Biol. Med. Model.* **4**, 13 (2007).
83. Lemaitre, F. *et al.* Propofol, midazolam, vancomycin and cyclosporine therapeutic drug monitoring in extracorporeal membrane oxygenation circuits primed with whole human blood. *Crit. Care* **19**, 40 (2015).
84. Björkman, S., Wada, D.R., Berling, B.M. & Benoni, G. Prediction of the disposition of midazolam in surgical patients by a physiologically based pharmacokinetic model. *J. Pharm. Sci.* **90**, 1226–41 (2001).
85. Patki, K.C., Moltke, L.L. Von & Greenblatt, D.J. In vitro metabolism of midazolam, triazolam, nifedipine, and testosterone by human liver microsomes and recombinant cytochromes p450: role of cyp3a4 and cyp3a5. *Drug Metab. Dispos.* **31**, 938–44 (2003).
86. Phimmasone, S. & Kharasch, E.D. A pilot evaluation of alfentanil-induced miosis as a noninvasive probe for hepatic cytochrome P450 3A4 (CYP3A4) activity in humans. *Clin. Pharmacol. Ther.* **70**, 505–17 (2001).
87. Wandel, C., Kim, R., Wood, M. & Wood, A. Interaction of morphine, fentanyl, sufentanil, alfentanil, and loperamide with the efflux drug transporter P-glycoprotein. *Anesthesiology* **96**, 913–920 (2002).
88. Meuldermans, W. *et al.* Alfentanil pharmacokinetics and metabolism in humans. *Anesthesiology* **69**, 527–534 (1988).
89. Kharasch, E.D. *et al.* Sensitivity of intravenous and oral alfentanil and pupillary miosis as minimal and noninvasive probes for hepatic and first-pass CYP3A induction. *Clin. Pharmacol. Ther.* **90**, 100–8 (2011).
90. Kharasch, E.D., Walker, A., Hoffer, C. & Sheffels, P. Intravenous and oral alfentanil as in vivo probes for hepatic and first-pass cytochrome P450 3A activity: noninvasive assessment by use of pupillary miosis. *Clin. Pharmacol. Ther.* **76**, 452–66 (2004).
91. Kharasch, E.D. *et al.* The role of cytochrome P450 3A4 in alfentanil clearance. Implications for interindividual variability in disposition and perioperative drug interactions. *Anesthesiology* **87**, 36–50 (1997).
92. Ferrier, C. *et al.* Alfentanil pharmacokinetics in patients with cirrhosis. *Anesthesiology* **62**, 480–484 (1985).
93. Jansson, R., Bredberg, U. & Ashton, M. Prediction of drug tissue to plasma concentration ratios using a measured volume of distribution in combination with lipophilicity. *J. Pharm. Sci.* **97**, 2324–39 (2008).
94. Edginton, A.N. & Willmann, S. Physiology-based simulations of a pathological condition: prediction of pharmacokinetics in patients with liver cirrhosis. *Clin. Pharmacokinet.* **47**, 743–52 (2008).
95. Almond, L.M. *et al.* Prediction of drug-drug interactions arising from CYP3A induction using a physiologically based dynamic model. *Drug Metab. Dispos.* **44**, 821–32 (2016).
96. Ochs, H.R., Greenblatt, D.J., Bodem, G. & Harmatz, J.S. Dose-independent pharmacokinetics of digoxin in humans. *Am. Heart J.* **96**, 507–11 (1978).
97. Bauer, L.A. *Applied Clinical Pharmacokinetics*. (2008).
98. Caldwell, J.H. & Cline, C.T. Biliary excretion of digoxin in man. *Clin. Pharmacol. Ther.* **19**, 410–5 (1976).

99. Wagner, J.G., Popat, K.D., Das, S.K., Sakmar, E. & Movahhed, H. Evidence of nonlinearity in digoxin pharmacokinetics. *J. Pharmacokinet. Biopharm.* **9**, 147–66 (1981).
100. Ding, R. *et al.* Substantial pharmacokinetic interaction between digoxin and ritonavir in healthy volunteers. *Clin. Pharmacol. Ther.* **76**, 73–84 (2004).
101. Tsutsumi, K. *et al.* The effect of erythromycin and clarithromycin on the pharmacokinetics of intravenous digoxin in healthy volunteers. *J. Clin. Pharmacol.* **42**, 1159–64 (2002).
102. Lalonde, R.L., Deshpande, R., Hamilton, P.P., McLean, W.M. & Greenway, D.C. Acceleration of digoxin clearance by activated charcoal. *Clin. Pharmacol. Ther.* **37**, 367–71 (1985).
103. Koup, J.R., Greenblatt, D.J., Jusko, W.J., Smith, T.W. & Koch-Weser, J. Pharmacokinetics of digoxin in normal subjects after intravenous bolus and infusion doses. *J. Pharmacokinet. Biopharm.* **3**, 181–92 (1975).
104. Kramer, W.G. *et al.* Pharmacokinetics of digoxin: relationship between response intensity and predicted compartmental drug levels in man. *J. Pharmacokinet. Biopharm.* **7**, 47–61 (1979).
105. Steiness, E., Waldorff, S. & Hansen, P.B. Renal digoxin clearance: dependence on plasma digoxin and diuresis. *Eur. J. Clin. Pharmacol.* **23**, 151–4 (1982).
106. Qiu, R. *et al.* Lack of a pharmacokinetic interaction between dimebon (latrepirdine) and digoxin in healthy subjects. *Am. Soc. Clin. Pharmacol. Ther. Meet. Atlanta, GA, USA* (2010).
107. Eckermann, G., Lahu, G., Nassr, N. & Bethke, T.D. Absence of pharmacokinetic interaction between roflumilast and digoxin in healthy adults. *J. Clin. Pharmacol.* **52**, 251–7 (2012).
108. Gurley, B.J., Swain, A., Williams, D.K., Barone, G. & Battu, S.K. Gauging the clinical significance of P-glycoprotein-mediated herb-drug interactions: comparative effects of St. John's wort, Echinacea, clarithromycin, and rifampin on digoxin pharmacokinetics. *Mol. Nutr. food Res.* **52**, 772–9 (2008).
109. U.S. Food and Drug Administration. *NDA 22-425 MULTAQ (dronedarone hydrochloride) Tablets, 400 mg*. (2009).
110. Friedrich, C. *et al.* Evaluation of the pharmacokinetic interaction after multiple oral doses of linagliptin and digoxin in healthy volunteers. *Eur. J. Drug Metab. Pharmacokinet.* **36**, 17–24 (2011).
111. Vaidyanathan, S. *et al.* Pharmacokinetics of the oral direct renin inhibitor aliskiren in combination with digoxin, atorvastatin, and ketoconazole in healthy subjects: the role of P-glycoprotein in the disposition of aliskiren. *J. Clin. Pharmacol.* **48**, 1323–38 (2008).
112. Johne, A. *et al.* Pharmacokinetic interaction of digoxin with an herbal extract from St John's wort (Hypericum perforatum). *Clin. Pharmacol. Ther.* **66**, 338–45 (1999).
113. Rodin, S.M., Johnson, B.F., Wilson, J., Ritchie, P. & Johnson, J. Comparative effects of verapamil and isradipine on steady-state digoxin kinetics. *Clin. Pharmacol. Ther.* **43**, 668–72 (1988).
114. Kirch, W., Hutt, H.J., Dylewicz, P., Gräf, K.J. & Ohnhaus, E.E. Dose-dependence of the nifedipine-digoxin interaction? *Clin. Pharmacol. Ther.* **39**, 35–9 (1986).
115. Larsen, U.L. *et al.* Human intestinal P-glycoprotein activity estimated by the model substrate digoxin. *Scand. J. Clin. Lab. Invest.* **67**, 123–34 (2007).
116. Becquemont, L. *et al.* Effect of grapefruit juice on digoxin pharmacokinetics in humans. *Clin. Pharmacol. Ther.* **70**, 311–6 (2001).
117. Jalava, K.M., Partanen, J. & Neuvonen, P.J. Itraconazole decreases renal clearance of digoxin. *Ther. Drug Monit.* **19**, 609–13 (1997).
118. Ragueneau, I. *et al.* Pharmacokinetic and pharmacodynamic drug interactions between digoxin and macrogol 4000, a laxative polymer, in healthy volunteers. *Br. J. Clin. Pharmacol.* **48**, 453–6 (1999).
119. Tayrouz, Y. *et al.* Pharmacokinetic and pharmaceutic interaction between digoxin and Cremophor RH40. *Clin. Pharmacol. Ther.* **73**, 397–405 (2003).

120. Verstuyft, C. *et al.* Dipyridamole enhances digoxin bioavailability via P-glycoprotein inhibition. *Clin. Pharmacol. Ther.* **73**, 51–60 (2003).
121. Westphal, K. *et al.* Oral bioavailability of digoxin is enhanced by talinolol: evidence for involvement of intestinal P-glycoprotein. *Clin. Pharmacol. Ther.* **68**, 6–12 (2000).
122. Martin, D.E. *et al.* Lack of effect of eprosartan on the single dose pharmacokinetics of orally administered digoxin in healthy male volunteers. *Br. J. Clin. Pharmacol.* **43**, 661–4 (1997).
123. Hayward, R.P., Greenwood, H. & Hamer, J. Comparison of digoxin and medigoxin in normal subjects. *Br. J. Clin. Pharmacol.* **6**, 81–6 (1978).
124. Oosterhuis, B., Jonkman, J.H., Andersson, T., Zuiderwijk, P.B. & Jedema, J.N. Minor effect of multiple dose omeprazole on the pharmacokinetics of digoxin after a single oral dose. *Br. J. Clin. Pharmacol.* **32**, 569–72 (1991).
125. Alsenz, J., Meister, E. & Haenel, E. Development of a partially automated solubility screening (PASS) assay for early drug development. *J. Pharm. Sci.* **96**, 1748–62 (2007).
126. Yalkowsky, S.H. & Dannenfelser, R.M. Aquasol database of aqueous solubility. (1992).
127. Hinderling, P.H. Kinetics of partitioning and binding of digoxin and its analogues in the subcompartments of blood. *J. Pharm. Sci.* **73**, 1042–53 (1984).
128. Atkinson, H.C. & Begg, E.J. Relationship between human milk lipid-ultrafiltrate and octanol-water partition coefficients. *J. Pharm. Sci.* **77**, 796–8 (1988).
129. Obach, R.S., Lombardo, F. & Waters, N.J. Trend analysis of a database of intravenous pharmacokinetic parameters in humans for 670 drug compounds. *Drug Metab. Dispos.* **36**, 1385–405 (2008).
130. Neuhoff, S. *et al.* Application of permeability-limited physiologically-based pharmacokinetic models: part I-digoxin pharmacokinetics incorporating P-glycoprotein-mediated efflux. *J. Pharm. Sci.* **102**, 3145–60 (2013).
131. Katz, A. *et al.* Selectivity of digitalis glycosides for isoforms of human Na,K-ATPase. *J. Biol. Chem.* **285**, 19582–92 (2010).
132. Troutman, M.D. & Thakker, D.R. Efflux ratio cannot assess P-glycoprotein-mediated attenuation of absorptive transport: asymmetric effect of P-glycoprotein on absorptive and secretory transport across Caco-2 cell monolayers. *Pharm. Res.* **20**, 1200–9 (2003).
133. Meyer, M., Schneckener, S., Ludewig, B., Kuepfer, L. & Lippert, J. Using expression data for quantification of active processes in physiologically based pharmacokinetic modeling. *Drug Metab. Dispos.* **40**, 892–901 (2012).
134. Nishimura, M. & Naito, S. Tissue-specific mRNA expression profiles of human phase I metabolizing enzymes except for cytochrome P450 and phase II metabolizing enzymes. *Drug Metab. Pharmacokinet.* **21**, 357–374 (2006).
135. Rodrigues, A.D. Integrated cytochrome P450 reaction phenotyping: attempting to bridge the gap between cDNA-expressed cytochromes P450 and native human liver microsomes. *Biochem. Pharmacol.* **57**, 465–80 (1999).
136. PK-Sim Ontogeny Database Documentation, Version 7.1. (2017).
137. Rowland Yeo, K., Walsky, R.L., Jamei, M., Rostami-Hodjegan, A. & Tucker, G.T. Prediction of time-dependent CYP3A4 drug-drug interactions by physiologically based pharmacokinetic modelling: impact of inactivation parameters and enzyme turnover. *Eur. J. Pharm. Sci.* **43**, 160–73 (2011).
138. Greenblatt, D.J. *et al.* Time course of recovery of cytochrome p450 3A function after single doses of grapefruit juice. *Clin. Pharmacol. Ther.* **74**, 121–9 (2003).
139. Prasad, B. *et al.* Interindividual variability in hepatic organic anion-transporting polypeptides and P-glycoprotein (ABCB1) protein expression: quantification by liquid chromatography tandem mass spectroscopy and influence of genotype, age, and sex. *Drug Metab. Dispos.* **42**, 78–88 (2014).

140. Nishimura, M. & Naito, S. Tissue-specific mRNA expression profiles of human ATP-binding cassette and solute carrier transporter superfamilies. *Drug Metab. Pharmacokinet.* **20**, 452–77 (2005).
141. Mills, J.B., Rose, K.A., Sadagopan, N., Sahi, J. & deMorais, S.M.F. Induction of drug metabolism enzymes and MDR1 using a novel human hepatocyte cell line. *J. Pharmacol. Exp. Ther.* **309**, 303–9 (2004).
142. Sahi, J. *et al.* Effect of troglitazone on cytochrome P450 enzymes in primary cultures of human and rat hepatocytes. *Xenobiotica.* **30**, 273–84 (2000).
143. Kolars, J.C., Schmiedlin-Ren, P., Schuetz, J.D., Fang, C. & Watkins, P.B. Identification of rifampin-inducible P450IIIA4 (CYP3A4) in human small bowel enterocytes. *J. Clin. Invest.* **90**, 1871–8 (1992).
144. Austin, R.P., Barton, P., Cockroft, S.L., Wenlock, M.C. & Riley, R.J. The influence of nonspecific microsomal binding on apparent intrinsic clearance, and its prediction from physicochemical properties. *Drug Metab. Dispos.* **30**, 1497–503 (2002).
145. Tucker, R.M. *et al.* Interaction of azoles with rifampin, phenytoin, and carbamazepine: in vitro and clinical observations. *Clin. Infect. Dis.* **14**, 165–74 (1992).
146. Xu, L., Chen, Y., Pan, Y., Skiles, G.L. & Shou, M. Prediction of human drug-drug interactions from time-dependent inactivation of CYP3A4 in primary hepatocytes using a population-based simulator. *Drug Metab. Dispos.* **37**, 2330–9 (2009).